Functional interactions of E2~Ubiquitin conjugates in and outside the ubiquitination pathway

Jonathan N. Pruneda

A dissertation

submitted in partial fulfillment of the

requirements for the degree of

Doctor of Philosophy

University of Washington

2012

Reading Committee:

Rachel E. Klevit, Chair

Wim G. J. Hol

Ning Zheng

Program Authorized to Offer Degree:

Department of Biochemistry

University of Washington

Abstract

Functional interactions of E2~Ubiquitin conjugates in and outside the ubiquitination pathway

Jonathan N. Pruneda

Chair of the Supervisory Committee:
Professor Rachel E. Klevit
Department of Biochemistry

Thirty years of research have implicated ubiquitin (Ub) signaling in nearly every aspect of eukaryotic cell biology. What appears to be a simple signaling molecule in fact has the ability to encode countless cellular fates that include proteasomal degradation, cell cycle control, and DNA damage repair. Although the enzymes within the Ub transfer pathway are well established (E1, E2, E3), the molecular details required for protein ubiquitination are largely unknown.

To address questions regarding the final stages of Ub transfer, we began with structural characterization of the pathway intermediate, the E2~Ub conjugate (~ indicates the thioester linkage between the E2 active site cysteine and the Ub C-terminus). NMR and SAXS techniques were used to describe the array of conformations populated by the flexibly linked UbcH5c~Ub and Ubc13~Ub conjugates. Unlike the Ubc13~Ub conjugate, the UbcH5c~Ub intermediate strongly prefers extended conformations in which the Ub is positioned directly below the E2 active site.

We determined that addition of RING/U-box E3 ligases induced a shift in the ensemble of UbcH5c~Ub populated states toward more “closed” conformations. A variety of biochemical assays were used to show that these closed conformations represent the activated states by which

E3 ligases promote Ub transfer. This mechanism of conformational activation is utilized by diverse RING/U-box E3:E2 pairs, and is mediated by an intermolecular hydrogen bond stemming from a conserved basic residue on the E3.

To identify mutations that augment the E3's ability to facilitate Ub transfer, we collaborated with the Stan Fields lab to screen nearly 100,000 E3 sequence variants for ubiquitination activity. Rare mutations were identified that increased ligase activity as much as 20-fold. NMR analysis showed that the mutations fall into two classes based on their effects; the first class of mutants enhance activity by increasing E3:E2 binding affinity while the second class does so by augmenting the ability to induce closed E2~Ub conformations.

Lastly, we characterized an interaction between the E2~Ub conjugate and *Shigella* effector kinase OspG to find that, while OspG has little effect on ubiquitination activity, formation of the OspG:UbcH5c~Ub complex results in a pronounced increase in OspG kinase activity.

TABLE OF CONTENTS

LIST OF FIGURES

LIST OF TABLES

ACKNOWLEDGEMENTS

"In the long history of humankind (and animal kind, too) those who learned to collaborate and improvise most effectively have prevailed."

-Apocryphally attributed to Charles Darwin

I believe that the best science is done through collaboration. Beyond the obvious benefits of sharing resources or skill sets, collaborations create an environment well suited for generating and refining ideas. Something so simple as a conversation over coffee can spark ideas that develop into hypotheses that lead to groundbreaking discoveries. For that reason I would like to acknowledge all contributions, large and small, that have lead to my cumulative dissertation work. Each section of my dissertation begins with an explanation of specific contributions toward that work. As for the more intangible collaborations that typically take place over coffee or beer, a more open thank you to my labmates, fellow graduate students, and family will have to suffice. I can only hope that I was able to repay you in kind.

DEDICATION

I dedicate this dissertation to all of my teachers over the past 26 years that have shaped me into the person I am today.

Chapter I - Introduction

A brief history

As the molecular machines of the cell, proteins require extremely precise regulation. Localization, activity, and stability all need to be carefully controlled, often with very sensitive time constraints. Exactly how protein fates are directed in the cellular milieu was a great mystery of early biochemistry. Proteolysis – the removal of damaged or otherwise unwanted proteins - proved to be a particularly puzzling phenomenon for early researchers. Early studies using stable isotope labeling showed that proteins are not as long-lived as the cells in which they reside[1]. Soon thereafter, Melvin Simpson made the curious observation that protein degradation in mammalian cells requires energy, despite the fact that the hydrolysis of a peptide bond is an exergonic process[2]. For decades though, protein degradation was primarily thought of as a straightforward process carried out by lysosomal vacuoles. It wasn't until Joseph Etlinger and Alfred Goldberg discovered an ATP-dependent proteolytic system in reticulocytes (which lack lysosomes) that researchers began to show a strong interest in the regulation of protein degradation[3]. Excited by Goldberg's discovery, Avram Hershko and Aaron Ciechanover fractionated reticulocyte lysate to separate and identify two critical components of the protein degradation pathway: a heat-stable component they named APF-1 (ATP-dependent Proteolysis Factor 1 in fraction I) and an ATP-binding component APF-2 (fraction II)[4,5]. With the help of Arthur Haas, they went on to show that APF-1 was incorporated into high molecular weight adducts after incubation with fraction II, in an ATP-dependent manner. Critically, they showed that these APF-1 adducts were covalent, suggesting some sort of post-translational modification[6].

The discovery of phosphorylation as a reversible, post-translational modification by Edmond Fischer and Edwin Krebs in the mid-1950's set the stage for future studies regarding

rapid alterations of protein chemistries[7]. It was on the shoulders of these types of studies that ubiquitin (Ub), a 76 amino acid protein first identified by Gideon Goldstein as a protein of unknown function present in many organisms, was shown to post-translationally modify histone H2A in 1977[8,9]. Recognizing the rarity of post-translational modification with another protein, in 1980 Keith Wilkinson, Michael Urban, and Arthur Haas showed somewhat serendipitously that Ub and APF-1 were, in fact, the same protein[10]. Over the next four years, Hershko, Ciechanover and others went on to identify a set of three enzymes, E1-E2-E3, that work in succession to move Ub onto the substrate[11]. Specifically, E1 uses ATP to adenylate the Ub C-terminus, which is then transferred onto the E1 active site cysteine to create a thioester linkage. The Ub is then passed onto an E2 enzyme active site cysteine to form the E2~Ub conjugate (~ denotes thioester linkage), which then works in coordination with an E3 to transfer Ub onto a substrate lysine, thusly creating a stable isopeptide linkage (Figure 1). Taking advantage of a temperature-sensitive mouse cell line called ts85, Dan Finley and Alexander Varshavsky showed that the Ub system was responsible for much of the regulated proteolysis within the cell[12]. These studies and those that followed sparked the creation of an entire field of research devoted to Ub biology. Now, thirty years later, hundreds of Ub researchers build upon the framework established by Ciechanover, Hershko, and Rose, who in 2004 received the Nobel Prize in Chemistry in honor of their work.

The ubiquitin signal

As with most biological research, each breakthrough in the Ub system comes with a new set of questions. Although the basis of the first described Ub system remains true today, the past thirty years of research has added many layers of complexity. As a prime example, the outcome of Ub modification has expanded beyond protein degradation to include many more processes,

including DNA damage response, protein localization, chromatin structure, and signaling. How a small protein such as Ub can signal for so many different protein fates is an interesting and ongoing area of research. For example, attachment of a single, mono-Ub can provide a sufficient signal for protein recruitment, as is the case for PCNA during response to DNA damage[13]. Much of the signal variety, however, is likely encoded within Ub chains (for a review, see Komander and Rape 2012[14]). Just as Ub can be covalently linked to target molecules through lysine side chains, Ub can also modify itself on any of its seven lysines or N-terminus to create polymers of Ub. Signals arise from the polymerization of Ub chains based upon specific linkages in Ub such as K48-linked chains (signal for proteasomal degradation[15]), K63-linked chains (associated with DNA damage response[16]), or linear N-terminally-linked Ub chains (implicated in NF-κB signaling[17]). Although all possible chain types have been observe in cells[18], the molecular roles of most are poorly understood, particularly K6, K27, K29, and K33 linkages. Even more complexity can be added through the polymerization of mixed (those made up of different linkage types) or branched (those that contain several modifications at a single Ub) chains. Additionally, Ub itself can be phosphorylated or acetylated, which could add to signal diversity[19,20].

Even the seemingly straightforward process of attaching Ub to a substrate has become more complicated. While the hierarchy of the E1-E2-E3 pathway identified by Ciechanover has remained, the numbers of each enzyme type have since grown. It is now thought that humans encode 2 E1 Ub-activating enzymes, 35-40 E2 Ub-conjugating enzymes, and over 600 E3 Ub-ligases. Although the ubiquitin-activating role of the E1 is seemingly universal, E2s and E3s are structurally and mechanistically much more diverse.

E2 Ub-conjugating enzymes:

All E2s contain a common "Ubc" α/β fold that carries the active site cysteine. Although the precise mechanics of the E2 active site are not fully understood, extensive mutational studies have identified a number of critical residues surrounding the E2~Ub thioester. E2s contain a conserved HPN motif near the active site, the Asn of which is thought to hydrogen bond the carbonyl of the thioester linkage and thusly stabilize the oxyanion intermediate during Ub transfer (the corresponding Asn in UbcH5c is N77)[21]. An additional requirement for transfer is a general base to aid in the deprotonation of the incoming lysine (thought to be D117 in UbcH5c)[22]. Lastly, a conserved Asp near the active site (D87 in UbcH5c) has been linked to Ub transfer activity[23]. Some E2s possess additional protein sequence before or after the Ubc domain, often with unknown function.

Minimally, interaction surfaces for the covalently linked Ub, E1, and E3 lie within the ~150 residue Ubc domain (for a review, see Wenzel, Stoll & Klevit 2010[24]). Some E2s have been observed to interact with a substrate-type molecule, such as Ub in the case of the chain building E2 Ubc1[25], and RanGAP1 in the case of the SUMO (a Ub-like modifier) E2 Ubc9[26]. Additionally, E2s have been reported to interact with a second Ub molecule[27], or accessory proteins[28]. Many interactions involving E2s are extremely weak and transient, making them difficult to study by conventional methods. Identifying which E2s function with a particular E3, for example, often cannot be accomplished by co-IP experiments because the interaction is too short-lived. While in the Klevit lab, Devin Christensen designed a yeast 2-hybrid experiment that screened for interactions between a breast cancer associated E3 ligase BRCA1 and the entire set of human E2s. From this screen, he identified 10 E2s that interact with BRCA1 and showed through *in vitro* ubiquitination assays that 9 of them are competent for ubiquitin transfer[29].

These assays reconstitute the ubiquitin system by combining recombinant E1, E2, E3, and Ub with ATP/Mg and observing the formation of high-molecular weight Ub adducts as a function of time. These products can take the form of either free Ub chains or modifications of the E3 itself outside of the ligase domain. Interestingly, even with a set E3 ligase, many of the E2s showed diverse product specificity ranging from mono-ubiquitination to poly-ubiquitination with either mixed, K48-specific, or K63-specific chain types. Further, he found that some poly-ubiquitinating E2s require a "priming" ubiquitination event catalyzed by a mono-ubiquitinating E2 before they could extend the Ub chain[29]. These results imply that, from its position at the crux of the Ub transfer pathway, E2s influence both E3- and product-specificity.

E3 Ub-ligases:

With numbers surpassing even kinases, E3 ligases represent the largest family of enzymes within the human proteome. E3s are roughly divided into two main classes based upon structural and mechanistic differences. HECT (Homologous to E6AP C-Terminus) E3s contain a bilobal ligase domain at their C-terminus. Within this domain, the N-terminal lobe binds an E2~Ub conjugate while the C-terminal lobe harbors a catalytic cysteine that accepts transfer of Ub. After recruitment of a substrate, Ub is passed from the high energy E3~Ub species to the incoming lysine. A crystal structure of a HECT domain in complex with an E2~Ub conjugate has recently been determined (Nedd4L:UbcH5b~Ub PDB code 3JW0)[30]. Several twists on the HECT-type mechanism exist. Some pathogenic bacteria have evolved a set of E3 ligases that they secrete during invasion to hijack our ubiquitination machinery. Of these, select examples in the NEL (Novel E3 Ligase) family utilize a HECT-type mechanism (i.e. contain a catalytic cysteine and require an additional transthiolation event) but display drastically unique structure[31].

RING (Really Interesting New Gene) ligases comprise the second (and largest) class of E3s (for a review, see Deshaies and Joazeiro 2009[32]). A canonical RING domain follows the sequence expression Cys-X_2-Cys-$X_{(9-39)}$-Cys-$X_{(1-3)}$-His-$X_{(2-3)}$-Cys-X_2-Cys-$X_{(4-48)}$-Cys-X_2-Cys where X is any amino acid. This sequence forms a cross-brace structure that is stabilized by the coordination of two zinc molecules. As illustrated with the RING domain of BRCA1, mutation of these conserved cysteines can result in severe structural instability[33]. Variations on RINGs include U-box domains, which maintain the same structure and function without coordinating zincs.

RING domains maintain a fairly low affinity for E2s (on the order of 100$M); significant exchange is likely required, though, because structural studies show that the E1 and E3 binding sites on the E2 overlap. In contrast to HECT E3 ligases that carry a bona fide active site, RING-type E3s have typically been considered to act as catalytically inert molecular scaffolds. Their role in ubiquitin transfer was described relatively simply; RING E3s bind E2~Ub and substrate, bringing them together and thusly facilitating transfer. The lingering question was: if E2s are predominantly in the Ub-loaded state in the cell[34], what prevents them from discharging their Ub cargo at every random protein encounter? Clearly unwanted ubiquitination events in the cell would not be tolerated, so logic argues that something must activate the E2~Ub at the opportune moment for transfer. As E2s typically do not recognize substrate in the absence of an E3, the question of whether RING domains contribute more to ubiquitination than E2 binding remained open for many years. Only a few specialized assays can illustrate an additional role played by RING domains. In the first, the E2 Ubc13 catalyzes the formation of free, K63-linked polyubiquitin chains in the presence of its accessory protein, Mms2. An elegant crystal structure of the Mms2:Ubc13~Ub complex has shown that Mms2 coordinates an incoming substrate Ub in

such a way that K63 is oriented directly toward the Ubc13~Ub thioester[35]. Essentially, this system does not require an E3 to coordinate substrate, yet Ub chain formation is dramatically enhanced in the presence of a minimal RING domain[36]. The second experiment, inspired by work of the late Cecile Pickart demonstrating E2-catalyzed Ub transfer onto the free amino acid lysine, demonstrates an increased rate of Ub discharge to small molecule nucleophiles in the presence of minimal RING domains[37,23]. With the advent of these substrate-independent assays researchers have begun to observe a second, catalytic role for RING-type E3s in the enhancement of Ub transfer reactions.

Open questions and statement of objectives

Crystallographic and solution-based structural studies have established a conserved interaction between RING domains and E2s. The "canonical" E3:E2 binding interaction established by nearly a dozen structures involves Loops 1, 2 and Helix 1 of the RING domain contacting Loops 4, 7 and Helix 1 of the Ubc domain (Figure 1). The ~15Å separation between the E3-binding site and the active site thioester implies that any role played by the RING domain in facilitating Ub transfer must be indirect. For each E3:E2 structure, though, comparisons of apo and E3-bound E2 enzymes have failed to identify a clear connection between E3 binding and the activation of Ub transfer. As the more physiologically relevant species, however, the key to RING-dependent allosteric activation may lie with the E2~Ub conjugate. At the inception of this thesis work, there were only two entries for E2~Ub conjugates in the Protein Data Bank. By 2010, two more structures were deposited. Among these entries, two were crystal structures and two were models based upon solution NMR data. Not only was each structure of a different E2, but the conformation of conjugated Ub was also unique in each case. This observation could stem from two nonexclusive possibilities: 1) each E2 positions its conjugated Ub in a distinct

conformation, and 2) E2~Ub conjugates are dynamic in solutions and, therefore, not accurately represented by structural snapshots. Understanding the behavior of an E2~Ub conjugate sets a basis for explaining how E3 ligases, in addition to other interacting proteins, manipulate this structure to suit their needs. Therefore, the objectives of this thesis are as follows:

1) Develop and apply methods to study the structure of an E2~Ub conjugate, keeping in mind the possible dynamic and E2-specific nature of this structure.
2) Using the E2~Ub structure as a starting point, understand how E3 ligases manipulate this structure with the goal of identifying and describing the allosteric activation of E2s by RING-type E3 ligases.
3) Leverage the discoveries in Objective 2 to further understand the molecular determinants of RING-type E3 allostery and use this information to identify and rationalize mutant E3s with hyperactive capacities for Ub transfer.
4) As an example of the E2~Ub conjugate working outside of the Ub system, characterize its interaction with the bacterial effector protein OspG. Describe the implications of this interaction for both the eukaryotic Ub pathway and for bacterial invasion and pathogenesis.

References:

1. Schoenheimer, R. (1942). The dynamic state of body constituents. Harvard University Press, Cambridge, MA.

2. McLean, J. R., Cohn, G. L., Brandt, I. K., and Simpson, M. V. (1958). Incorporation of labeled amino acids into the protein of muscle and liver mitochondria. J. Biol. Chem. *201*, 143-154.

3. Etlinger, J. D. and Goldberg, A. L. (1977). A soluble ATP-dependent proteolytic system responsible for the degradation of abnormal proteins in reticulocytes. Proc. Natl. Acad. Sci. USA. *74*, 54-58.

4. Ciechanover, A., Hod, Y., and Hershko, A. (1978). A heat-stable polypeptide component of an ATP-dependent proteolytic system from reticulocytes. Biochem. Biophys. Res. Commun. *81*, 1100-1105.

5. Hershko, A., Ciechanover, A., and Rose, I. A. (1979). Resolution of the ATP-dependent proteolytic system from reticulocytes: a component that interacts with ATP. Proc. Natl. Acad. Sci. USA. *76*, 3107-3110.

6. Ciechanover, A., Heller, H., Elias, S., Haas, A. L., and Hershko, A. (1980). ATP-dependent conjugation of reticulocyte proteins with the polypeptide required for protein degradation. Proc. Natl. Acad. Sci. USA. *77*, 1365-1368.

7. Fischer, E. H. and Krebs, E. G. (1955). Conversion of Phosphorylase *b* to Phosphorylase *a* in muscle extracts. J. Biol. Chem. *216*, 121-132.

8. Goldstein, G., Scheid, M., Hammerling, U., Schlesinger, D. H., Niall, H. D., and Boyse, E. A. (1975) Isolation of a polypeptide that has lymphocyte-differentiating properties and is probably represented universally in living cells. Proc. Natl. Acad. Sci. USA. *72*, 11-15.

9. Goldknopf, I. L. and Busch, H. (1977). Isopeptide linkage between nonhistone and histone 2A polypeptides of chromosomal conjugate-protein A24. Proc. Natl. Acad. Sci. USA. *74*, 864-868.

10. Wilkinson, K. D., Urban, M. K., and Haas, A. L. (1980). Ubiquitin is the ATP-dependent proteolysis factor I of rabbit reticulocytes. J. Biol. Chem. *255*, 7529-7532.

11. Hershko, A., Heller, H., Elias, S., and Ciechanover, A. (1983). Components of the ubiquitin-protein ligase system. Resolution, affinity purification, and role in protein breakdown. J. Biol. Chem. *258*, 8206-8214.

12. Finley, D., Ciechanover, A., and Varshavsky, A. (1984). Thermolability of ubiquitin activating enzyme from the mammalian cell cycle mutant ts85. Cell. *37*, 43-55.

13. Hoege, C., Pfander, B., Moldovan, G. L., Pyrowolakis, G., and Jentsch, S. (2002). RAD6-dependent DNA repair is linked to modification of PCNA by ubiquitin and SUMO. Nature. *419*, 135-141.

14. Komander, D. and Rape, M. (2012). The ubiquitin code. Annu. Rev. Biochem. *81*, 203-229.

15. Chau, V., Tobias, J. W., Bachmair, A., Marriott, D., Ecker, D. J., Gonda, D. K., and Varshavsky, A. (1989). A multiubiquitin chain is confined to specific lysine in a targeted short-lived protein. Science. *243*, 1576-1583.

16. Al-Hakim, A., Escribano-Diaz, C., Landry, M. C., O'Donnell, L, Panier, S. Szilard, R. K., and Durocher, D. (2010). The ubiquitous role of ubiquitin in the DNA damage response. DNA Repair. *9*, 1229-1240.

17. Rahighi, S., Ikeda, F., Kawasaki, M., Akutsu, M., Suzuki, N., Kato, R., Kensche, T., Uejima, T., Bloor, S., Komander, D., Randow, F., Wakatsuki, S., and Dikic, I. Specific recognition of linear ubiquitin chains by NEMO is important for NF-kB activation. Cell. *136*, 1098-1109.

18. Peng, J., Schwartz, D., Elias, J. E., Thoreen, C. C., Cheng, D., Marsischky, G., Roelofs, J., Finley, D., and Gygi, S. P. (2003). A proteomics approach to understanding protein ubiquitination. Nat. Biotech. *21*, 921-926.

19. Olsen, J. V., Blagoev, B., Gnad, F., Macek, B., Kumar, C., Mortensen, P., and Mann, M. (2006). Global, in vivo, and site-specific phosphorylation dynamics in signaling networks. Cell. *127*, 635-648.

20. Choudhary, C., Kumar, C., Gnad, F., Nielsen, M. L., Rehman, M., Walther, T., Olsen, J. V., and Mann, M. (2009). Lysine acetylation targets protein complexes and co-regulates major cellular functions. Science. *325*, 834-840.

21. Wu, P. Y., Hanlon, M., Eddins, M., Tsui, C., Rogers, R. S., Jensen, J. P., Matunis, M. J., Weissman, A. M., Wolberger, C. P., and Pickart, C. M. (2003) A conserved catalytic residue in the ubiquitin-conjugating enzyme family. EMBO J. *22*, 5241-5250.

22. Plechanovová, A., Jeffray, E. G., Tatham, M. H., Naismith, J. H., and Hay, R. T. (2012). Structure of a RING E3 ligase and ubiquitin-loaded E2 primed for catalysis. Nature. *489*, 115-120.

23. Wenzel, D. M., Lissounov, A., Brzovic, P. S., and Klevit, R. E. (2011). UBCH7 reactivity profile reveals parkin and HHARI to be RING/HECT hybrids. Nature. *474*, 105-108.

24. Wenzel, D. M., Stoll, K. E., and Klevit, R. E. (2010). E2s: structurally economical and functionally replete. Biochem. J. *433*, 31-42.

25. Rodrigo-Brenni, M. C., Foster, S. A., and Morgan, D. O. (2010). Catalysis of lysine 48-specific ubiquitin chain assembly by residues in E2 and ubiquitin. Mol. Cell. *39*, 548-559.

26. Bernier-Villamor, V., Sampson, D. A., Matunis, M. J., and Lima, C. D. (2002). Structural basis for E2-mediated SUMO conjugation revealed by a complex between ubiquitin-conjugating enzyme Ubc9 and RanGAP1. Cell. *108*, 345-356.

27. Brzovic, P. S., Lissounov, A., Christensen, D. E., Hoyt, D. W., and Klevit, R. E. (2006). A UbcH5/ubiquitin noncovalent complex is required for processive BRCA1-directed ubiquitination. Mol. Cell. *21*, 873-880.

28. Moraes, T. F., Edwards, R. A., McKenna, S., Pastushok, L., Xiao, W., Glover, J. N., and Ellison, M. J. (2001). Crystal structure of the human ubiquitin conjugating enzyme complex, hMms2-hUbc13. Nat. Struct. Mol. Biol. *8*, 669-673.

29. Christensen, D. E., Brzovic, P. S., and Klevit, R. E. (2007). E2-BRCA1 RING interactions dictate synthesis of mono- or specific polyubiquitin chain linkages. Nat. Struct. Mol. Biol. *14*, 941-948.

30. Kamadurai, H. B., Souphron, J., Scott, D. C., Duda, D. M., Miller, D. J., Stringer, D., Piper, R. C., and Schulman, B. A. (2009) Insights into ubiquitin transfer cascades from a structure of a UbcH5B~ubiquitin-HECT(NEDD4L) complex. Mol. Cell. *36*, 1095-1102.

31. Rohde, J. R., Breitkreutz, A., Chenal, A., Sansonetti, P. J., and Parsot, C. (2007). Type III secretion effectors of the IpaH family are E3 ubiquitin ligases. Cell Host Microbe. *1*, 77-83.

32. Deshaies, R. J. and Joazeiro, C. A. (2009). RING domain E3 ubiquitin ligases. Annu. Rev. Biochem. *78*, 399-434.

33. Brzovic, P. S., Meza, J. E., King, M. C., and Klevit, R. E. (2001). BRCA1 RING domain cancer-predisposing mutations: Structural consequences and effects on protein-protein interactions. J. Biol. Chem. *276*, 41399-41406.

34. Haas, A. L. and Rose, I. A. (1982). The mechanism of ubiquitin activating enzyme. A kinetic and equilibrium analysis. J. Biol. Chem. *257*, 10329-10337.

35. Eddins, M. J., Carlile, C. M., Gomez, K. M., Pickart, C. M., and Wolberger, C. (2006). Mms2-Ubc13 covalently bound to ubiquitin reveals the structural basis of linkage-specific polyubiquitin chain formation. Nat. Struct. Mol. Biol. *10*, 915-920.

36. Yin, Q., Lin, S. C., Lamothe, B., Lu, M., Lo, Y. C., Hura, G., Zheng, L., Rich, R. L., Campos, A. D., Myszka, D. G., Lenardo, M. J., Darnay, B. G., and Wu, H. (2009). E2 interaction and dimerization in the crystal structure of TRAF6. Nat. Struct. Mol. Biol. *6*, 658-666.

37. Pickart, C. M. and Rose, I. A. (1985). Functional heterogeneity of ubiquitin carrier proteins. J. Biol. Chem. *260*, 1573-1581.

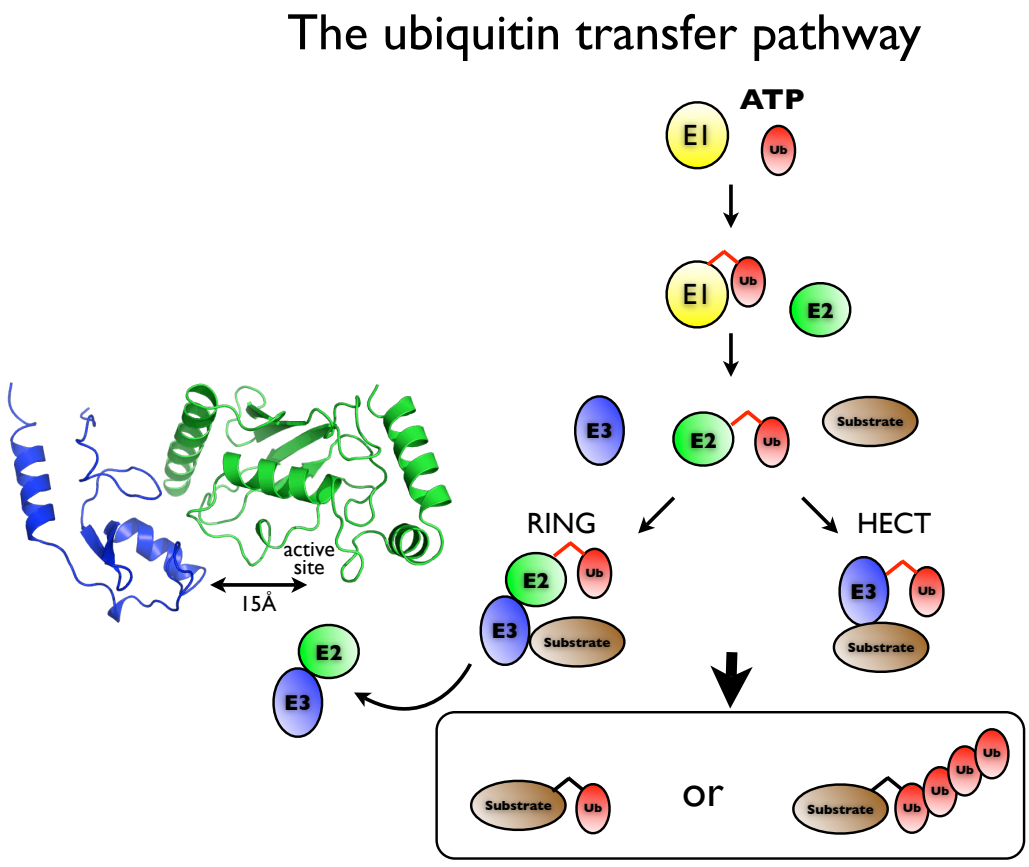

Figure 1: The Ubiquitination Pathway. In an ATP-dependent process, the E1 enzyme (yellow) activates Ub (red) and forms an E1~Ub thioester linkage (red lines). The Ub is then passed onto an E2 (green) active site cysteine, which works with an E3 ligase (blue) to ultimately form a stable isopeptide linkage between a substrate (brown) lysine and the Ub C-terminus (black lines). RING-type E3s (left) facilitate the direct transfer of Ub from E2 to substrate, while HECT-type E3s (right) rely upon an E3~Ub thioester intermediate. The E3:E2 complex that has been the focus of many structural studies (ribbon structure, PDB ID 3L1Z), in fact, represents a byproduct of the Ub transfer reaction

Chapter II - Ubiquitin in Motion: Structural studies of the E2~Ub conjugate

The following chapter was published in the journal *Biochemistry*.

Reprinted with permission from
Pruneda, J. N.*, Stoll, K. E.*, Bolton, L. J., Brzovic, P. S., and Klevit, R. E. (2011) Ubiquitin in Motion: Structural studies of the ubiquitin-conjugating enzyme~ubiquitin conjugate. *Biochemistry. 50*, 1624-1633.

*Authors contributed equally to this work

Author Contributions: J.N.P. performed all NMR experiments involving UbcH5c and the UbcH5c~Ub conjugate, in addition to all SAXS experiments. K.E.S. performed all NMR experiments pertaining to Ubc13 and the Ubc13~Ub conjugate. L.J.B. performed the assay shown in Figure 7. J.N.P, K.E.S., P.S.B., and R.E.K. wrote the manuscript.

Abbreviations: Ub, ubiquitin; E2, ubiquitin-conjugating enzyme; E3, ubiquitin ligase; E1, ubiquitin-activating enzyme; RING, Really Interesting New Gene; HECT, Homologous to E6AP Carboxy Terminus; NMR, nuclear magnetic resonance; SAXS, small angle x-ray scattering; PRE, paramagnetic relaxation enhancement; CSP, chemical shift perturbation.

Introduction

Covalent attachment of the 8.6 kDa Ubiquitin (Ub) to target proteins is an essential step in eukaryotic signaling pathways. The type of Ub modification can vary, inducing distinct signals. For example, mono-ubiquitination may elicit a signal for protein transport while poly-ubiquitination (attachment of a chain of Ubs to the target) may mark a protein for proteasome-mediated degradation. Covalent attachment of Ub to a substrate proceeds through a multi-enzyme process consisting of a Ub-activating enzyme (E1), a Ub-conjugating enzyme (E2), and a Ub ligase (E3)[1]. The human genome contains two Ub E1s, ~35 E2s, and many hundreds of E3s[2]. Despite the large number of E2s, they share significant similarity at both the sequence and structure levels. The E2 plays a central role in the ubiquitination cascade, shuttling Ub from an E1 to an E3/substrate complex. The E2 holds Ub in its activated form *via* formation of a thioester bond between the carboxy-terminus of Ub and the E2's active site cysteine (denoted as E2~Ub).

The small size and high solubility of many E2s have made them prime candidates for structural investigations. There are ~100 structures of E2s in the Protein Data Bank (PDB) and 23 of the ~35 human E2s have their structures deposited. This wealth of information reveals that all E2s are related by their conserved catalytic cores which fold into an α/β topology. Significantly fewer structures of E2~Ub complexes have been solved, due probably to the technical challenges that the labile thioester conjugate poses. There are presently five structures of E2~Ub conjugates or close structural analogs that have been determined by X-ray crystallography or NMR: Ubc13~Ub (PDB code 2GMI)[3]; Ubc1~Ub (PDB code 1FXT)[4]; UbcH8~Ub (PDB code 2KJH)[5]; and UbcH5b~Ub (PDB codes 3A33[6], and 3JW0[7]). In each case,

the backbone of the E2 and Ub moieties are not significantly altered from their free structures. However, each structure presents a unique relative orientation of the E2 and Ub units.

Despite the wealth of atomic-level structural information on E2s, on E2/E3 complexes, and a growing number of E2~Ub conjugates, the ways in which E3s catalyze Ub transfer from an E2~Ub remain poorly understood. It is clear that one function of the E3 is to bind a substrate simultaneously with binding an E2~Ub, thereby bringing the two components into proximity. However, even in the absence of a protein substrate, E3s have been shown to enhance the rate at which Ub is released from an E2~Ub conjugate, presumably due to reaction of the thioester bond with solvent or buffer components[8,9]. Although this so-called hydrolysis or release rate may not be the mechanistic equivalent of the reaction involving a substrate lysine side chain, the ability of an E3 to enhance the reactivity of an E2~Ub suggests that an E2 active site can somehow be tuned in response to E3 binding. As a step towards understanding how an E3 ligase regulates E2~Ub activity, a more complete description of the E2~Ub conjugate is needed. Furthermore, the *in vivo* steady-state equilibrium of the human E2 Ubc2b favors the conjugated form and this is likely a general feature of E2s because E1 is efficient at maintaining E2s in the conjugated state[10,11]. Thus, E3s and other cellular proteins are more likely to encounter E2~Ubs than free E2s. We have chosen to focus on UbcH5c and Ubc13, two highly related E2 enzymes (45.6% sequence identity and 61% similarity) with divergent activities and specificities (Figure S3). Orthologues of both UbcH5c and Ubc13 play key roles in all organisms from yeast to human[12]. These two E2s are well characterized, with structures determined for each in their free and Ub-conjugated states (Ubc13 PDB IDs 1J7D[13], 2GMI; UbcH5 PDB IDs 1X23, 3A33), both alone and in complex with interacting proteins. These studies and our own make use of an active site Cys-to-Ser mutation to generate a more stable oxyester-linked E2-O~Ub. In this study, we use

NMR chemical shift mapping, site-specific paramagnetic labeling, and small angle X-ray scattering (SAXS) to examine the ensemble of E2~Ub conformations populated by UbcH5c~Ub and Ubc13~Ub in solution. Characterization of the E2~Ub conjugate in solution will facilitate future structural studies with interacting proteins, including E3 ligases.

Results

We have previously reported the NMR chemical shift perturbations observed for UbcH5c-O~Ub relative to the free protein counterparts[15]. The most notable feature of the UbcH5-O~Ub conjugate was its asymmetric perturbations in which significant chemical shift perturbations were observed to emanate away from the active site in the E2 but were highly localized to the extreme C-terminus of the Ub moiety. Ub chemical shifts beyond the C-terminal residues are small (<0.05 ppm). While over one third (45/126) of UbcH5c resonances are shifted by greater than one peakwidth, only twelve are shifted by greater than one standard deviation from the mean. Mapping these twelve residues onto the 3-dimensional structure reveals a spotted surface spanning the crossover helix (Helix-2), active site, Loop 5 (residues 75-77), and the C-terminal helices (helices 3 and 4) (see figure 3C in reference *15*). Such a distributed perturbation surface is consistent with either a conformational adjustment in interior hydrophobics (aromatics) or a dynamic UbcH5c-O~Ub species in which activated Ub makes transient contact with multiple E2 surfaces.

Mapping the Ubc13~Ub interface by Chemical Shift Perturbation Analysis.

To allow for study of the Ubc13-O~Ub conjugate by NMR, the 2D HSQC-TROSY spectrum of ^{15}N-Ubc13-O~Ub was assigned. The lifetime of the Ubc13-O~Ub species in

solution is too short for collection of 3D spectra such as HNCA or HNCACB. Based on the observation that E2 structures do not change significantly in their Ub-conjugated state[3,5,6], we turned to HNCO spectra which can be collected in shorter acquisition times. The chemical shifts of backbone carbonyl groups are largely determined by the structure in which they are found, so the spectrum of conjugated Ubc13 could be assigned by matching HNCO carbonyl assignments between free and conjugated Ubc13 (Table S1). Comparison of the $^{1}H^{15}N$ chemical shifts of the free and conjugated protein reveals significant chemical shift perturbations (CSPs) in backbone amide resonances beyond the active site of Ubc13 (Figure 1A, C). In contrast to UbcH5-O~Ub, ^{15}N-Ub exhibits significant CSPs beyond its C-terminal tail when conjugated to Ubc13 (Fig 1B, C, D).

When mapped onto the crystal structure of Ubc13-O~Ub (PDB ID 2GMI), the CSPs resulting from the conjugation of Ub to Ubc13 reveal discrete surfaces on each protein component. The surface on Ubc13 is comprised of Helix-2 ("crossover helix"; residues 100-114), Loop 8 (residues 114-123) and, to a smaller extent, the penultimate C-terminal helix (See Table S2 for residue-level information). The I44 hydrophobic surface of Ub is perturbed upon conjugation to Ubc13 (Figure 1C and 1D and Table S2). The chemical shifts in Ub arising from conjugation to Ubc13 are remarkably different than those observed for conjugation to UbcH5c, both in profile and magnitude (Figure 1D). The perturbations observed when Ubc13 is conjugated to Ub are not congruent with those expected for an E2~Ub complex in an extended state, as observed in the crystal structure of Ubc13-O~Ub. The simplest interpretation of the observed perturbations is that they identify surfaces on Ubc13 and Ub that are in close proximity in the conjugate, suggesting a closed conformation in which the Ub is folded up towards the crossover helix of Ubc13. A similar closed state has been proposed for yeast Ubc1~Ub based on

NMR observations[4], however because this E2~Ub was created using a wildtype thioester linkage, it suffered from a short half-life and incomplete NMR assignments. The chemical shift perturbations observed for the oxyester forms of UbcH5-O~Ub and Ubc13-O~Ub allow direct comparison and suggest that Ubc13-O~Ub populates closed conformations more frequently than does UbcH5c-O~Ub.

Mapping the RING E3 binding surface of Ubc13 by Chemical Shift Perturbation Analysis.

To determine an E3's ability to bind the closed Ubc13-O~Ub conformation, we measured CSPs for free Ubc13 and Ubc13-O~Ub upon the addition of 1.1 equivalents of the minimal RING domains of the heterodimeric RING E3 BRCA1/BARD1. The chemical shift perturbations on ^{15}N-Ubc13 induced by BRCA1/BARD1 binding map to the conventional E3 binding surface comprised of Helix 1 and Loops 4 and 7 of Ubc13 (Fig 2b, Table S2 for residue level information). Resonances perturbed upon BRCA1/BARD1 addition to Ubc13-O~Ub map to the same surface as for free Ubc13. Conjugation-induced CSPs in Ubc13 residues (e.g., D44, T51) are not affected by E3 binding (Fig. 2A). These observations indicate that E3 binding does not preclude or detectably perturb the closed conformation of Ubc13-O~Ub.

E2~Ub species are highly dynamic.

To observe the resonances of the E2 and Ub moieties simultaneously, UbcH5c-O~Ub and Ubc13-O~Ub conjugates were generated using ^{15}N-labeled E2 and ^{15}N-labeled Ub. The ^{1}H, ^{15}N-HSQC-TROSY spectra of the resulting species display two classes of resonances distinguished by sharper peaks with higher intensities or broader peaks with lower intensities. NMR linewidths are a function of T_2 relaxation and therefore reflect the dynamics of individual groups

within a protein. An E2~Ub conjugate in which both proteins behave as a globular complex would be expected to display similar linewidths throughout the spectrum. In both UbcH5c-O~Ub and Ubc13-O~Ub, the sharper, more intense resonances arise from the 8.6 kDa Ub subunit (Figure 3A), consistent with Ub behaving as a flexibly tethered protein that is largely independent of the 17 kDa E2 to which it is conjugated.

T_1 and T_2 relaxation times were measured for UbcH5c, Ub, and UbcH5c-O~Ub (Figure 3B). Within the conjugate, T_1/T_2 ratios differed significantly between the UbcH5c and Ub moieties (average values: 26.3 and 14.7, respectively). Average T_1/T_2 values for free UbcH5c and Ub were measured to be 9.2 and 3.3, respectively. The lifetime of the Ubc13-O~Ub oxyester conjugate (half life at pH 7 and 25°C ~10 hours) did not allow for collection of high quality ^{15}N-T_1 and T_2 relaxation measurements. In summary, both observed linewidths and ^{15}N relaxation parameters indicate that the Ub moieties within the UbcH5-O~Ub and Ubc13-O~Ub conjugates behave as highly flexible entities independent of the E2s to which they are attached.

Investigation of the solution conformations of E2~Ub: use of spin-labeled Ub.

While the asymmetric CSPs observed for UbcH5c-O~Ub seem consistent with the dynamic behavior evidenced by the linewidths, the implied closed conformations for Ubc13-O~Ub based on CSPs seem contradictory to its dynamic behavior. The dynamics indicate that while Ubc13~Ub may populate a closed conformation that gives rise to the observed CSPs, this conformation must be in equilibrium with others, on a timescale that is consistent with the sharper linewidths for Ub. Exploiting the lack of cysteines in wild-type Ub, site-specific cysteine mutations were used to incorporate a thiol-reactive paramagnetic nitroxide probe into Ub at positions 11 (K11SL), 39 (D39SL), 48 (K48SL), and 63 (K63SL). A spin label accelerates

the T_2 relaxation rate of nearby nuclei, resulting in broadening of linewidths in an HSQC-type NMR spectrum, referred to as the paramagnetic relaxation effect (PRE). The large magnitude of the paramagnetic effect provides sufficient sensitivity to allow for the observation of structures that are either transient or lowly populated, making it an excellent approach for studying the dynamic E2~Ub species.

PRE experiments recapitulate the UbcH5c – Ub non-covalent complex.

Our intention was to observe line broadening effects of spin-labeled Ub on an E2 to which it is conjugated. In light of the dynamic behavior described above, we first sought to ascertain whether broadening effects are detectable in a short-lived, transient species. We used a previously characterized low-affinity (non-covalent) complex formed between wild-type UbcH5c and Ub as a test case (PDB ID 2FUH[15]). Ub-K48SL (1 molar eq.) was added to ^{15}N-UbcH5c and HSQC-TROSY spectra were collected in the absence ("active") and presence ("reduced") of ascorbate. Peak intensities were measured in both spectra and the ratios of active/reduced intensities were used as indicators for residues in close proximity to the paramagnetic probe. A majority of UbcH5c resonances exhibit a ratio close to 1.0, indicating that these resonances are not affected by the spin label and confirming that there are no non-specific interactions between the spin label and the E2. The strongest effect is observed for UbcH5 residue G27, as this resonance is undetectable in the "active" spectrum. Residues that were significantly affected by the spin label were identified as those with ratios differing from the mean by more than one standard deviation. When mapped onto the 3-dimensional structure, the affected residues define a surface that coincides with what is expected based on the solution structure solved on the basis of observed NOEs (Figure 4A, Table S3)[15].

Investigation of E2~Ub Conformations: E2~UbSL experiments indicate a range of conformations within the conjugate.

HSQC-TROSY spectra were collected for active and ascorbate-reduced ^{15}N-UbcH5c-O~UbSL (with the S22R mutation) and ^{15}N-Ubc13-O~UbSL for each spin label position in Ub (residues 11, 39, 48, and 63). Spectra in which one molar equivalent of each UbSL was added but not conjugated to ^{15}N-UbcH5c/Ubc13 were also collected as controls for potential inter-molecular spin label effects. In general, the E2 + Ub-SL spectra showed no spin label-affected peaks, with the exception of small effects observed on the "backside" of UbcH5c in the K48SL and K11SL cases, most likely a result of some residual non-covalent interaction with Ub despite the S22R mutation (see Experimental Procedures). These small backside effects were also observed in UbcH5c-O~Ub experiments (Figure 5). Several lines of evidence confirm that the modification of Ub with TEMPO does not alter its structural or functional properties. First, Ub-K11SL functions equivalent to wild-type Ub in an *in vitro* ubiquitination assay with UbcH5c and BRCA1/BARD1 (Figure S1). Second, spectral overlays of reduced PRE experiments at all spin label positions show no significant differences in the E2 spectra (Figure S2).

Results for the four spin label positions in the UbcH5c-O~Ub and Ubc13-O~Ub conjugates are summarized in Table 1, and residue-level histograms of intensity ratios for each species are included as Figure S4. In every spectral pair, the measured intensity ratios averaged over all E2 resonances is close to 1.0, confirming a lack of non-specific intensity loss that might be expected to affect random surface residues to some extent. The average measured intensity ratios over all data sets is 0.98 for both E2s, indicating that the samples and spectra were well-matched and providing high confidence in the intensities measured. Of the four Ub spin label

positions, K48 gives the strongest PRE in the context of UbcH5c-O~Ub, with a lowest intensity ratio of 0.2 for residues E122 and R131, while labels at Ub positions K11 and D39 give the strongest effects in the context of Ubc13-O~Ub, with lowest ratios of 0.25 for Ubc13 residues I108 and K82, A122, respectively (Table 1). Of particular note is the clear difference in the K63 position, which shows no significant effects in the context of UbcH5c-O~Ub but strong effects (lowest ratio is 0.1) in Ubc13-O~Ub. Given the concurrence among all the E2-O~Ub PRE data sets, we chose to use a global threshold of 0.7 as the intensity ratio below which significance was assigned (i.e., an intensity loss greater than 30% of a peak's original intensity). (Table S3).

Comparison of E2~Ub conjugates.

Each of the four spin label positions in the context of UbcH5c-O~Ub affect a unique set of resonances. Affected UbcH5 residues reside in the crossover helix, the active site and C-terminal helices, and Loop 6. No single orientation of Ub relative to UbcH5 can satisfy all the observations, consistent with the flexible nature of the conjugate. To satisfy all the PRE effects, the conjugated Ub moiety must swing *via* its flexible C-terminal residues from closed conformations in which it approaches the E2 crossover helix, through extended conformations in which it resides below the active site and C-terminal helices, and up to Loops 5 and 6 in "backbent" conformations (Figure 5, left). Considering the two sequential glycines at the Ub C-terminus, remarkably little "twisting" of ubiquitin's C-terminal tail is required to move among these radically different conformations. Like the UbcH5c-O~Ub conjugate, no single Ubc13-O~Ub conformation can satisfy all of the PRE-affected surfaces. Together, the four spin label positions suggest a similar Ub trajectory as in the UbcH5c-O~Ub conjugate, except that the Ub moiety must twist to enable its hydrophobic I44 surface to face the two sides of the E2, as

indicated by the K48SL effect observed on both the C-terminal helices and the β-sheet (Figure 5, right).

Small angle X-ray scattering (SAXS) of the E2~Ub conjugates confirms NMR-based models.

SAXS curves were collected on samples of UbcH5c, His_6-Ubc13, UbcH5c-O~Ub, and His_6-Ubc13-O~Ub at 25°C (Figure 6 A, B). No concentration-dependent effects or radiation damage was observed. Preliminary analysis of SAXS curves offers information on the shape (R_g) and size (D_{max}) of the sample proteins. The two free E2s give similar values for R_g and D_{max} that are consistent with monomeric E2s based on their known structures. UbcH5c-O~Ub and His_6-Ubc13-O~Ub also give similar values for R_g (23.0 Å and 23.7 Å, respectively) and D_{max} (70 Å and 75 Å, respectively). A D_{max} value of approximately 72 Å is predicted for the open conformation of Ubc13-O~Ub observed in the crystal structure (2GMI). Thus, the SAXS data indicate that extended conformations are populated in solution both by Ubc13~Ub and UbcH5c~Ub.

We reasoned the five atomic-level structures of E2~Ub species (or their mimics) available in the PDB may represent a sampling of the allowable conformations available to E2~Ubs. Therefore, the structures were used as a basis set for further analysis of the SAXS data. Theoretical scattering curves were generated for each of the five E2~Ub structures using the programs CRYSOL and OLIGOMER for comparison with the measured curves for UbcH5c-O~Ub and Ubc13-O~Ub (Figure S5). Not surprisingly, no single structure produced a theoretical scattering curve that fits the experimental data (Figure S6A). Furthermore, no linear combination of 2, 3, 4, or 5 conformations chosen from a pool of existing E2~Ub structures could recapitulate the experimental curves (OLIGOMER; Figure 6 A, B). Among all possible

combinations, conformations from the 2KJH and 1FXT structures fit the UbcH5c~Ub experimental data with χ^2=5.45, while conformations of the Ubc13~Ub conjugate from the 3JW0 and 1FXT structures fit the data with χ^2=3.87 (Figure S6B). Flexible systems such as the E2~Ub conjugate, however, likely populate a continuum of conformations that may differ from existing solved structures.

To better account for the flexibility of the E2~Ub conjugate, an ensemble optimization method (RanCh/GAJOE) was used to search for a minimal ensemble of UbcH5c~Ub orientations that recapitulate the experimental data. Our initial analysis of UbcH5c-O~Ub was based upon a 20-member ensemble (generated from a pool of 10,000 random conformations; see Experimental Methods) and included Ub orientations ranging from a closed state in which Ub is proximal to the E2 crossover helix, to an extended or open state in which Ub hangs below the E2 active site and C-terminal helices, to a backbent state in which Ub has swung to the opposite face of the E2 and is proximal to Loops 5 and 6 (χ^2 value of 2.26; Figure 6A). The ensemble shows a slight preference for extended E2~Ub conformations, consistent with the weak CSPs observed in Ub upon conjugation to UbcH5c.

In contrast to the UbcH5~Ub ensemble, a 20-member Ubc13~Ub ensemble contains more conformers that represent a closed conformation with additional conformations that include the extended state and a weakly populated conformation placing Ub near the surface of Ubc13 that also binds Mms2 (χ^2 value of 2.75), see Figure 6 B. The highly populated closed state observed in the SAXS ensemble coincides with the CSPs observed upon Ubc13~Ub conjugation.

In both cases, the ensembles of 20 E2~Ub models represent one possible set of conformations that fit the data and fine structural details should be analyzed in that light. Repeating the calculations to obtain additional ensembles, however, resulted in similar trends for

both the pattern and density of E2~Ub orientations, with associated χ^2 values remaining consistent in each case (Figure S6C). Furthermore, calculated ensembles comprised of fewer models yielded similar trends in E2~Ub conformations and comparable χ^2 values (Figure S6D and E). Ensembles comprised of fewer than five structures were unable to satisfy both the pattern and density of E2~Ub models observed in larger ensembles and, as a result, yielded poorer χ^2 values. Although there is little statistical difference between ensembles containing five or twenty models, we believe that a twenty-member ensemble better reflects properties of an E2~Ub species as it reveals lowly-populated conformations.

Discussion

E2~Ub species are essential components of the multi-protein complex required for the transfer of Ub to substrates. Several recent crystal structures and static NMR-based models have significantly increased the structural information available, but the solution-state behavior of E2~Ubs reported here and previously by other groups[22,23] suggest that such structures provide a snapshot of what is a conformationally dynamic species. Here we present a more comprehensive description of the conjugate forms of two human E2s, UbcH5c and Ubc13, and find distinct differences between the two closely related E2s.

The NMR spectral features of both UbcH5c~Ub and Ubc13~Ub are consistent with flexibly linked domains, as indicated by linewidth analysis and ^{15}N relaxation data. Chemical shift perturbations, paramagnetic relaxation enhancement, and small angle X-ray scattering identify distinct features of the two E2~Ub species. Despite the strong CSPs observed in Ubc13 and Ub upon conjugation, analyses of linewidth, PRE, and SAXS data indicate a flexible species that inhabits multiple E2~Ub conformations. Chemical shift perturbations suggest that the

preferred state of the flexibly linked Ub is folded up towards the crossover helix of Ubc13, in what we call the closed conformer. Notably, the Ub swings "backwards" toward loop 4 and β-strand 4 of Ubc13 more rarely than it swings up into the closed conformation, based upon SAXS and CSP data. This is in contrast to UbcH5c~Ub, which appears to prefer a more open state, based on analysis of SAXS data and the general lack of Ub CSPs upon activation. Another notable difference is in Ub's C-terminus: PRE data indicate that the I44 hydrophobic face of Ub approaches both the front and back of Ubc13, implying that a twist in the Ub C-terminus must occur, whereas there is no evidence that the UbcH5c~Ub conjugate undergoes such a pronounced twist.

Currently, there are two deposited crystal structures of UbcH5~Ub. In one structure (PDB 3A33), the conjugated Ub is in a conformation similar to the backbent orientation included in the UbcH5c~Ub ensemble[6]. The other is a structure of a complex formed between UbcH5b~Ub and the HECT-type E3, Nedd4L[7]. In this case, the conjugated Ub is in an extended-twisted conformation that places Ub residue D39 near UbcH5 Loop 8, a state that is also included in the UbcH5c~Ub ensemble. These structures suggest how additional binding interactions may select a particular E2~Ub conformation from among manifold possibilities.

The conjugation-induced CSPs in human Ubc13 agree with a previous report[24], although our complete ^{15}N-^{1}H assignments afford a more detailed view of the Ubc13~Ub species. An extended state of Ubc13~Ub as observed in the crystal structure (PDB 2GMI) is represented among the conformations in the solution ensemble. The presence of Ubc13 binding partner, Mms2, which can interact with a Ub moiety from another Ubc13~Ub conjugate, may shift the equilibrium towards the extended state seen in the crystal. It is beyond the technical scope of the present study to characterize the conjugated Ubc13/Mms2 heterodimer in solution, so we cannot

comment further on the effects of Mms2 binding. Overall, our results indicate that Ubc13~Ub populates a closed state with highest frequency. Furthermore, our NMR data indicate that binding of the RING E3, BRCA1/BARD1 to Ubc13~Ub does not preclude the closed state observed in the ensemble.

There are a growing number of reports of proteins that selectively recognize E2~Ub conjugates, but not the free protein components. To date, three proteins have been identified that specifically bind an E2~Ub conjugate: bacterial E3 ligase SspH2 (binds UbcH5c~Ub)[23], bacterial effector protein OspG (binds UbcH5b~Ub)[25], and nuclear import protein importin-11 (binds UbcM2~Ub)[26]. Ub and E2 enzymes individually contain a number of potential binding sites; conjugation of the two proteins creates new combinatorial possibilities that may create unique binding modes. Based on the two crystal structures available, it appears that (at least in these cases) interacting proteins make use of available E2~Ub orientations in their modes of binding. Multiple conformations assumed by the E2~Ub conjugate allow for diverse binding modes. Such flexibility allows the E2~Ub conjugate to participate in a variety of complexes, ultimately resulting in diverse biological roles. Commonalities among E2~Ub structures might be related to common binding partners. For example, neither the Ubc13~Ub model nor the UbcH5c~Ub model place Ub in an orientation that is likely to interfere with binding to a RING E3. On the other hand, differences in E2~Ub structures could be linked to differences in binding partners, including non-canonical E3 ligases. As a result, studying molecular interactions with the free E2 may not directly translate to the E2~Ub conjugate.

Despite the technical challenges posed, it is clear that studying the active, conjugated form of E2 Ub-conjugating enzymes can provide insights not readily apparent from the structures of isolated E2s. Understanding the combinatorial effect of E2 and Ub binding sites

and the E2-specific conformational ensembles will be key to deciphering the E2 protein interactome. The NMR-based spin labeling approach described herein will be generally applicable to the study of other E2~Ub conjugates as well as to E2~Ub species in complex with interacting proteins, including E3 ligases.

Experimental Procedures

Plasmids, Protein Expression, and Purification. N-terminal His_6-tagged Ubc13 was expressed from the pET24 vector. UbcH5c was expressed from the pET28N vector. UbcH5c and BRCA1_1-112/BARD1_25-139 were purified as previously described[14]. Proteins were expressed in *E. coli* (BL21 star DE3 cells) at 37°C, and induced with 1mM IPTG for four hours, or at 16°C induced with 200 μM IPTG for 18 hours. His_6-Ubc13 was purified using a Ni^{2+} affinity column, followed by size exclusion chromatography on SDX75 resin in 25 mM sodium phosphate, 150 mM NaCl buffer at pH 7.0, the buffer used for all NMR experiments.

Spin Label Modification. Four mutant forms of Ub were generated using site-directed mutagenesis (K11C, D39C, K48C, K63C) to incorporate a cysteine for chemical modification with the thiol-reactive relaxation probe 4-(2-Iodoacetamido)-TEMPO (Sigma-Aldrich) to form a covalently-linked, non-transferable adduct. Reactions between TEMPO and each cysteine mutant of Ub were performed at 25°C overnight in a 1:5 Ub:TEMPO molar ratio. Reaction yields were quantified by MALDI-MS; in all cases the reaction went essentially to completion (>95%). Unreacted TEMPO was removed by dialysis prior to the conjugation reaction. Paramagnetic activity was confirmed by incorporating a spin label into ^{15}N-Ub K63C and collecting HSQC spectra before and after reducing the nitroxide probe with ascorbate.

Comparison of the ^{15}N-Ub K63SL ascorbate-reduced spectrum with wildtype Ub showed little spectral perturbation associated with the cysteine mutation and subsequent modification with the spin label.

Formation of the E2~Ub conjugate. To characterize the conjugated forms of the E2s UbcH5c and Ubc13, we used an active site Cys-to-Ser mutation (C85S in UbcH5; C87S in Ubc13) to generate an oxyester between the C-terminus of Ub and the E2. The resulting bond is only one atom different than the wildtype thioester and significantly more stable. All structural work described in this study utilized the active site Cys-to-Ser mutation; the conjugates formed with these E2s are denoted as E2-O~Ub. NMR studies of the UbcH5c-O~Ub conjugate were performed in the context of the S22R mutation to prevent non-covalent Ub binding[15]. ^{15}N E2-O~Ub oxyester conjugates were generated by reaction of 5-10 μM E1, 600 μM TEMPO-modified or wildtype Ub, 300 μM ^{15}N E2s (^{15}N C85S-S22R-UbcH5c or ^{15}N C87S-Ubc13), 5 mM $MgCl_2$, and 2.5 mM ATP at 30°C for 3 to 6 hours. E2-O~Ub conjugates were purified from unreacted material by gel filtration on SDX75 resin and homogeneity of the E2-O~Ub species was confirmed by SDS-PAGE. 2D (^{1}H, ^{15}N)-TROSY-HSQC spectra were collected on samples containing 150 μM E2~Ub before and after reduction of the paramagnetic probe with 5 molar equivalents of ascorbate.

NMR Spectroscopy. Chemical shift perturbation and paramagnetic relaxation enhancement (PRE) data were collected at 25ºC on a Bruker 500 MHz AVANCE II NMR spectrometer (University of Washington). Relaxation data were collected at 25ºC on a Varian 600 MHz INOVA NMR spectrometer (Pacific Northwest National Labs). Data processing and analysis

were performed using NMRPipe[16] and NMRView[17]. Peak intensities were measured in NMRView and intensity ratios for individual NH peaks in the active and ascorbate-reduced spectra (I/I_{red}) were calculated. Spin label-affected E2 resonances were identified as those with a peak intensity ratio below 0.70. In general, this cutoff was approximately one standard deviation from the mean. Chemical shift perturbations observed by 2D TROSY-HSQC NMR were quantified in ppm with the equation $\Delta\delta_j=((\Delta\delta_j{}^{15}N/5)^2+(\Delta\delta_j{}^{1}H)^2)^{1/2}$.

Small Angle X-ray Scattering. SAXS data were collected at the Stanford Synchrotron Radiation Lightsource beamline 4-2. Data were collected for UbcH5c, UbcH5c~Ub, and His_6-Ubc13~Ub at 10, 5, and 0.5 mg/mL concentrations in 25mM sodium phosphate, 150mM NaCl, 2mM DTT (free radical scavenger), pH 7.0 at 25˚C. Data on His_6-Ubc13 was collected at 7, 5, and 0.5 mg/mL in the same buffer without DTT. Initial data subtraction and averaging was performed with SSRL in-house software and confirmed using PRIMUS[18]. R_g values calculated from the Guinier plot, the Porod plot, and the P(r) function were all consistent. The P(r) functions were calculated using GNOM[19] and theoretical scattering profiles of published structures were calculated using CRYSOL[20] and OLIGOMER[18]. Existing E2~Ub structures were substituted with the appropriate E2 structure prior to calculation of the theoretical scattering profile. Flexibility analysis using the ensemble optimization method (EOM)[21] was performed using RanCh to create a pool of 10,000 random E2~Ub conformations based upon flexibility in Ub residues 72-76. The GAJOE genetic algorithm was used as described previously to select an ensemble of 20 conformations that, together, best fit the scattering data[21]. SAXS data for free His_6-Ubc13 was used to model a single conformation of the His_6-tag that is consistent with the

measured SAXS curve. The His-tag model was then used to represent the Ubc13 component within the His-Ubc13~Ub RanCh/GAJOE analysis.

References

1. Pickart, C. M. (2001) Mechanisms underlying ubiquitination. *Annu Rev Biochem 70*, 503-533.
2. Ye, Y. & Rape, M. (2009) Building ubiquitin chains: E2 enzymes at work. *Nat Rev Mol Cell Biol 10*, 755-764.
3. Eddins, M. J., Carlile, C. M., Gomez, K. M., Pickart, C. M., & Wolberger, C. (2006) Mms2-Ubc13 covalently bound to ubiquitin reveals the structural basis of linkage-specific polyubiquitin chain formation. *Nat Struct Mol Biol 13*, 915-920.
4. Hamilton, K. S., Ellison, M. J., Barber, K. R., Williams, R. S., Huzil, J. T., McKenna, S., Ptak, C., Glover, M., & Shaw, G. S. (2001) Structure of a conjugating enzyme-ubiquitin thiolester intermediate reveals a novel role for the ubiquitin tail. *Structure 9*, 897-904.
5. Serniwka, S. A. & Shaw, G. S. (2009) The structure of the UbcH8-ubiquitin complex shows a unique ubiquitin interaction site. *Biochemistry 48*, 12169-12179.
6. Sakata, E., Satoh, T., Yamamoto, S., Yamaguchi, Y., Yagi-Utsumi, M., Kurimoto, E., Tanaka, K., Wakatsuki, S., & Kato, K. (2010) Crystal structure of UbcH5b~ubiquitin intermediate: insight into the formation of the self-assembled E2~Ub conjugates. *Structure 18*, 138-147.
7. Kamadurai, H. B., Souphron, J., Scott, D. C., Duda, D. M., Miller, D. J., Stringer, D., Piper, R. C., & Schulman, B. A. (2009) Insights into ubiquitin transfer cascades from a structure of a UbcH5B~ubiquitin-HECT(NEDD4L) complex. *Mol Cell 36*, 1095-1102.
8. Ozkan, E., Yu, H., & Deisenhofer, J. (2005) Mechanistic insight into the allosteric activation of a ubiquitin-conjugating enzyme by RING-type ubiquitin ligases. *Proc Natl Acad Sci USA 102*, 18890-18895.
9. Huang, A., de Jong, R. N., Wienk, H., Winkler, G. S., Timmers, H. T. M., and Boelens, R. (2009) E2-c-Cbl recognition is necessary but not sufficient for ubiquitination activity. *J Mol Biol 385*, 507-519.
10. Siepmann, T. J., Bohnsack, R. N., Tokgöz, Z., Baboshina, O. V., & Haas, A. L. (2003) Protein interactions within the N-end rule ubiquitin ligation pathway. *J Biol Chem 278*, 9448-9457.
11. Haas, A. L. & Rose, I. A. (1982) The mechanism of ubiquitin activating enzyme. A kinetic and equilibrium analysis. *J Biol Chem 257*, 10329-10337.
12. Michelle, C., Vourc'h, P., Mignon, L., & Andres, C. R. (2009) What was the set of ubiquitin and ubiquitin-like conjugating enzymes in the eukaryote common ancestor?. *J Mol Evol 68*, 616-628.

13. Moraes, T. F., Edwards, R. A., McKenna, S., Pastushok, L., Xiao, W., Glover, J. N. M., & Ellison, M. J. (2001) Crystal structure of the human ubiquitin conjugating enzyme complex, hMms2-hUbc13. *Nat Struct Mol Biol 8*, 669-673.

14. Brzovic, P. S., Keeffe, J. R., Nishikawa, H., Miyamoto, K., Fox, 3rd, D., Fukuda, M., Ohta, T., & Klevit, R. (2003) Binding and recognition in the assembly of an active BRCA1/BARD1 ubiquitin-ligase complex. *Proc Natl Acad Sci USA 100*, 5646-5651.

15. Brzovic, P. S., Lissounov, A., Christensen, D. E., Hoyt, D. W., & Klevit, R. E. (2006) A UbcH5/ubiquitin noncovalent complex is required for processive BRCA1-directed ubiquitination. *Mol Cell 21*, 873-880.

16. Delaglio, F., Grzesiek, S., Vuister, G. W., Zhu, G., Pfeifer, J., & Bax, A. (1995) NMRPipe: a multidimensional spectral processing system based on UNIX pipes. *J Biomol NMR 6*, 277-293.

17. Johnson, B. A. & Blevins, R. A. (1994) NMR View: A computer program for the visualization and analysis of NMR data. *J Biomol NMR 4*, 603-614.

18. Konarev, P. V., Volkov, V. V., Sokolova, A. V., Koch, M. H. J., & Svergun, D. I. (2003) PRIMUS: a Windows PC-based system for small-angle scattering data analysis. *J Appl Crystallogr 36*, 1277-1282.

19. Svergun, D. I. (1992) Determination of the regularization parameter in indirect-transform methods using perceptual criteria. *J Appl Crystallogr 25*, 495-503.

20. Svergun, D., Barberato, C., & Koch, M. H. J. (1995) CRYSOL - a Program to Evaluate X-ray Solution Scattering of Biological Macromolecules from Atomic Coordinates. *J Appl Crystallogr 28*, 768-773.

21. Bernadó, P., Mylonas, E., Petoukhov, M. V., Blackledge, M., & Svergun, D. I. (2007) Structural Characterization of Flexible Proteins Using Small-Angle X-ray Scattering. *J Am Chem Soc 129*, 5656-5664.

22. Miura, T., Klaus, W., Gsell, B., Miyamoto, C., & Senn, H. (1999) Characterization of the binding interface between ubiquitin and class I human ubiquitin-conjugating enzyme 2b by multidimensional heteronuclear NMR spectroscopy in solution. *J Mol Biol 290*, 213-228.

23. Levin, I., Eakin, C., Blanc, M.-P., Klevit, R. E., Miller, S. I., & Brzovic, P. S. (2010) Identification of an unconventional E3 binding surface on the UbcH5 ~ Ub conjugate recognized by a pathogenic bacterial E3 ligase. *Proc Natl Acad Sci USA 107*, 2848-2853.

24. McKenna, S., Moraes, T., Pastushok, L., Ptak, C., Xiao, W., Spyracopoulos, L., & Ellison, M. J. (2003) An NMR-based model of the ubiquitin-bound human ubiquitin conjugation complex Mms2.Ubc13. The structural basis for lysine 63 chain catalysis. *J Biol Chem 278*, 13151-13158.

25. Kim, D. W., Lenzen, G., Page, A.-L., Legrain, P., Sansonetti, P. J., & Parsot, C. (2005) The Shigella flexneri effector OspG interferes with innate immune responses by targeting ubiquitin-conjugating enzymes. *Proc Natl Acad Sci USA 102*, 14046-14051.

26. Plafker, S. M., Plafker, K. S., Weissman, A. M., & Macara, I. G. (2004) Ubiquitin charging of human class III ubiquitin-conjugating enzymes triggers their nuclear import. *J Cell Biol 167*, 649-659.

Acknowledgements

We thank SSRL and PNNL for beam time and the use of magnets. Portions of this research were carried out at the Stanford Synchrotron Radiation Laboratory Beamline 4-2, a national user facility operated by Stanford University on behalf of the U.S. Department of Energy, Office of Basic Energy Sciences. The SSRL Structural Molecular Biology Program is supported by the Department of Energy, Office of Biological and Environmental Research, and by the National Institutes of Health, National Center for Research Resources, Biomedical Technology Program. A portion of the research was performed using EMSL, a national scientific user facility sponsored by the Department of Energy's Office of Biological and Environmental Research and located at Pacific Northwest National Laboratory. We gratefully acknowledge Walter Chazin and members of the Klevit lab for helpful discussions and critical reading of the manuscript.

UbcH5c-O~Ub	Ave. I/I_{red} Ratio	STDEV	Lowest I/I_{red} Ratio	Res. w/lowest I/I_{red} ratio	# of Significant Residues
K11SL	0.9	0.22	0.36	109	21
D39SL	0.9	0.22	0.38	84 and 87	23
K48SL	0.96	0.22	0.2	122 and 131	14
K63SL	1.14	0.12	0.86	94	0
Ubc13-O~Ub					
K11SL	0.93	0.16	0.25	108	8
D39SL	0.88	0.22	0.25	82, 122	18
K48SL	0.96	0.21	0.38	134	17
K63SL	1.13	0.2	0.1	149	4
UbcH5c+Ub					
K48SL	1.06	0.2	0.28	26	14

Table 1. Comparison of the spin label effects between UbcH5c-O~Ub, Ubc13-O~Ub, and UbcH5c + Ub.

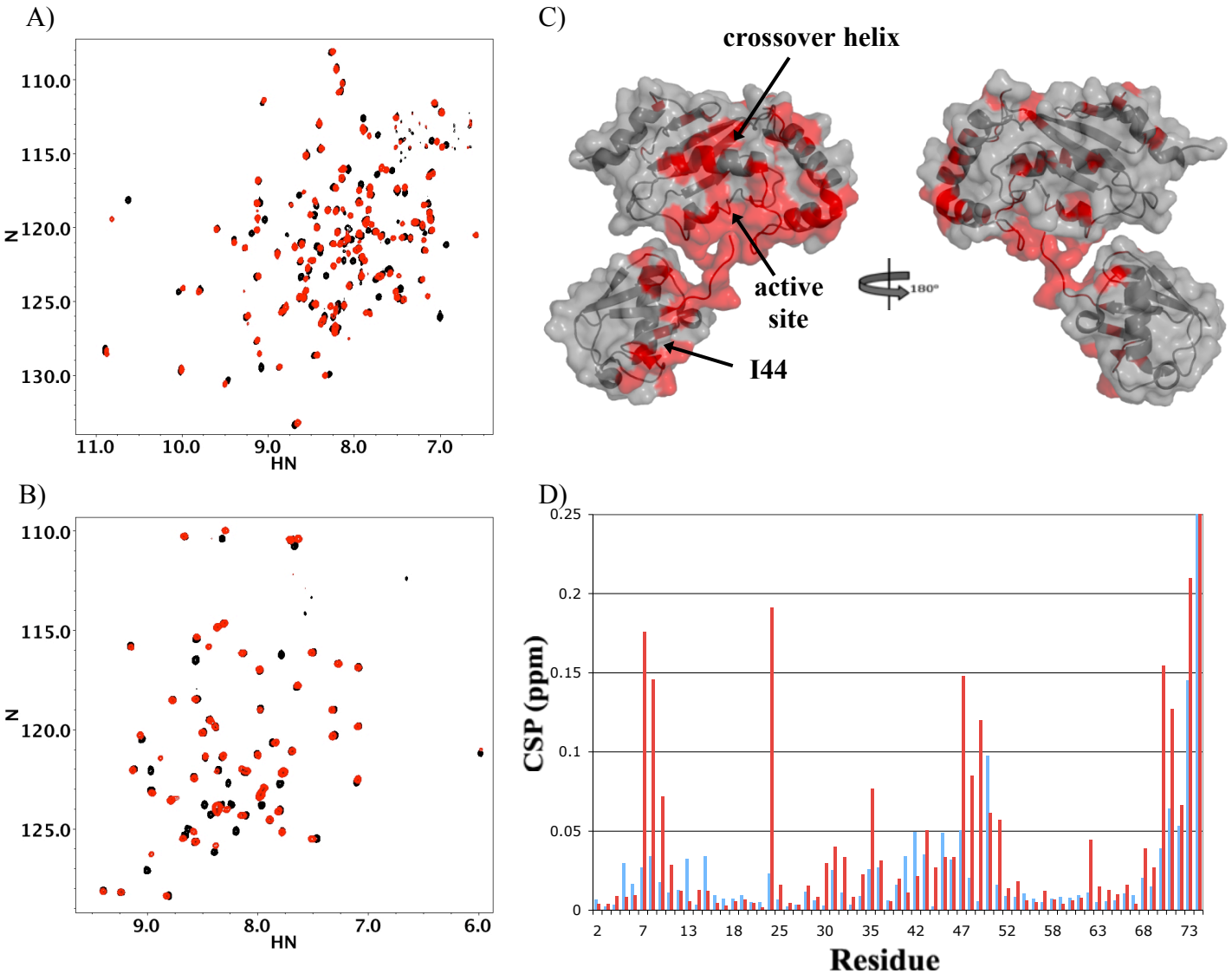

Figure 1. Spectral perturbations observed in Ubc13 and Ub upon formation of Ubc13-O~Ub conjugate. A) 2D HSQC-TROSY spectrum of ^{15}N-Ubc13 (black) is overlaid with spectrum of oxy-ester linked ^{15}N-Ubc13-O~Ub (red). **B)** 2D HSQC-TROSY spectrum of ^{15}N-Ub (black) is overlaid with ^{15}N-Ub~O-Ubc13 (red). **C)** Combined ^{1}H and ^{15}N chemical shift perturbations greater than 0.05 ppm are mapped in red onto the structure of conjugated Ubc13-O~Ub (PDB code 2GMI with human Ubc13 structure overlaid PDB code 1J7D). Perturbations reveal surfaces on both Ubc13 and Ub, suggestive of a protein-protein interaction in which the hydrophobic I44 surface of Ub rotates to meet the surface mapped on Ubc13. **D)** Histogram showing Ub CSPs upon activation to Ubc13 (red) and UbcH5c (blue). Comparison of the two profiles reveals differences in both the identity of affected residues and the degree to which they are perturbed.

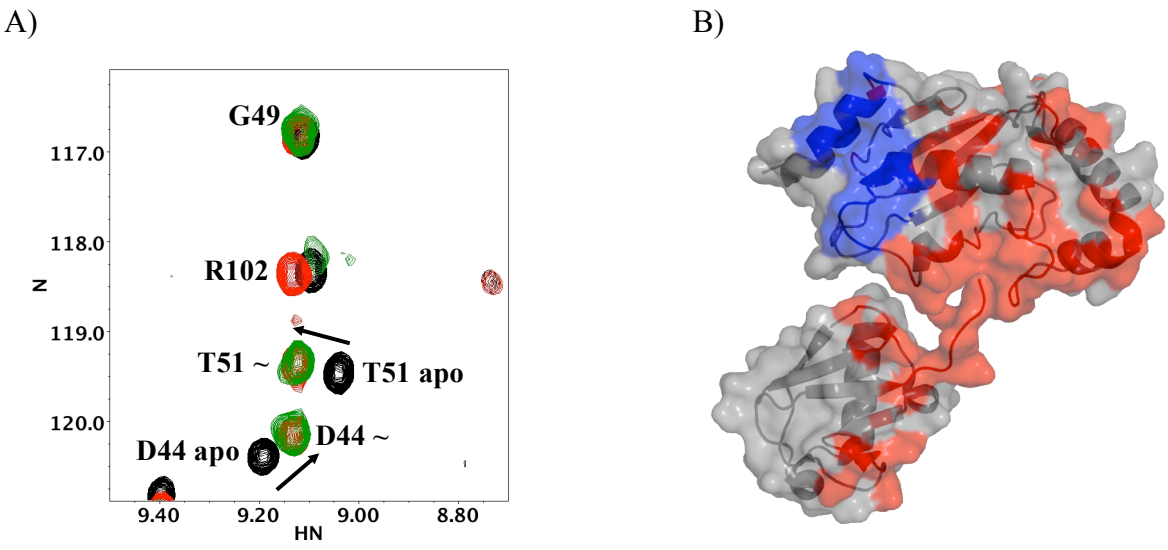

Figure 2. E3 binding does not disrupt the closed state. A) 2D HSQC-TROSY spectrum of ^{15}N-Ubc13 (black) is overlaid with ^{15}N-Ubc13-O~Ub (red) and with ^{15}N-Ubc13-O~Ub plus 1.1 mol. equiv. BRCA1 1-112/BARD1 1-114 RING domains (green). Ubc13 residues D44 and T51 which are perturbed upon conjugation with Ub are not affected by BRCA1 binding to the E2~Ub conjugate, indicating Ubc13~Ub can adopt the closed conformation even when bound to BRCA1. **B)** CSP greater than 0.05 ppm upon the addition of 1.1 equivalent RING E3 BRCA1/BARD1 are mapped in blue onto the structure of conjugated Ubc13~Ub (PDB code 2GMI with human Ubc13 structure overlaid PDB code 1J7D). CSPs upon conjugation to Ub as in Figure 1C are mapped in red.

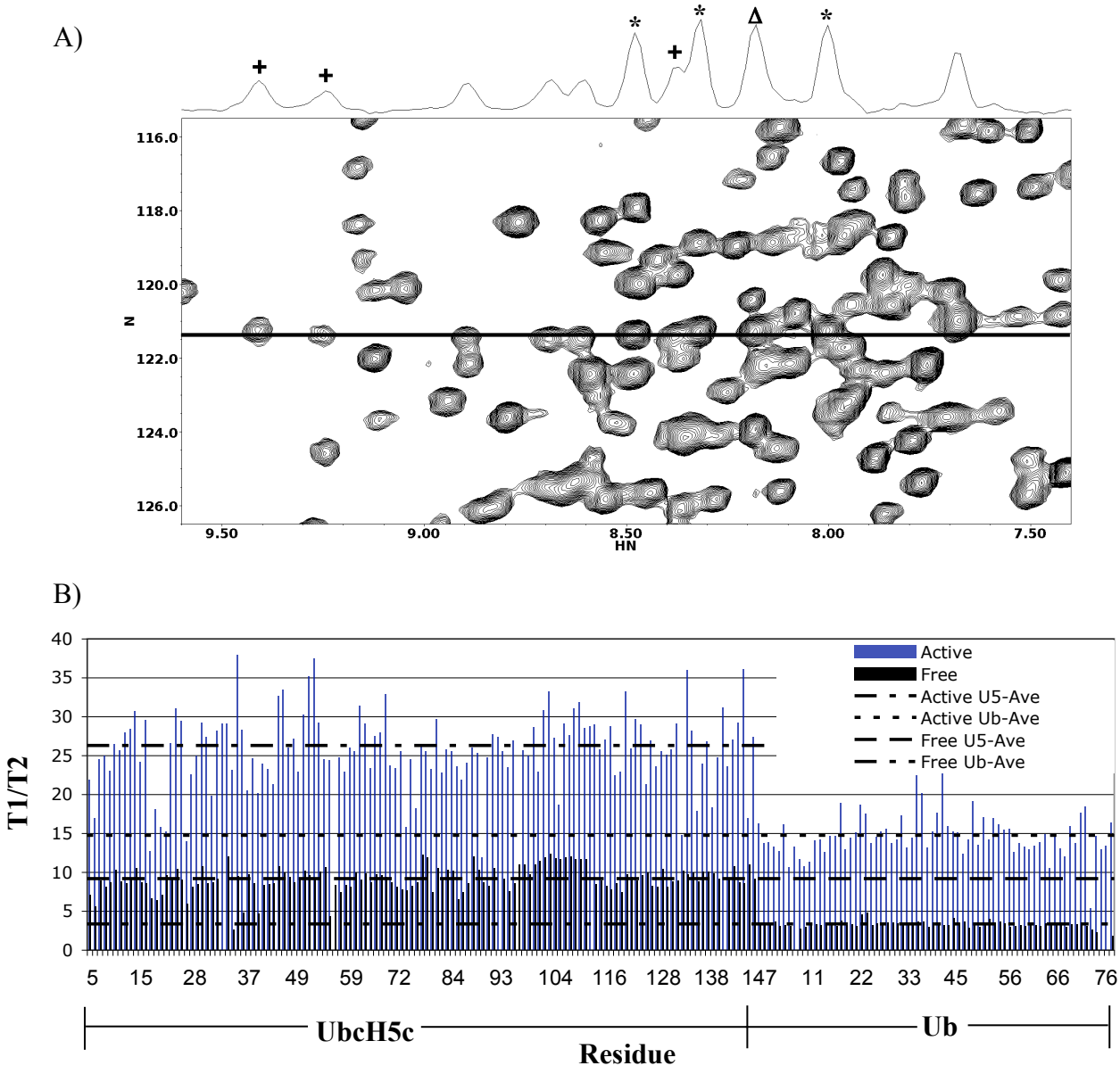

Figure 3. NMR resonance linewidths and intensities indicate that the E2~Ub conjugate is a dynamic species. A) 2D HSQC-TROSY spectrum of ^{15}N-Ubc13-O~^{15}N-Ub shows two classes of peaks based on intensity. In general, peaks that are sharper (more intense) arise from Ub residues, while the broader (weaker) peaks arise from Ubc13 residues. A 1D slice taken at the ^{15}N frequency denoted by the black horizontal line in the 2D spectrum illustrates the distinction between Ub (*) and Ubc13 (+) resonances. A limited number of more intense Ubc13 resonances are observed (Δ); these arise from residues in loops or near the C-terminus. Off-center peaks are not labeled. **B)** Histogram of T_1/T_2 values for UbcH5c and Ub residues in their conjugated (blue) and free (black) forms.

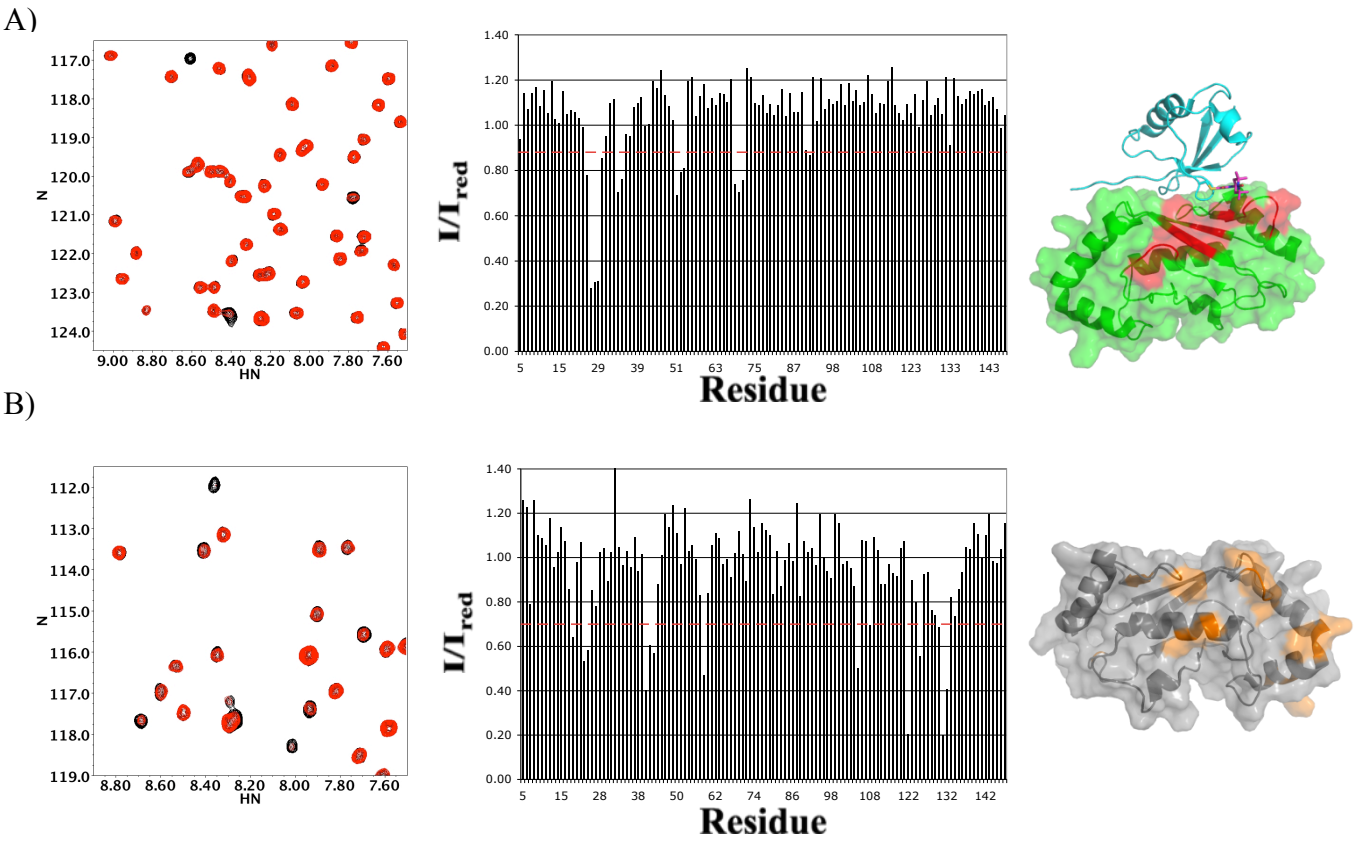

Figure 4. Paramagnetic Relaxation Enhancement data analysis. A) 2D HSQC-TROSY spectra were taken of ^{15}N-UbcH5c with 1 molar equiv. of Ub-K48SL before (red) and after reduction with ascorbate (black, left). Peak intensities were measured and plotted as ratios of I/I_{red} (center). Residues corresponding to intensity ratios lower than one standard deviation from the mean were mapped onto the 3-D structure (right). **B)** As in A) for the ^{15}N-UbcH5c-O~Ub-K48SL experiment.

A)

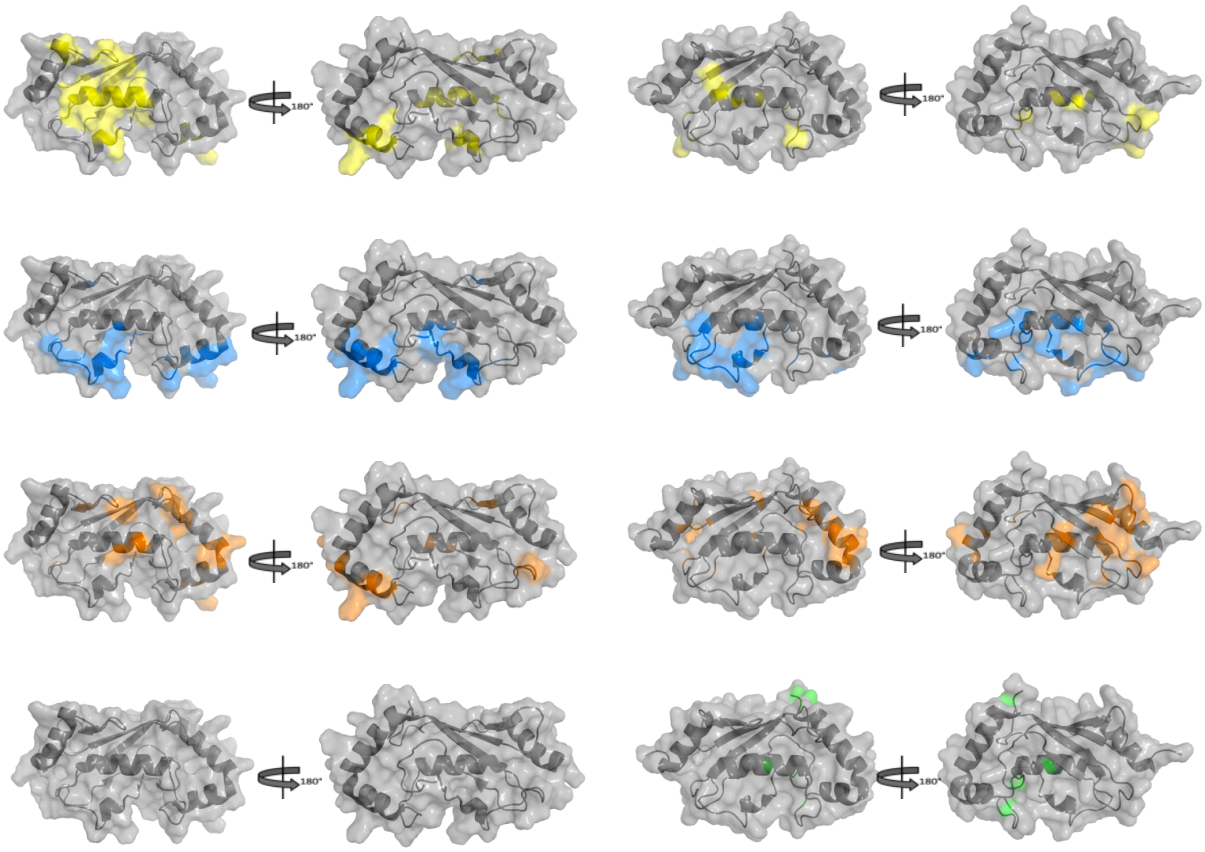

B)

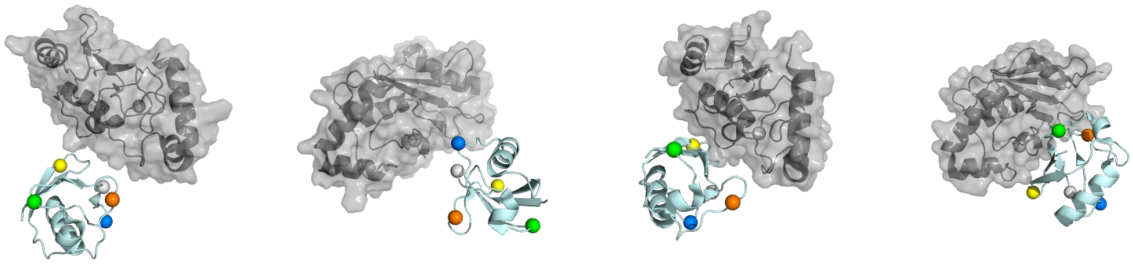

Figure 5. Observed PREs are specific to both spin label position and E2 identity. A) Highlighted residues in UbcH5c (2FUH, left) and Ubc13 (1J7D, right) are those whose resonances show PRE effects upon conjugation with Ub-SL at positions K11 (yellow), D39 (blue), K48 (orange), and K63 (green). Colored residues correspond to HSQC peaks with an I/I_{red} intensity ratio of ≤0.7. **B)** Illustrative extreme E2~Ub conformations. SL positions shown as colored spheres to match affected regions shown above, Ub core C-terminus and E2 active sites shown as gray spheres.

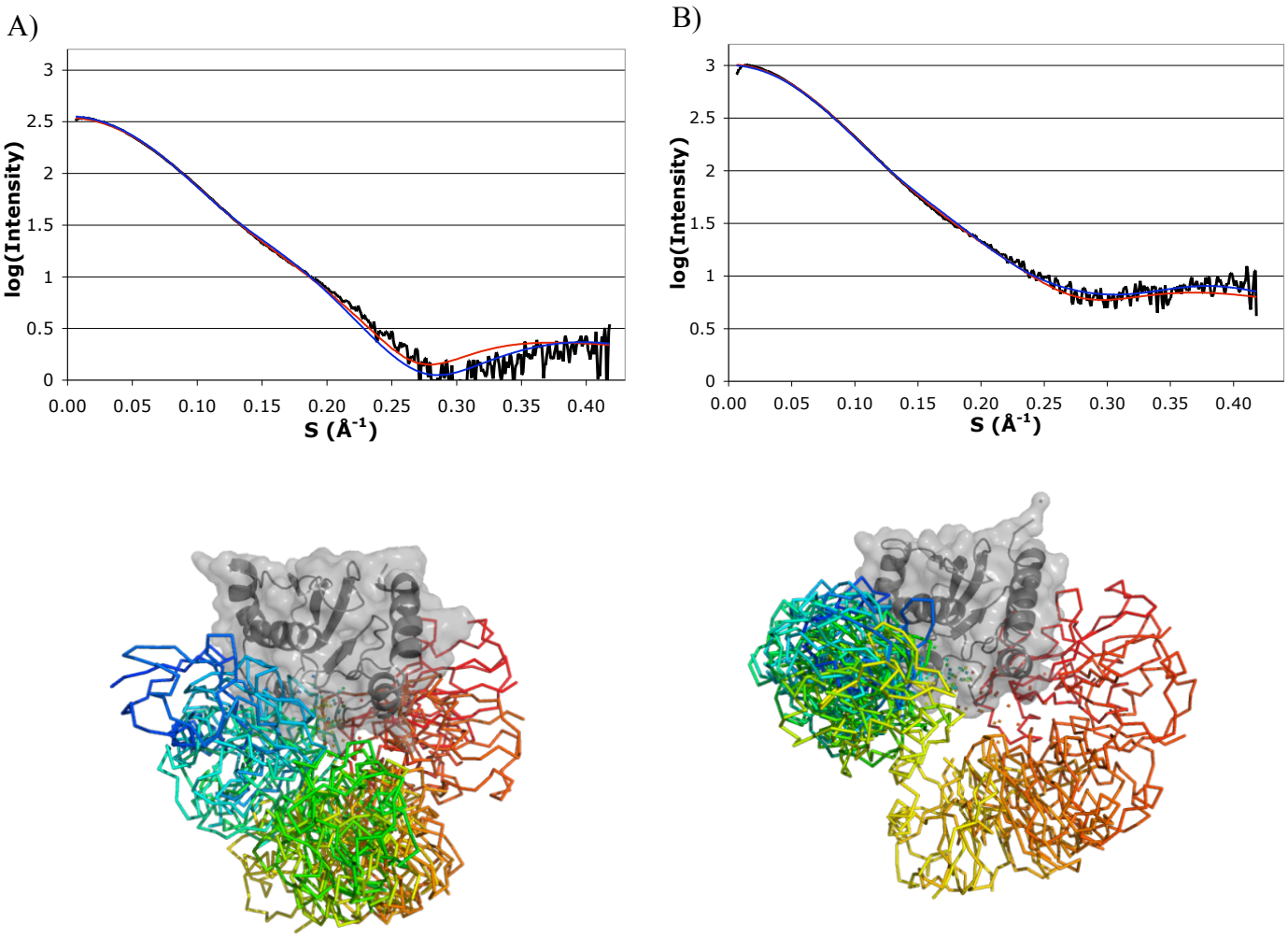

Figure 6. Analysis of SAXS curves reveals a range of E2~Ub conformations. A) Experimental SAXS data of the UbcH5c-O~Ub conjugate (upper, black) overlaid with calculated fits produced from OLIGOMER (blue, based on 5 published E2~Ub structures) and EOM (red; RanCh/GAJOE) analysis. Ensemble of 20 UbcH5c~Ub conformations produced by EOM analysis is shown (lower). **B)** As in A) for the Ubc13-O~Ub conjugate.

Ubc13 residue #	Free Ubc13 C=O chemical shift (ppm)	Conjugated Ubc13 C=O chemical shift (ppm)	Ubc13 residue #	Free Ubc13 C=O chemical shift (ppm)	Conjugated Ubc13 C=O chemical shift (ppm)	Ubc13 residue #	Free Ubc13 C=O chemical shift (ppm)	Conjugated Ubc13 C=O chemical shift (ppm)
8	180.4	180.3	50	173.6	173.6	92	178.9	178.6
9	181.5	181.4	51	172.1	172.1	93	176.8	176.6
10	180.7	180.6	52	170.2	170.2	94	177.9	177.8
11	183.4	184.0	53	172.7	172.8	95	175.0	175.2
12	183.3	183.3	54	176.8	176.8	96	177.2	177.0
13	175.5	175.5	55	173.5	173.5	98	175.8	175.6
14	182.8	182.8	56	172.7	172.7	99	181.7	181.6
15	180.5		57	171.1	171.1	100	171.5	171.6
16	180.9	180.9	58	173.4		101	178.3	178.4
17	181.7	181.7	60	177.9	177.9	102	182.1	182.3
18	180.2	180.3	61	180.6	180.6	103	177.1	177.3
20	179.3	179.3	62	179.0.	178.9	104	179.9	179.6
22	179.5	179.6	64	174.3	174.3	105	178.4	178.4
23	172.5	172.4	65	176.6	176.5	106	180.7	180.4
24	174.8	174.8	66	172.4	172.4	107	184.2	184.4
25	174.3	174.2	68	173.4	173.4	108	172.8	172.8
26	174.4	174.4	69	177.2	177.2	109	177.6	177.6
29	177.7	177.7	70	173.0	172.7	110	180.0	179.8
30	178.5	178.5	71	176.4	176.2	111	183.5	183.1
31	173.5	173.5	72	177.0	177.0	112	184.2	184.3
32		172.5	73	177.5	177.5	113	177.7	177.6
33	176.6	176.6	74	172.1	172.2	114	173.3	172.0
34	174.0	174.0	75	178.4	178.4	116	175.2	175.1
35	172.5	172.4	76	167.2		118	173.2	176.1
36	173.5	173.6	77	168.3	168.3	119	174.9	
37	175.2		79	175.7	176.6	122	177.1	177.7
38	174.3	174.2	80	169.5	169.0	126	174.8	175.1
39	175.3	175.3	81	174.8	176.2	127	181.4	181.1
40	174.8	174.8	82	181.4	181.1	128	183.0	181.7
41	181.5	181.5	83	179.6	179.8	130	179.8	
43	179.2	179.1	84	174.2	174.1	131	181.6	
44	176.7	176.5	85	174.4	174.2	132	174.5	174.4
45	173.1	173.0	88	170.3	167.9	133	172.4	172.5
47	173.3	173.1	89	177.8		134	178.6	178.6
48	175.3	175.2	90	184.1	184.3	135	185.2	185.2
49	177.5	177.5	91	171.2	171.0	136	180.2	180.2

Ubc13 residue #	Free Ubc13 C=O chemical shift (ppm)	Conjugated Ubc13 C=O chemical shift (ppm)
137	181.2	181.4
138	180.3	180.4
139	183.7	183.6
140	174.5	174.4
141	187.4	187.4
142	182.1	182.0
143	186.0	186.1
144	185.6	185.6
145	176.1	175.9
146	180.2	180.1
147	182.4	182.3
148	176.9	176.8
149	176.3	176.3
150	175.9	175.8
151	174.1	174.1
152	172.9	172.9

Table S1: HNCO assignments of free and conjugated Ubc13 carbonyl resonances (n-1 reported).

Ubc13~Ub CSP upon conjugation	
Ubc13	16, 23, 25, 32, 44-45, 51-52, 56, 71, 79-81, 87-89, 91, 93-94, 103, 106-107, 109, 112, 114-122, 126, 128, 130-132, 139, 141-142, 149, 151
Ub	7, 8, 10, 23, 35, 43, 47-51, 70-76
Ubc13 CSP upon BRCA1 binding	9-12, 14-15, 17-18, 68, 96-103

Table S2: List of all residues whose CSP > 0.05 ppm upon the indicated binding event.

UbcH5c	***Residues with spin label intensity ratios ≤0.7***
K11SL	16, 19-21, 23, 87-89, 97-98, 100-101, 103-109, 122-123, 125
D39SL	23, 81, 83-84, 86-90, 92-94, 96, 105, 116, 120, 122-126, 128-129
K48SL	20, 23-24, 41-43, 58, 105, 108, 122, 125, 130-132
K63SL	-
Ubc13	
K11SL	60, 64, 69, 81, 85, 102, 104, 108, 116
D39SL	64-66, 69, 81-82, 85, 88, 90, 93-100, 107-108, 122, 127
K48SL	11, 22, 30-32, 34, 44-45, 57, 60, 66, 70, 85, 133-135, 137
K63SL	81, 108, 122, 149
UbcH5c+Ub	***Residues perturbed by > 1 standard deviation from the mean***
K48SL	24, 26-30, 34-35, 51-53, 70-72

Table S3: List of all E2 residues affected by each spin label position on Ub in the E2~Ub species.

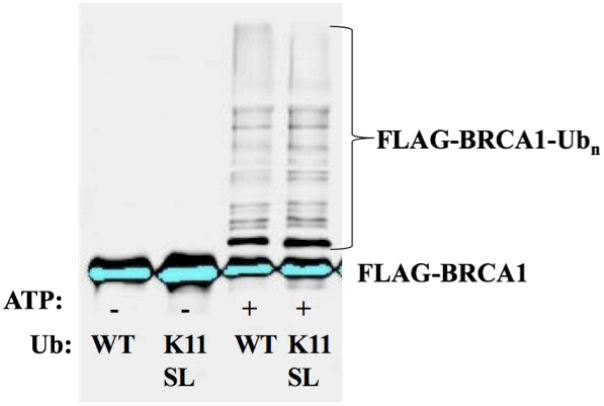

Figure S1. Spin-label modified Ub is active in transfer with UbcH5c and BRCA1/BARD1. Auto-ubiquitination assay of proxy substrate BRCA1 in the presence of wildtype Ub or Ub spin label-modified at residue 11, as followed by a western blot of FLAG-BRCA 1-304, confirms that the spin label does not interfere with the native function of Ub.

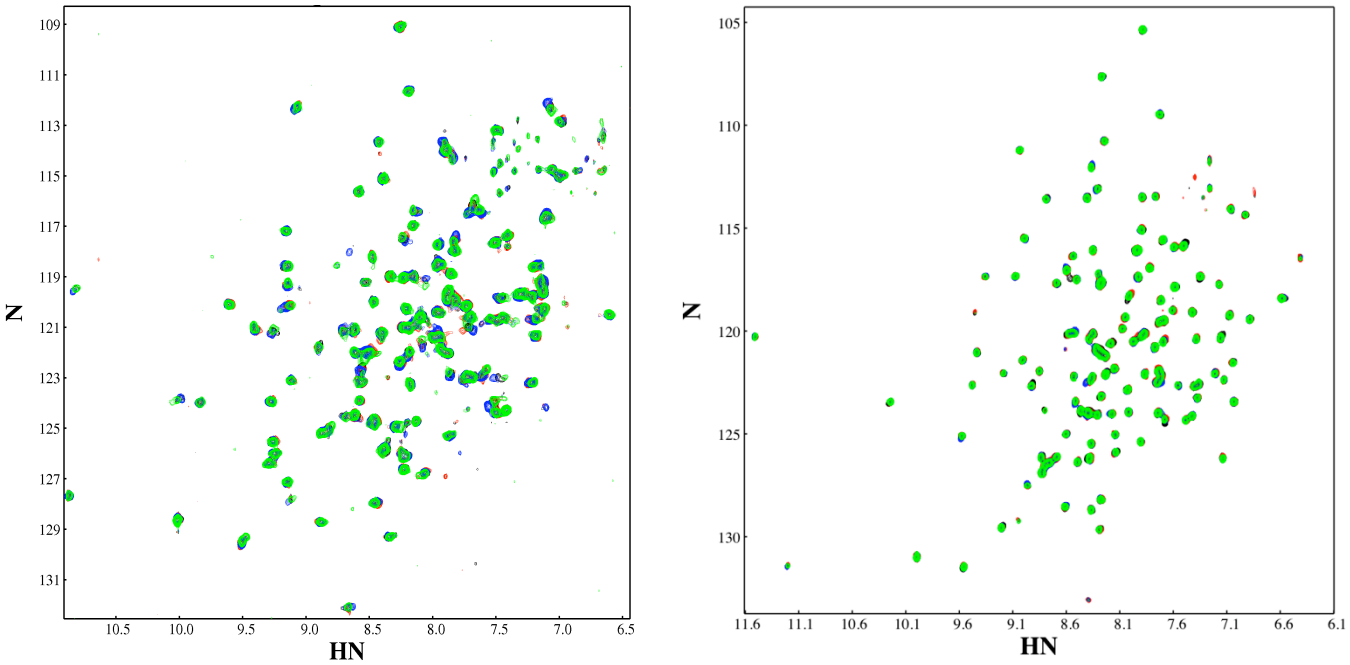

Figure S2. 2D HSQC-TROSY spectra of ^{15}N-Ubc13-O~Ub (left) and ^{15}N-UbcH5c-O~Ub (right). To assess presence of non-native interactions in the presence of spin labeled Ub, ^{15}N-E2~Ub spectra with each of the four spin labeled positions were overlaid. If the spin labels were inducing non-native protein interactions, one would expect these spectra to be significantly different from each other.

A)

```
UbcH5c,        4 KRINKELSDLARDPPAQCSAGPVGDDMFHWQATIMGPNDSPYQGGVFFLTIHFPTDYPFK
Ubc13,         6 RRIIKETQRLLAEPVPGIKAEPDESNARYFHVVIAGPQDSPFEGGTFKLELFLPEEYPMA
                  ** **   *   *     * *           * ** ***  ** * *    *  **

UbcH5c,       64 PPKVAFTTRIYHPNINSNGSICLDILRSQWSPALTISKVLLSICSLLCDPNPDDPLVPEI
Ubc13,        66 APKVRFMTKIYHPNVDKLGRICLDILKDKWSPALQIRTVLLSIQALLSAPNPDDPLANDV
                  *** * * *****    * ******   ***** *  *****  **  *******

UbcH5c,      124 ARIYKTDRDKYNRISREWTQKYAM
Ubc13,       126 AEQWKTNEAQAIETARAWTRLYAM
                  *   **         * **  ***
```

B)

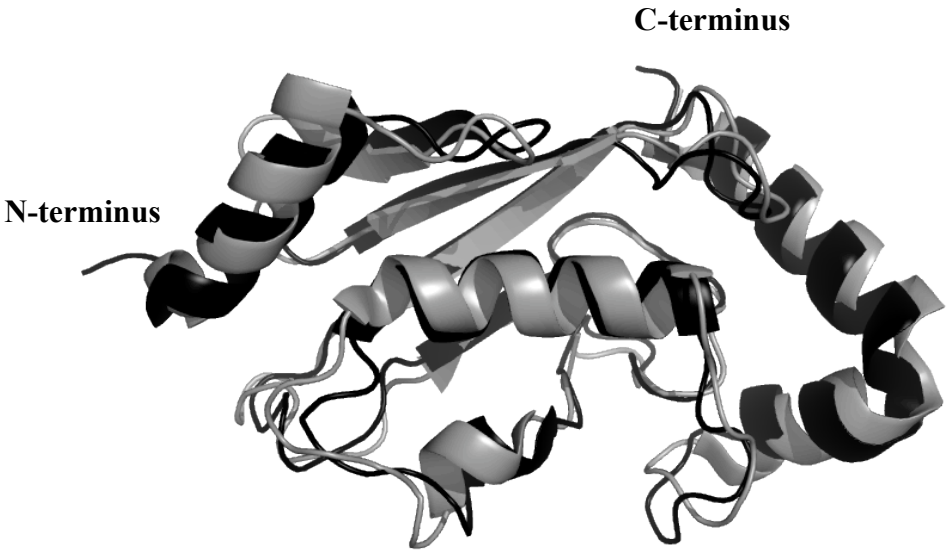

Figure S3. UbcH5c and Ubc13 are highly related human E2s, with similar sequences and structures. A) Sequence alignment of UbcH5c and Ubc13 with 45.6% identity and 61% similarity by residue. Structural alignment of UbcH5c (grey; PDB ID 2FUH) and Ubc13 (black; PDB ID 1J7D) with an RMSD of 1.97Å.

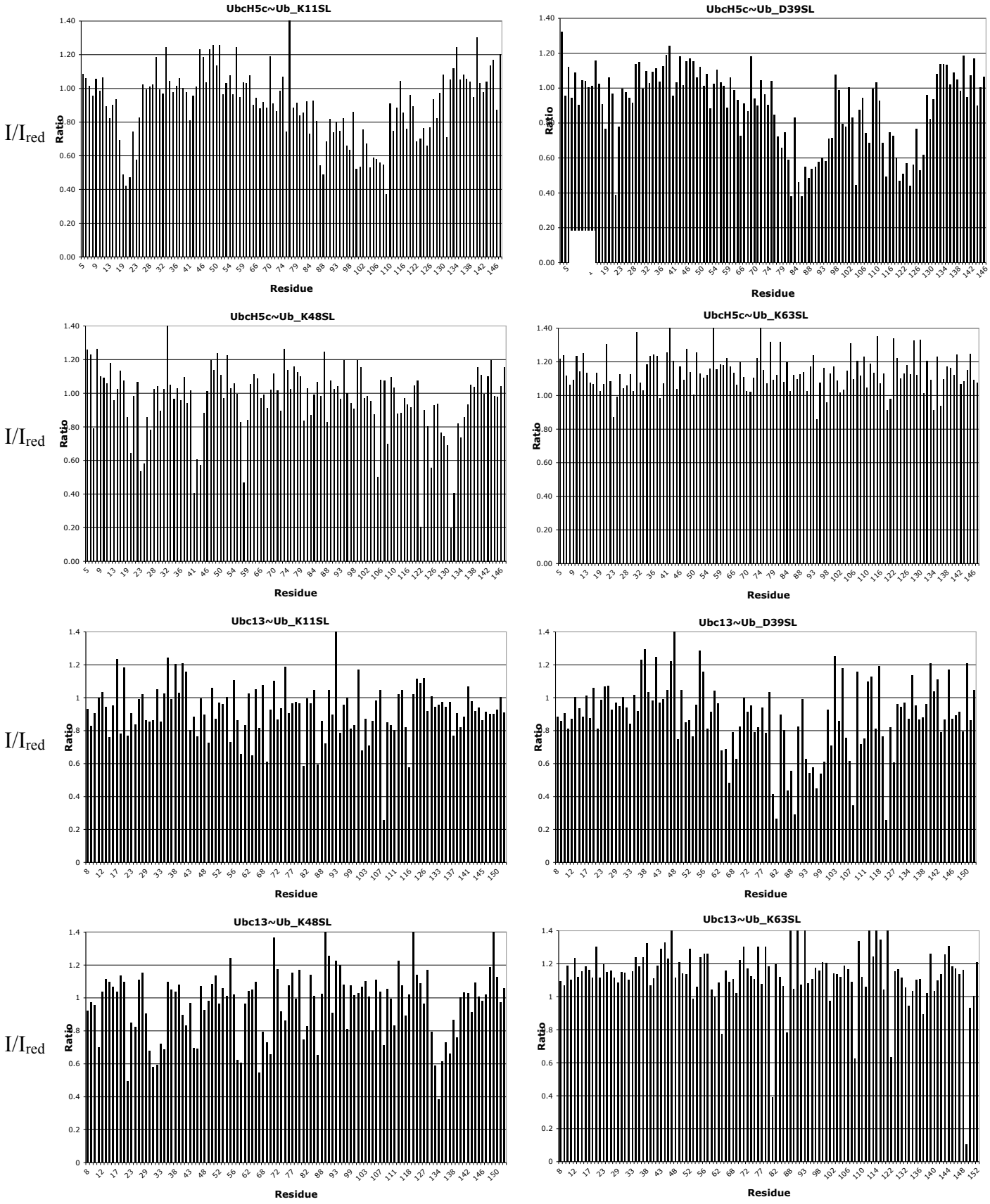

Figure S4. Histogram representation of the intensity ratios (I/I_{red}) of ^{15}N-E2~Ub as affected by the presence of a spin label on the conjugated Ub.

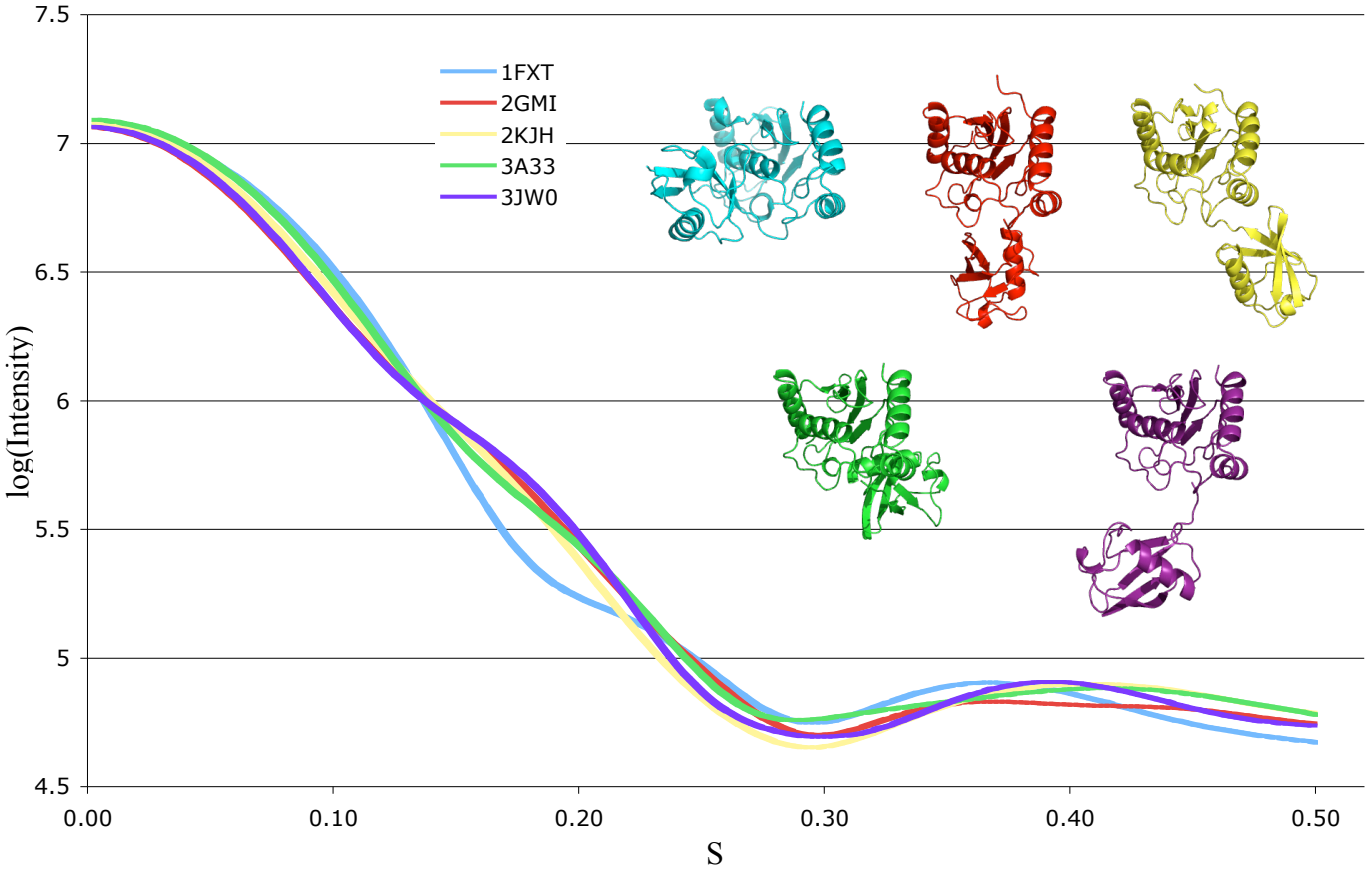

Figure S5. Theoretical scattering profiles for the five published E2~Ub structures (generated using the program OLIGOMER).

Figure S6. SAXS statistics

A) Chi-squared values for CRYSOL-based fits to experimental data

	3JW0	1FXT	2GMI	2KJH	3A33
UbcH5c-O~Ub	6.218	NA	7.283	3.762	7.075
Ubc13-O~Ub	8.554	NA	9.051	5.917	8.070

B) Chi-squared and percent contributions for OLIGOMER linear combination fits

	Chi-squared	3JW0	1FXT	2GMI	2KJH	3A33
UbcH5c-O~Ub	5.45	0%	1%	0%	99%	0%
Ubc13-O~Ub	3.87	70.4%	29.6%	0%	0%	0%

C) Chi-squared values for repeated GAJOE calculations

	Run 1	Run 2	Run 3
UbcH5c-O~Ub	2.247	2.271	2.264
Ubc13-O~Ub	2.751	2.742	2.754

D) Decreasing ensemble size for GAJOE calculations

	20	15	10	5	3	1
UbcH5c-O~Ub	2.247	2.238	2.220	2.185	2.234	2.674
Ubc13-O~Ub	2.751	2.667	2.644	2.559	2.448	3.401

E) GAJOE-calculated ensembles for 5-component systems

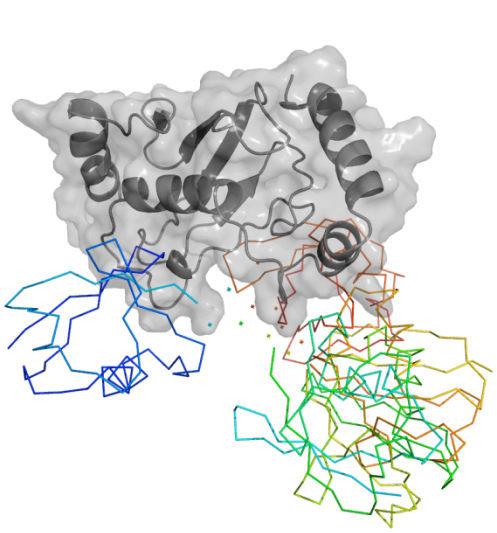

UbcH5c-O~Ub

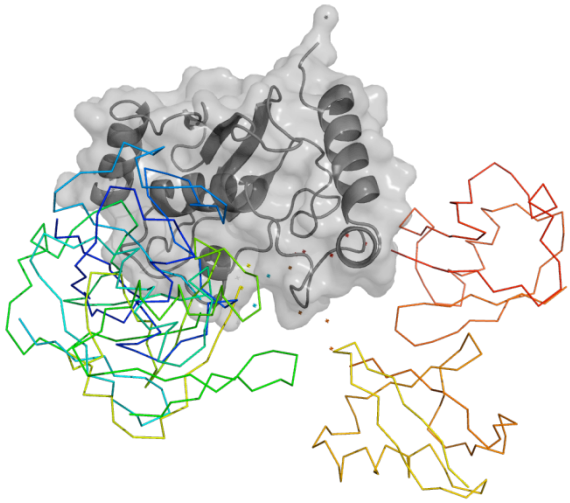

Ubc13-O~Ub

Chapter III - Structure of an E3:E2~Ub complex reveals an allosteric mechanism shared among RING/U-box ligases

The following chapter was published in the journal *Molecular Cell*.

Reprinted with permission from
Pruneda, J. N., Littlefield, P. J., Soss, S. E., Nordquist, K. A., Chazin, W. J., Brzovic, P. S., and Klevit, R. E. (2012) Structure of an E3:E2~Ub complex reveals an allosteric mechanism shared among RING/U-box ligases. *Molecular Cell*. *47*, 933-942.

Author Contributions

J.N.P and P.J.L. performed all experiments, with the exception of NMR relaxation studies performed by S.E.S. and E4B auto-ubiquitination assays performed by K.A.N. J.N.P., P.J.L., P.S.B., and R.E.K. designed the overall study and J.N.P., P.J.L., P.S.B., W. J. C., and R.E.K. analyzed the data and wrote the manuscript.

Abbreviations: Ub, ubiquitin; E2, ubiquitin-conjugating enzyme; E3, ubiquitin ligase; E1, ubiquitin-activating enzyme; RING, Really Interesting New Gene; HECT, Homologous to E6AP Carboxy Terminus; NMR, nuclear magnetic resonance; CSP, chemical shift perturbation.

Introduction

Post-translational protein modification by ubiquitin (Ub) is critical for control of a broad range of cellular pathways. Yet mechanistic details of Ub transfer are poorly understood. The basic scheme of Ub activation and transfer requires the sequential activity of three enzymes; an E1 Ub-activating enzyme, an E2 Ub-conjugating enzyme, and an E3 Ub-ligase. There are two predominant classes of E3s: 1) HECT ligases, which act via obligate formation of an E3~Ub thioester intermediate, and 2) RING/U-box ligases, which facilitate the direct transfer of Ub from an E2~Ub conjugate to a target substrate. In the absence of an E3, the reactivity of E2~Ub conjugates toward small nucleophiles is significantly reduced. This behavior presumably prevents nonproductive hydrolysis of the Ub-thioester bond before assembly into an E3-ligase Ub-transfer complex. Thus, RING/U-box E3 ligases not only coordinately bind E2~Ub conjugate and substrate, but must also activate the E2~Ub thioester to enhance the direct transfer of Ub to a target lysine[1,2].

The structural basis for RING/U-box-mediated E2~Ub activation has been elusive. Numerous structural studies have allowed definition of a consensus E3:E2 contact surface comprised of E2 residues located in Helix 1, Loop 4, and Loop 7, and RING/U-box residues in Loops 1, 2, and the central Helix (Fig 1A). This arrangement places the E2 active site ~15Å away from the E3:E2 interface[3-9]. No clear structural differences between free and E3-bound E2s are apparent that explain E3 enhancement of E2~Ub reactivity. Using statistical coupling analysis, Ozkan et. al.[10] identified clusters of co-evolving residues in UbcH5b that link the E3-binding interface to the E2 active site. Based upon mutational analysis, they suggested that RING-type E3s may allosterically activate E2s, but the structural basis for the E3-dependent

activation was not defined[10]. Here we report structural and biochemical studies that define how RING/U-box E3 ligases allosterically activate E2~Ub conjugates.

Our studies focus on interactions of UbcH5c~Ub with two RING/U-box E3s, BRCA1/BARD1[11-14] and E4B[15,16]. The UbcH5 family of E2 Ub-conjugating enzymes are among the most thoroughly characterized, both structurally and biochemically, including interactions between unconjugated UbcH5 and BRCA1/BARD1[17,18] and E4B[4,19]. Analysis of the UbcH5c~Ub conjugate in the absence of an E3 revealed it to be highly dynamic. UbcH5c~Ub displays a preference for highly extended and open conformations (few non-covalent interactions between E2 and Ub domains) and only occasionally samples closed conformations in which the Ub subunit directly contacts Helix 2 of the E2 (Fig 1B)[20]. Closed E2~Ub conformations were first proposed for Ub conjugated to the yeast E2 Ubc1, and recent studies have linked closed E2~Ub conformational states to the ability of the E2s Ube2s and Cdc34 to transfer Ub in E3-*independent* reactions[21-23]. While it might seem logical to extend these observations to infer that E3 binding is associated with closed E2~Ub, states, there is no experimental evidence that directly addresses this point.

Here, we present an experimentally-based structural model for an E3:E2~Ub ternary complex. We show that binding of either BRCA1/BARD1 or E4B promotes a shift in the dynamic ensemble of UbcH5c~Ub, biasing the conjugate toward closed conformations that are more reactive for Ub transfer. Structural analysis of an E3:E2~Ub complex allowed us to design targeted mutations that selectively disrupt E3-enhanced Ub transfer without affecting consensus E3:E2 interactions, thereby uncoupling E3 binding from activation. We identify a highly conserved E3 sequence motif and an essential E3:E2 hydrogen bond that serves as the linchpin for activation of E2~Ub conjugates. This work supports a model in which RING/U-box E3

ligases allosterically activate E2~Ub conjugates for transfer through a broadly conserved mechanism.

Results

Interactions of protein subunits within the E4BU:UbcH5c~Ub ligase complex

Assembly of a RING or U-box E3:E2~Ub complex poised for Ub transfer involves simultaneous interactions among multiple components. The interactions are of moderate to weak affinity, resulting in the formation of a dynamic E3:E2~Ub structural ensemble. To generate a structural model of the E4B:UbcH5c~Ub complex we used NMR chemical shift perturbations (CSPs) and paramagnetic relaxation probes to characterize interactions among the various protein subunits. NMR experiments for structural analysis were performed with the E4B minimal U-Box construct (E4BU; residues 1092-1173) and UbcH5c (free and Ub-conjugated) with a Cys85Ser mutation to produce a more stable oxyester-linked UbcH5c-O~Ub conjugate[24]. Separate isotopic labeling of E4BU, UbcH5c, and Ub subunits allowed for the identification of each protein-protein interaction surface within the ternary complex using $^{1}H,^{15}N$-HSQC-TROSY NMR titration experiments (Fig S1). Criteria used for determining contact residues included solvent accessibility and chemical shift perturbations greater than one standard deviation above the mean. Results from NMR titration experiments were used to generate sets of ambiguous interaction restraints (AIRs), which in turn were used for the structure calculations and docking in HADDOCK[25]. A complete list of restraints is provided in Table S1. For the E4BU:UbcH5~Ub complex, 200 structures were calculated and the top-scoring cluster was selected. This cluster contained 36 structures with an average pairwise RMSD of 2.87Å (Fig 1C).

Chemical shift perturbations (CSPs) similar in trajectory and magnitude (Fig S1A, S1B, S1H) are observed for residues comprising the consensus E3:E2 contact surface for E4BU binding to both free UbcH5c and UbcH5c~Ub. These data indicate that the consensus contact surface between E4BU and UbcH5c is maintained whether or not conjugated Ub is present (Fig 1A, 1C). Consistent with this observation, comparison of the E4BU and UbcH5c subunits in the NMR-based ensemble to an E4BU:UbcH5c co-crystal structure yields an average pairwise RMSD of 1.68Å over all members of the cluster[4].

Additional CSPs outside the consensus E3:E2 interaction site are observed in both the UbcH5c and Ub subunits upon formation of the E4BU:UbcH5c~Ub ternary complex (Fig S1A, S1C). In UbcH5c, the additional CSPs observed are for residues in Helix 2 (centered around Leu104) and surrounding the E2 active site (residues His75, Asn77, and Leu86) (Fig S1B). The CSPs in Ub map to a region centered about Leu8, Ile44, and V70, which form a surface exposed hydrophobic patch utilized in many Ub-protein interactions (Fig S1D). As compared to UbcH5c~Ub in the absence of an E3, which populates mainly extended conformations[20], these data show that the I44 surface of the Ub subunit interacts more frequently with solvent exposed residues centered around Leu 104 in Helix 2 of UbcH5c while in the ternary complex. These CSPs for resonances in the regions of UbcH5c and Ub serve as signatures for adjustments in the UbcH5c~Ub ensemble toward closed conformations. Similar observations were made in NMR titrations performed with the BRCA1/BARD1 RING heterodimer reveal that RING E3 interactions also shift UbcH5c~Ub conformations toward more closed conformational states (Fig S1I).

Within the structural ensemble of the ternary complex, the relative position of Ub displays the largest variability. In individual members of the ensemble, the potential E4BU:Ub

interface varies from essentially no contact to almost 300Å^2. Within the ensemble, residues in Ub b-strand 2 approach residues in C-terminal region of E4BU Loop 2. The interaction between Ub and UbcH5c is more defined and extensive, comprised of a combination of hydrophobic and electrostatic interactions. The most prominent of the electrostatic contacts are between a negatively-charged patch on UbcH5c comprised of Asp42, Asp112, Asp116, Asp117 and a positively-charged patch on Ub formed by Arg42, Lys48, and Arg72 (Fig 1D).

TEMPO spin labels incorporated into various positions of Ub provide independent verification of the ternary complex calculated from CSPs. NMR spectra were collected to identify UbcH5c and E4BU residues affected by proximity to a paramagnetic probe in the E3:E2~Ub complex. Ub-K11SL affected many of the same residues in UbcH5c reported previously for the conjugate alone[20] (i.e. Loop 1 and Helix 2), but the effects in Loop 7 are of significantly greater magnitude in the ternary complex (Fig 1E, S1J). Ub-K11SL also affected E4BU residues in Loop 1, the β1/β2 turn, Helix 1, and Loop 2 (Fig 1E, S1K). Together, the paramagnetic spin label data confirm both the interacting surfaces and the orientation of subunits in the structural model of the complex derived from CSPs.

NMR heteronuclear relaxation measurements were performed to ascertain whether the closed conformations of UbcH5~Ub observed in the structural ensemble of the ternary complex are associated with a change in the dynamics of the E2~Ub conjugate. The relaxation parameters were used to define diffusion tensors that describe the overall tumbling for Ub in the isolated UbcH5c~Ub conjugate and within the E4BU:UbcH5c~Ub ternary complex[26]. Figure 1F shows a mesh representation of the diffusion tensor of ubiquitin in the UbcH5c conjugate alone and in complex with E4BU. There is a 16% reduction in the volume of the tensor calculated for the E4BU complex compared to the UbcH5c~Ub conjugate alone (Fig 1F, Table S2). This analysis

demonstrates that the motion of the conjugated Ub is significantly slowed upon E4BU binding to the conjugate.

E2~Ub closed conformations are necessary for E3-mediated Ub transfer

The E4BU:UbcH5c~Ub structural ensemble predicts contact residues that should be important for stabilizing the complex in closed conformations. Point mutations in UbcH5c and in Ub were generated to test these predictions (Fig 2A). UbcH5c Leu104 is a solvent exposed hydrophobic residue on Helix 2 for which significant CSPs are observed upon formation of the E4BU:UbcH5c-O~Ub complex. The structurally analogous position is widely conserved as a hydrophobic residue among E2s that function with RING/U-box E3s (Fig S2A). Hence, Leu104 was mutated to glutamine to disrupt hydrophobic non-covalent interactions between UbcH5c and Ub. For Ub, each residue of the Leu8-Ile44-Val70 hydrophobic surface was mutated to Ala. Titration of unlabeled E4BU into ^{15}N-UbcH5c^{L104Q}-O~^{15}N-Ub or ^{15}N-UbcH5c-O~^{15}N-Ub^{I44A} produced CSPs nearly identical to those observed for free UbcH5c (Fig S1, S3). Notably, CSP signatures for UbcH5c~Ub closed conformational states were not observed, even though the designed point mutations do not appear to affect consensus E3:E2 interactions. From the perspective of the E3, titration of ^{15}N-E4BU with either UbcH5c-O~Ub^{I44A} or UbcH5c^{L104Q}-O~Ub resulted in CSPs in E4BU nearly identical to those observed for interactions between E4BU and free UbcH5c (Fig S1E, S1G). Thus, the designed mutations in Ub and UbcH5c uncouple the E3-induced conformational shift in the UbcH5c~Ub ensemble from consensus E3:E2 binding and can, therefore, be used to assess the functional role of closed conformational states in E3-mediated Ub transfer reactions.

The impact of the designed mutations on Ub transfer reactions were examined using auto-ubiquitination assays in which the E3 serves as both ligase and proxy substrate. The BC_{304}/BD_{327} heterodimer (BRCA1 residues 1-304, BARD1 residues 26-327) and $E4BU^{+20}$ (E4BU with an additional 20 N-terminal residues) were used in activity assays as these longer constructs are more efficient proxy substrates than the minimal RING or U-box domains used in NMR experiments[18,19]. In these experiments, no auto-ubiquitination of either BC_{304}/BD_{327} or $E4BU^{+20}$ was observed in reactions involving $UbcH5c^{L104Q}$, Ub^{L8A}, Ub^{I44A}, or Ub^{V70A} (Fig 2B, S4A, S4B). More conservative substitutions, $UbcH5c^{L104V}$ and Ub^{V70I}, display intermediate levels of Ub transfer activity (Fig S4A, S4B). None of the UbcH5c and Ub mutations affected charging of Ub onto the E2. Thus, inclusion of mutant versions of either component (E2 or Ub) severely diminishes or abrogates Ub transfer activity and the differences in activity reflect changes in the final step of Ub transfer from the E2 onto a substrate lysine.

Reaction of the UbcH5c~Ub thioester with the ε-amino group of free lysine provides a direct measure for the intrinsic aminolysis activity of an E2~Ub conjugate in the absence and presence of a RING/U-box E3[2]. The ability of UbcH5c~Ub to transfer Ub to free lysine was monitored in the presence of BC_{112}/BD_{140} (BRCA1 residues 1-112, BARD1 residues 26-140). Compared to a $BRCA1^{I26A}$ control that abrogates UbcH5c binding[17], the reactivity of the UbcH5c~Ub conjugate toward lysine is dramatically increased by the presence of BC_{112}/BD_{140}, indicating an E3-induced activation of the UbcH5c~Ub thioester to nucleophilic attack[2]. Mutant E2~Ub conjugates comprised of either $UbcH5c^{L104Q}$ or Ub^{I44A} are marginally slower in E3-independent aminolysis assays, consistent with previous reports[22,23]. Importantly, no enhancement of reactivity is observed upon addition of BC_{112}/BD_{140}, despite the ability of the

mutant UbcH5c~Ub conjugates to bind the E3 (Fig 2C). Therefore, the consensus E2:E3 interaction is necessary but not sufficient to enhance UbcH5c~Ub reactivity.

Though the UbcH5c-O~Ub conjugate used in our NMR experiments is more stable toward hydrolysis than the thioester conjugate, the oxyester-linked conjugate undergoes enhanced hydrolysis in the presence of stoichiometric amounts of E4BU. As a quantitative measure of the E3 rate enhancement, UbcH5c-O~Ub hydrolysis was monitored by 1D-NMR. The Asn77 backbone amide resonance undergoes a well-resolved chemical shift change upon formation of the UbcH5c-O~Ub conjugate and serves as an indicator of the relative amounts of E2~Ub and free E2 present. 1D ^{1}H spectra were collected at twenty-minute intervals after addition of E4BU and the area of the conjugated-Asn77 resonance was plotted as a function of time. In the absence of E4BU, the UbcH5c-O~Ub oxyester hydrolyzed slowly, with a half-life of approximately 58 hours at 25°C. Addition of an equimolar amount of E4BU decreased the oxyester half-life to less than 10 hours. The E3-mediated rate enhancement (i.e., $k_{obs}(E3)/k_{obs}(no\ E3)$) corresponds to a $\Delta\Delta G^{\ddagger}$ of approximately 1 kcal/mol. Complexes formed with mutations that disfavor closed conformations (ie. UbcH5c^{L104Q} or Ub^{I44A}) have rates of hydrolysis nearly identical to the no-E3 control (Fig 2D). Taken together, the activity assays reveal a strong correlation between E3-mediated Ub transfer and the induced UbcH5c~Ub closed conformations observed in NMR CSP experiments. Thus, mutations that block the ability of E3 to shift the UbcH5c~Ub ensemble toward closed conformations also block E3 enhancement of Ub transfer.

Conformational activation is a general feature of RING/U-box E3:E2~Ub function

Of the twenty human Ub-conjugating E2s with known structures, twelve have a leucine that is structurally analogous to UbcH5c Leu104, and two others have methionine at this

position, suggesting the position plays a similar role in other E2s. A set of E2s that function with BRCA1/BARD1 was used to examine the generalizability of the conformational activation mechanism among E2s. The representative E2s investigated were Ube2e1 (transfers monoubiquitin), Ube2K (synthesizes K48-linked chains), and Ube2n (synthesizes K63-linked chains with Uev1A)[18]. In each E2, the mutation analogous to UbcH5c L104Q substantially decreases BRCA1/BARD1-enhanced reactivity toward lysine (Fig 3A).

To assess whether other RING/U-box E3s function via similar mechanisms to activate the UbcH5c~Ub conjugate, assays were performed using either wild-type or L104Q UbcH5c and the RING E3s MDM2 (a homodimeric C-terminal RING), RNF8 (a structurally uncharacterized N-terminal RING), and SCF-Fbw7 (a multi-component RING E3). MDM2 and RNF8 auto-ubiquitination activity is drastically decreased when UbcH5c L104Q is the E2 (Fig 3B). SCF-Fbw7-dependent ubiquitination of the substrate cyclin E was similarly affected (Fig S4C). In stark contrast, Ub transfer catalyzed by HECT-type E3 ligases (which proceeds via a transthiolation reaction to generate an E3~Ub thioester intermediate) is unaffected by the UbcH5c L104Q mutation, as shown in assays using E6AP, SspH1 (a bacterial effector protein), and HHARI (a RBR RING/HECT hybrid) as the E3 (Fig 3C). Thus, diverse E2s and RING/U-box E3s utilize a similar mechanism whereby activation of an E2~Ub conjugate by a RING/U-box E3 ligase requires that E2~Ub closed conformations be populated. This shared mechanism implies that a conserved feature in RING/U-box E3s is responsible for the activation of E2~Ub conjugates, but to date no such feature has been identified.

Formation of a conserved E3:E2 hydrogen bond increases the population of E2~Ub closed conformations

The structural model of E4BU:UbcH5c~Ub indicates that Loop 2 of E4BU occupies conformations in which it is in intimate contact with UbcH5c. Comparison of the sequence of this loop across RING and U-box E3s revealed a highly conserved Φ-x-(K/R) motif, where Φ is a hydrophobic residue and x is either the final Cys of RING domains or a corresponding polar residue of U-box domains that is important for structural stability (for example E4B residues F1141-N1142-R1143 or BRCA1 residues L63-C64-K65) (Fig S2B). Analysis of structurally homologous E3 residues in all available high-resolution RING/U-box E3:E2 co-crystal structures (PDB IDs 1FBV, 2C2V, 2OXQ, 3HCT, 3L1Z, and 3RPG) revealed that the conserved K/R side chain forms a hydrogen bond with an E2 backbone carbonyl preceding Loop 7 (corresponding to UbcH5c residue 92) (Fig 4A, S5A). This hydrogen bond is strictly conserved among all deposited structures (in the case of TRAF6:Ubc13, the connection is made through a water molecule). The sole notable exception is the cCbl:UbcH7 complex, which is in fact an inactive E3:E2 pair despite its common use as a primary example of how RING E3s bind E2s. Mutation of R1143 in E4BU (E4BU^{R1143A}) generates an E3 unable to shift the population of the UbcH5c-O~Ub conjugate toward closed states, even though consensus E3:E2 interactions remain intact as judged by NMR binding experiments (Fig 4B). Titrations of ^{15}N-labeled UbcH5c with either wild-type E4BU or E4BU^{R1143A} demonstrate that there is little or no significant change in the strength of the E2:E3 binding interaction associated with loss of the hydrogen bond (Fig S5B). Importantly, the hydrogen bond-defective mutants E4BU^{R1143A} or E4BU^{R1143M} show no ability to activate Ub transfer in auto-ubiquitination or oxyester hydrolysis assays (Fig 4C, 2D, S4D). Our results establish that formation of the E3:E2 intermolecular hydrogen bond is required for

activation of the E2~Ub conjugate for transfer, even though the contact point is ~15Å from the E2 active site. We propose the hydrogen bond is a key molecular linchpin for initiating the allosteric activation of the E2~Ub conjugate.

Discussion

Previous structural analyses of the assembly of Ub-transfer complexes involving RING/U-box E3 ligases focused primarily on E3:E2 complexes and, more recently, on E2~Ub conjugates in the absence of an E3[3-10,19-23]. In general, E2~Ub conjugates exhibit substantial flexibility between the Ub and E2 subunits and display modest to weak interactions with E3s. Thus, binding to an E3 generates a dynamic E3:E2~Ub ensemble that is difficult to define in terms of a single static structure. To structurally characterize such E3:E2~Ub complexes, we employed a variety of NMR-based techniques that 1) directly demonstrate that binding to RING/U-box E3s shifts the ensemble population of E2~Ub conjugates toward more closed, active conformations, 2) expand the "consensus" E3:E2 contact surface required for E3:E2~Ub assembly, and 3) define critical E3:E2 interactions required for activation of E2~Ub conjugates.

Characterization of UbcH5c~Ub and Ubc13~Ub conjugates by SAXS showed that E2~Ubs sample closed conformations in the absence of an E3, but the E2~Ub closed state is sparsely populated[20]. Despite observations of closed E2~Ub conformations in the absence of an E3, direct evidence regarding the nature of the conjugate within the active E3:E2~Ub complex has been elusive. The NMR and mutational studies presented here demonstrate that binding to RING and U-box E3s increases the population of closed conformations in UbcH5c~Ub and other E2~Ub conjugates. Mutations that selectively disrupt closed conformations (e.g., Ub^{I44A} and $UbcH5c^{L104Q}$) also disrupt Ub transfer activity and E3-enhanced aminolysis (Fig 2) despite our

finding that "consensus" E3:E2 binding interactions remain intact (see Fig 1A). Introduction of the L104Q mutation into the structurally analogous position in several other E2s similarly impairs E3-enhanced reactivity of the E2~Ub conjugates. Such mutations not only abrogate the ability of E4BU and BRCA1 to facilitate Ub transfer, but also disrupt Ub-transfer activity catalyzed by other diverse RING E3s (Fig 3B). Thus, we demonstrate that there is a direct link between RING/U-box-facilitated Ub transfer and the induction of an E2~Ub closed conformational state, and that conformational biasing toward closed populations is a feature shared by numerous RING and U-box E3s to activate cognate E2~Ub conjugates for Ub transfer.

How do RING/U-box E3s enhance the population of reactive E2~Ub conjugates? Our studies of the E4BU:UbcH5c~Ub ternary complex identify E4BU R1143 as a key determinant. R1143 is part of a Φ-x-(K/R) motif (F1141, N1142, and R1143 in E4B; L63, C64, and K65 in BRCA1) that is highly conserved among RINGs and U-box E3s. Even the class of bacterial effector E3s that is structurally homologous to eukaryotic U-boxes shows conservation at the analogous position. This is remarkable as bacterial and eukaryotic U-box-type E3s share almost no sequence homology despite having similar structures, suggesting their convergent evolution and highlighting the pivotal role played by the E3 hydrogen bond donor residue in Ub transfer (Fig S2B).

Our NMR studies on wild-type and ligase-inactive mutant proteins allow us to define three discrete requirements for the formation of an active E3:E2~Ub complex and subsequent catalyzed Ub transfer (Fig 5A, wild-type). The first requirement involves formation of the consensus E3:E2 binding interaction as observed in previous crystallographic and NMR studies (Fig 5, dark blue). This interaction is largely conserved among various E3:E2 complexes and can be disrupted with point mutations in the binding interface (e.g. UbcH5c^{A96D} or BRCA1^{I26A};

Fig 5B, class "a" mutation). The second requirement for an active E3:E2~Ub complex involves the formation of an intermolecular hydrogen bond from a side chain in the E3 Loop 2 Φ-x-(K/R) motif to a backbone carbonyl at the C-terminal end of the 3_{10} helix in the E2. This interaction does not significantly contribute to the affinity of the E3:E2 complex, but its formation (detected as CSPs in E2 resonances 87-93 within the E2 3_{10} helix) is essential for catalysis. CSPs resulting from the E3:E2 hydrogen bond define an allosteric pathway that links the E3 binding interface to the E2 active site (Fig 5, cyan). Direct experimental evidence shows that the effects of the hydrogen bond extend to the N-terminal end of the 3_{10} helix where a conserved Asp (UbcH5c Asp87) occupies a cleft near the E2 active site. UbcH5c Asp87 is sensitive to steric mutations suggesting it may play a role in controlling access to E2~Ub closed conformations[2]. Consistent with this model, preliminary analysis of the UbcH5c^{D87E}-O~Ub conjugate indicates an inability to adopt closed conformations in response to E4BU binding. The allosteric linkage can be broken by mutation of the conserved E3 K/R residue (e.g., E4B R1143A), a mutation that also abrogates formation of closed E2~Ub conformations and the ability to transfer Ub *in vitro* (Fig 5C, class "b" mutation).

The third requirement for an active E3:E2~Ub complex is E3:E2 interactions that allow E2~Ub conjugates to adopt closed conformational states with high frequency. Direct experimental evidence for the closed states comes from the observation of CSPs in the residues surrounding the hydrophobic Ile44 surface of Ub and exposed hydrophobic residues in Helix 2 of the E2 (Fig 5, red). CSPs associated with closed E2~Ub conformations are also observed in E2 active site residues 75, 77, and 86. Point mutations in the E2:Ub interface (e.g. UbcH5c^{L104Q} and Ub^{I44A}) selectively disrupt E3-mediated formation of E2~Ub closed conformations (Fig 5D, class "c" mutations). The three types of interactions are each necessary but none is sufficient on its

own. Thus, distinct sets of interactions link E3:E2 binding to increases in the population of closed E2~Ub conformational states and to E3-mediated enhancement of Ub transfer activity. This linkage between E3 binding and the resulting shift toward E2~Ub closed conformations (Fig 5, dark blue – cyan – red) defines a model for the allosteric activation of E2~Ub conjugates by RING and U-box E3s.

The E3:E2~Ub structural model (Fig 1C) suggests additional interactions that could stabilize E2~Ub closed conformations. The N-terminal region of Ub b-strand 2 in some closed states are in proximity to the E3 suggesting a potential E3:Ub contact surface. Such an interaction could enhance the affinity of an E3 for an E2~Ub conjugate over a free E2. Recently, a difference in affinity of nearly 50-fold was reported for binding of the E3 Rbx1 to Cdc34~Ub over free Cdc34[27]. However, binding of free UbcH5c or UbcH5c~Ub to either E4BU or BRCA1 shows remarkably little difference in apparent affinities, as observed in NMR-based competition measurements (Fig S5C). Our model of the E4BU:UbcH5c~Ub complex predicts only few interactions between the C-terminal regions of E4BU Loop 2 and β-strand 2 of Ub. Small CSPs are observed in this region of Ub, but are more consistent with infrequent contacts between E3 and Ub rather than a defined E3:Ub contact surface. The Ub residue that most frequently approaches E4BU is Thr12, but its mutation to Ala or Glu has no impact on observed Ub transfer activity (Fig S4E). Furthermore, the region of RING/U-box E3s that might mediate E3:Ub contacts shows poor sequence conservation outside of the Φ-x-(K/R) motif. Together, these observations argue against the presence of an E3:Ub interaction surface that is broadly shared among the family of RING/U-box E3 ligases.

Our model for assembly and activation of E3:E2~Ub complexes provides a framework for understanding how both post-translational E2~Ub modifications and small molecule ligands

may impact Ub transfer activity. UbcH5 contains several acidic residues (Asp42, Asp112, Asp116, and Asp117) that interact with basic residues on Ub (Arg42, Lys48, and Arg72). In other E2s, structurally analogous sites contain serine residues that have been found to be sites of phosphorylation. This suggests that Ub transfer can be regulated by modulating the negative electrostatic potential in regions of the E2:Ub interface which, in turn, alter the ability of E2~Ub conjugates to adopt closed conformations. For example, positions that correspond structurally to UbcH5c Asp112 are conserved as either Asp or Ser in a large number of E2s. Yeast E2 Ubc1 Ser115 is a site of reversible phosphorylation associated with a phenotype in which yeast display enhanced tolerance to environmental stresses[28]. Our E4BU:UbcH5c~Ub model predicts that the phosphorylation of Ubc1 Ser115 would enhance the E2:Ub electrostatic interaction, thereby promoting the activation of Ub transfer. Another example involves the bacterial effector protein CHBP which catalyzes deamidation of Ub Gln40 to yield Glu[29]. The Ub Q40E modification would create an unfavorable electrostatic contact in the closed E2:Ub interface and, in fact, Ub modified at this position is not active in ubiquitination reactions[29]. A third example is the highly specific inhibitor of the E2 Cdc34 found in a high-throughput small molecule screen, which blocks E3-mediated Ub transfer without affecting assembly of the ubiquitination machinery[30]. A Cdc34/inhibitor co-crystal structure revealed that the inhibitor binds Cdc34 directly above Helix 2 causing a 2Å shift in Helix 2 and active site residues relative to the unliganded E2. Our structural analysis of the RING/U-box E3:E2~Ub complex suggests that such a structural perturbation may block adoption of a Cdc34~Ub closed conformation and E3-mediated Ub transfer by preventing Ub:Cdc34 interactions in the closed state.

RING/U-box E3s have traditionally been thought to function by simultaneously binding both substrate and E2~Ub conjugate to facilitate Ub transfer. The results presented here define

an additional essential role for RING/U-box E3 ligases in promoting ubiquitin transfer. Assembly of a RING/U-box E3:E2~Ub ligase complex biases the E2~Ub conjugate toward closed conformational states that are more reactive toward lysine. The linchpin of the E2~Ub activation is formation of a conserved E3:E2 intermolecular hydrogen bond that allows for E2~Ub allosteric activation, not by stabilizing a discrete protein conformation, but by shifting the E2~Ub conformational ensemble toward more reactive states. The ability to form a closed E2~Ub complex is essential to the function of a diverse array of both E2s and RING/U-box E3s, illuminating a general strategy that can be exploited by other RING/U-box family members. The molecular basis for allosteric activation of E2~Ub conjugates presented here provides new insights into how RING/U-box E3s function and offers valuable tools for investigation of the biological function of the largest class of E3 Ub-ligases.

Experimental Procedures

Plasmids, protein expression and purification. Plasmid constructs, expression, and purification of E1, Ub, UbcH5c, BRCA1$^{1-112}$/BARD1$^{26-140}$, BRCA1$^{1-304}$/BARD1$^{26-327}$, Ube2k, Ube2n, Ube2e1, E4BU, E4BU^{+20}, E6AP**,** and HHARI were previously described[18,17,19,31,2]. SspH1 was produced and purified as described for SspH2[32]. Point mutations were produced via Quikchange site-directed mutagenesis (Stratagene) and confirmed by DNA sequencing. All proteins were expressed in BL21 *Escherichia coli* (Invitrogen) in either rich LB media or isotope supplemented minimal MOPS media (Cambridge Isotopes). Proteins were stored in 25 mM sodium phosphate 150 mM NaCl (pH 7.0) at either 4^{o}C or -80^{o}C.

NMR Spectroscopy – Chemical Shift Perturbation and Paramagnetic Relaxation Enhancement. NMR spectra were recorded on either a 500 MHz Bruker Avance II (University of Washington) or a 750 MHz Varian INOVA spectrometer (Pacific Northwest National Laboratories, Richland, WA). UbcH5c-O~Ub was prepared as previously described using the structurally analogous active site Cys-to-Ser mutation in UbcH5c to improve conjugate stability, and the S22R mutation to prevent noncovalent Ub binding on the "backside" of UbcH5c[24]. Spectra were recorded at 25°C in 25 mM sodium phosphate 150 mM NaCl (pH 7.0) 10% D_2O. All titration datasets were collected using $^{1}H,^{15}N$-HSQC-TROSY experiments with 220 μM labeled protein with or without addition of unlabeled partners. Data were processed using NMRPipe/NMRDraw[33], and visualized with NMRView[34]. Chemical shift perturbations were calculated with the formula $\Delta\delta_j = [(\Delta\delta_j{}^{15}N/5)^2 + (\Delta\delta_j{}^{1}H)^2]^{1/2}$. Ub-K11C, covalently modified with 4-(2-iodoacetamido)-TEMPO (Sigma-Aldrich) as previously described[20], was conjugated to UbcH5c, and the conjugate was purified by gel filtration. Active and ascorbate-reduced spectra were recorded in the presence of >1 molar equivalent E4BU, and resonances with an I/I_{red} ratio lower than 1.5 standard deviation from the mean were deemed significantly affected by the probe.

NMR Spectroscopy- Relaxation Analysis. Heteronuclear R1 and NOE parameters were measured using standard protocols (Palmer, 2004). NMR spectra were recorded on 600 and 900 MHz Bruker Avance III spectrometers (Vanderbilt University). ^{15}N-UbcH5c-O~^{15}N-Ub and E4BU were prepared as described above and data were collected at 20°C in 30 mM sodium citrate (pH 5.75), 150 mM NaCl, 8% D_2O. Samples contained 200 μM labeled UbcH5c-O~Ub with or without 600 μM unlabeled E4BU. The conjugate slowly hydrolyzes when bound to E4BU, so multiple samples were used for the ternary complex. These samples were prepared just before

use from concentrated stocks and were limited to 1.5 days of data collection. Attempts to acquire ^{15}N-R2 experiments for the ternary complex were stymied by the limited hydrolysis of conjugate, since the signals from free Ub dominated the spectrum. We therefore resorted to measuring R1 and NOE at multiple fields. The recovery delays for ^{15}N-R1 experiments were 7.5 s and 12 s (600 and 900 MHz, respectively), and a three second saturation period was used for the $\{^1H\}$-^{15}N NOE. Time delays for the R1 measurements were 0.1, 0.4, 0.8, 1.2, 1.8, 2.5, and 4 s at 600 MHz, and 0.1, 0.4, 0.8, 1.2, 2, 3, and 5 s at 900 MHz. The data were processed in Topspin (Bruker) and analyzed in Sparky[35]. The NOE was calculated as the ratio of intensities I_{sat}/I_{ref}, and the NOE error was calculated such that $(\text{NOE err/NOE})^2 = [(I_{ref}\ \text{err}/I_{ref})^2 + (I_{sat}\ \text{err}/I_{sat})^2]$ and the error of each intensity measurement is the rmsd noise of each plane. Residues with NOE < 0.7 or having fewer than 3 of the 4 points determined were removed from analysis. The remaining Ub residues (48 for UbcH5c-O~Ub sample and 51 for ternary complex with E4BU) were each fit to a local isotropic correlation time (τiso) using relax[36]. These values were then input into the quadric_diffusion program (AG Palmer, based on reference *37*) to fit global diffusion tensors when using a structural model of Ub oriented to the inertial mass tensor. Among the isotropic, axial, and anisotropic models, the best statistical fit was obtained using axial symmetric diffusion tensors. Models of the diffusion tensors were created with relax and visualized using PYMOL.

Computational Modeling. Docking experiments were performed using HADDOCK 2.1[25]. Previous studies have shown that the E4BU, UbcH5c, and Ub subunits do not undergo detectable conformational changes when interacting with their protein partners[4,20]. Therefore, available NMR and X-ray crystallographic structures of the individual protein components were used as

input. Input structures for UbcH5c, Ub, and E4BU were taken from solution NMR ensembles of Protein Data Bank entries 2FUH (chain A), 1XQQ, and 2KR4, respectively. Unambiguous distance and dihedral restraints were used to model conjugation of the Ub C-terminus to the UbcH5c active site cysteine, and Ub residues 72-76 were allowed full flexibility. Definition of active and passive residues for ambiguous restraints was based on chemical shift perturbation data and was filtered for solvent accessibility. Ambiguous interaction restraints are listed in Table S1.

Small nucleophile reactivity assays. Reactivity assays involving Ub transfer to free lysine were performed as previously described[2]. Briefly, an E2~HA-Ub(K0) conjugate is formed (this ubiquitin construct contains arginine or methionine mutations at all lysine positions to prevent Ub chain formation). The conjugate is then combined with BC_{112}/BD_{140} and free lysine. Reaction samples are quenched in non-reducing SDS load buffer. Ub transfer to lysine is monitored by disappearance of the E2~Ub species, as observed by western blot probing for the HA epitope on Ub.

Hydrolysis of the UbcH5c-O~Ub conjugate was monitored by ^{1}H-NMR spectra recorded in 25 mM sodium phosphate 150 mM NaCl (pH 7.0) 10% D_2O at 25°C. 220 μM UbcH5c-O~Ub was combined (when applicable) with a 1:1 molar equivalency of E4BU. Spectra were processed and analyzed using MestReNova (Mestrelab Research). The integral of a 0.2 ppm window spanning the conjugated-Asn77 backbone amide resonance was calculated for each spectrum; baseline correction within each spectrum was performed by subtraction of the integral from a 0.2 ppm window in a neighboring region with no observable resonances.

E3 auto-ubiquitination reactions. Auto-ubiquitination reactions with BC_{304}/BD_{327} and $E4BU^{+20}$ were performed as previously described[2,18,19]. Reactions including $RNF8^{239-485}$, $MDM2^{FL}$, $E6AP^{494-875}$, $SspH1^{FL}$, and $HHARI^{177-395}$ were performed similarly to those with BC_{304}/BD_{327}. Briefly, a mixture of E1, E2, E3, and Ub is incubated with ATP/$MgCl_2$ to initiate the reaction. Samples are quenched by boiling in SDS loading buffer and ubiquitination products are visualized either by Coomassie staining or western blotting for FLAG-BRCA1 or HA-Ub components.

References

1. Song, J., Wang, J., Jozwiak, A. A., Hu, W., Swiderski, P. M., and Chen, Y. (2009). Stability of thioester intermediates in ubiquitin-like modifications. Protein Sci. *18*, 2492-2499.
2. Wenzel, D. M., Lissounov, A., Brzovic, P. S., and Klevit, R. E. (2011). UBCH7 reactivity profile reveals parkin and HHARI to be RING/HECT hybrids. Nature *474*, 105-108.
3. Zheng, N., Wang, P., Jeffrey, P. D., and Pavletich, N. P. (2000). Structure of a c-Cbl-UbcH7 complex: RING domain function in ubiquitin-protein ligases. Cell *102*, 533-539.
4. Benirschke, R. C., Thompson, J. R., Nomine, Y., Wasielewski, E., Juranic, N., Macura, S., Hatakeyama, S., Nakayama, K. I., Botuyan, M. V., and Mer, G. (2010). Molecular Basis for the Association of Human E4B U Box Ubiquitin Ligase with E2-Conjugating Enzymes UbcH5c and Ubc4. Structure *18*, 955-965.
5. Yin, Q., Lin, S. C., Lamothe, B., Lu, M., Lo, Y. C., Hura, G., Zheng, L., Rich, R. L., Campos, A. D., Myszka, D. G., et al (2009). E2 interaction and dimerization in the crystal structure of TRAF6. Nat. Struct. Mol. Biol. *16*, 658-666.
6. Xu, Z., Kohli, E., Devlin, K. I., Bold, M., Nix, J. C., and Misra, S. (2008). Interactions between the quality control ubiquitin ligase CHIP and ubiquitin conjugating enzymes. BMC Struct. Biol. *8*, 26.
7. Deshaies, R. J. and Joazeiro, C. A. (2009). RING domain E3 ubiquitin ligases. Annu. Rev. Biochem. *78*, 399-434.
8. Zhang, M., Windheim, M., Roe, S. M., Peggie, M., Cohen, P., Prodromou, C., and Pearl, L. H. (2005). Chaperoned ubiquitylation - crystal structures of the CHIP U-box E3 ubiquitin ligase and a CHIP-Ubc13-Uev1a complex. Mol. Cell *20*, 525-538.
9. Bentley, M. L., Corn, J. E., Dong, K. C., Phung, Q., Cheung, T. K., and Cochran, A. G. (2011). Recognition of UbcH5c and the nucleosome by the Bmi1/Ring1b ubiquitin ligase

complex. EMBO J. *30*, 3285-3297.

10. Ozkan, E., Yu, H., and Deisenhofer, J. (2005). Mechanistic insight into the allosteric activation of a ubiquitin-conjugating enzyme by RING-type ubiquitin ligases. PNAS *102*, 18890-18895.

11. Welcsh, P. L., Owens, K. N., and King, M. C. (2000). Insights into the functions of BRCA1 and BRCA2. Trends Genet. *16*, 69-74.

12. Welcsh, P. L. and King, M. C. (2001). BRCA1 and BRCA2 and the genetics of breast and ovarian cancer. Hum. Mol. Genet. *10*, 705-13.

13. Yu, V. (2000). Caretaker Brca1: keeping the genome in the straight and narrow. Breast Cancer Res. *2*, 82-85.

14. Scully, R. and Puget, N. (2002). BRCA1 and BRCA2 in hereditary breast cancer. Biochimie *84*, 95-102.

15. Cyr, D. M., Höhfeld, J., and Patterson, C. (2002). Protein quality control: U-box-containing E3 ubiquitin ligases join the fold. Trends Biochem. Sci. *27*, 368-375.

16. Richly, H., Rape, M., Braun, S., Rumpf, S., Hoege, C., and Jentsch, S. (2005). A series of ubiquitin binding factors connects CDC48/p97 to substrate multiubiquitylation and proteasomal targeting. Cell *120*, 73-84.

17. Brzovic, P. S., Keeffe, J. R., Nishikawa, H., Miyamoto, K., Fox, D., Fukuda, M., Ohta, T., and Klevit, R. E. (2003). Binding and recognition in the assembly of an active BRCA1/BARD1 ubiquitin-ligase complex. PNAS *100*, 5646-5651.

18. Christensen, D. E., Brzovic, P. S., and Klevit, R. E. (2007). E2-BRCA1 RING interactions dictate synthesis of mono- or specific polyubiquitin chain linkages. Nat. Struct. Mol. Biol. *14*, 941-948.

19. Nordquist, K. A., Dimitrova, Y. N., Brzovic, P. S., Ridenour, W. B., Munro, K. A., Soss, S. E., Caprioli, R. M., Klevit, R. E., and Chazin, W. J. (2010). Structural and functional characterization of the monomeric U-box domain from E4B. Biochemistry *49*, 347-355.

20. Pruneda, J. N., Stoll, K. E., Bolton, L. J., Brzovic, P. S., and Klevit, R. E. (2011). Ubiquitin in Motion: Structural studies of the E2~Ub conjugate. Biochemistry *50*, 1624-1633.

21. Hamilton, K. S., Ellison, M. J., Barber, K. R., Williams, R. S., Huzil, J. T., McKenna, S., Ptak C., Glover, M., and Shaw, G. S. (2001). Structure of a conjugating enzyme-ubiquitin thiolester intermediate reveals a novel role for the ubiquitin tail. Structure *9*, 897-904.

22. Wickliffe, K. E., Lorenz, S., Wemmer, D. E., Kuriyan, J., and Rape, M. (2011). The mechanism of linkage-specific ubiquitin chain elongation by a single-subunit E2. Cell *144*, 769-781.

23. Saha, A., Lewis, S., Kleiger, G., Kuhlman, B., and Deshaies, R. J. (2011). Essential role for ubiquitin-ubiquitin-conjugating enzyme interaction in ubiquitin discharge from cdc34 to substrate. Mol. Cell *42*, 75-83.

24. Brzovic, P. S., Lissounov, A., Christensen, D. E., Hoyt, D. W., and Klevit, R. E. (2006). A UbcH5c/Ubiquitin noncovalent complex is required for processive BRCA1-directed ubiquitination. Mol. Cell *21*, 873-880.

25. de Vries, S. J., van Dijk, M., and Bonvin, A. M. (2010). The HADDOCK web server for data-driven biomolecular docking. Nat. Protoc. *5*, 883-897.

26. Palmer, A. G. (2004). NMR Characterization of the dynamics of biomacromolecules. Chem. Rev. *104*, 3623-3640.

27. Spratt, D. E., Wu, K., Kovacev, J., Pan Z. Q., and Shaw. G. S. (2012). Selective recruitment of an E2~ubiquitin complex by an E3 ubiquitin ligase. J. Biol. Chem. Epub ahead of print, doi: 10.1074/jbc.M112.353748.

28. Meena, R. C., Thakur, S., Nath, S., and Chakrabarti, A. (2011). Tolerance to thermal and reductive stress in Saccharomyces cerevisiae is amenable to regulation by phosphorylation-dephosphorylation of ubiquitin conjugating enzyme (Ubc1) S97 and S115. Yeast *28*, 783-793.

29. Cui, J., Yao, Q., Li, S., Ding, X., Lu, Q., Mao, H., Liu, L., Zheng, N., Chen, S., and Shao, F. (2010). Glutamine deamidation and dysfunction of ubiquitin/NEDD8 induced by a bacterial effector family. Science *329*, 1215-1218.

30. Ceccarelli, D. F., Tang, X., Pelletier, B., Orlicky, S., Xie, W., Plantevin, V., Neculai, D., Chou, Y. C., Ogunjimi, A., Al-Hakim, A., et al. (2011). An allosteric inhibitor of the human Cdc34 ubiquitin-conjugating enzyme. Cell *145*, 1075-1087.

31. Huang, L., Kinnucan, E., Wang, G., Beaudenon, S., Howley, P. M., Huibregtse, J. M., and Pavletich, N. P. (1999). Structure of an E6AP-UbcH7 Complex: Insights into Ubiquitination by the E2-E3 Enzyme Cascade. Science *286*, 1321-1326.

32. Levin, I., Eakin, C., Blanc, M. P., Klevit, R. E., Miller, S. I., and Brzovic, P. S. (2010). Identification of an unconventional E3 binding surface on the UbcH5~Ub conjugate recognized by a pathogenic bacterial E3 ligase. PNAS *107*, 2848-2853.

33. Delaglio, F., Grzesiek, S., Vuister, G. W., Zhu, G., Pfeifer, J., Bax, A. (1994). NMRPipe: A multidimensional spectral processing system based on UNIX pipes. J. Biomol. NMR. *6*, 277-293.

34. Johnson, B. A. and Blevins, R. A. (1994). NMRView: a computer program for the visualization and analysis of NMR data. J. Biomol. NMR. *4*, 603-614.

35. Goddard, T. D. and Kneller, D. G. SPARKY 3. University of California, San Francisco.

36. d'Auvergne, E. J. and Gooley, P. R. (2008). Optimisation of NMR dynamic models I. Minimisation algorithms and their performance within the model-free and Brownian rotational diffusion spaces. J. Biomol. NMR. *40*, 107-119.

37. Lee, L. K., Rance, M., Chazin, W. J., and Palmer, A. G. (1997). Rotational diffusion anisotropy of proteins from simultaneous analysis of 15N and 13Calpha nuclear spin

relaxation. J. Biomol. NMR. *9*, 287-298.

Acknowledgements

We thank V. Vittal, K. Dove, N. Zheng, A.G. Palmer, and W. Hol for discussions and critical reading of the manuscript. We acknowledge B. Larimore for performing the experiment shown in Supplemental Figure 7C in the N. Zheng and B. Clurman laboratories. A portion of this research was performed using EMSL, a national user facility sponsored by the Department of Energy's Office of Biological and Environmental Research and located at PNNL. This work was supported by National Institutes of Health Grants R01 GM088055 (R.E.K.) and R01 GM075156 (W.J.C.), and the U.S. Public Health Service Grant NRSA 2T32 GM007270 from the National Institute of General Medical Sciences (J.N.P.). Access to instrumentation was supported by grants P30 ES0000267 (Vanderbilt University Center in Molecular Toxicology) and P50 CA068485 (Vanderbilt-Ingram Cancer Center) from the National Institutes of Health.

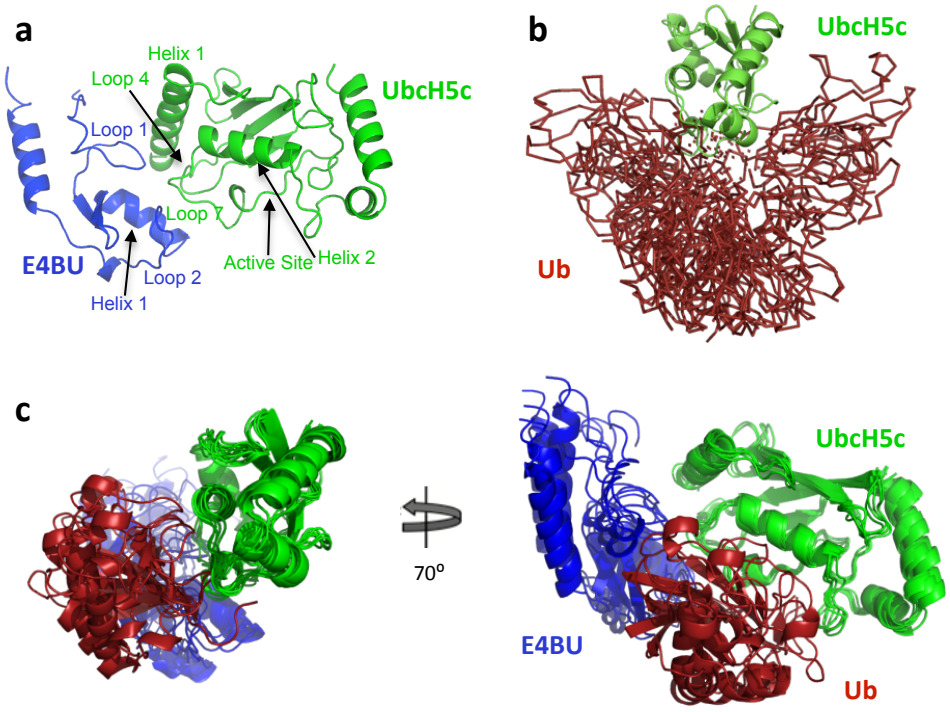

Figure 1. Model of the E4BU:UbcH5c~Ub complex. a) The E4BU:UbcH5 complex (PDB ID 3L1Z) is shown as a representative structure of RING/U-box E3:E2 structures. Structural features relevant to this work are noted. **b)** A side-on view of the UbcH5c~Ub structural ensemble generated from small angle X-ray data (Pruneda et al., 2011). **c)** Five representative structures of the top-scored HADDOCK cluster, aligned on UbcH5c (green); E4BU and Ub are shown in blue and red, respectively. For comparison, the view on the left is comparable to that shown in panel b).

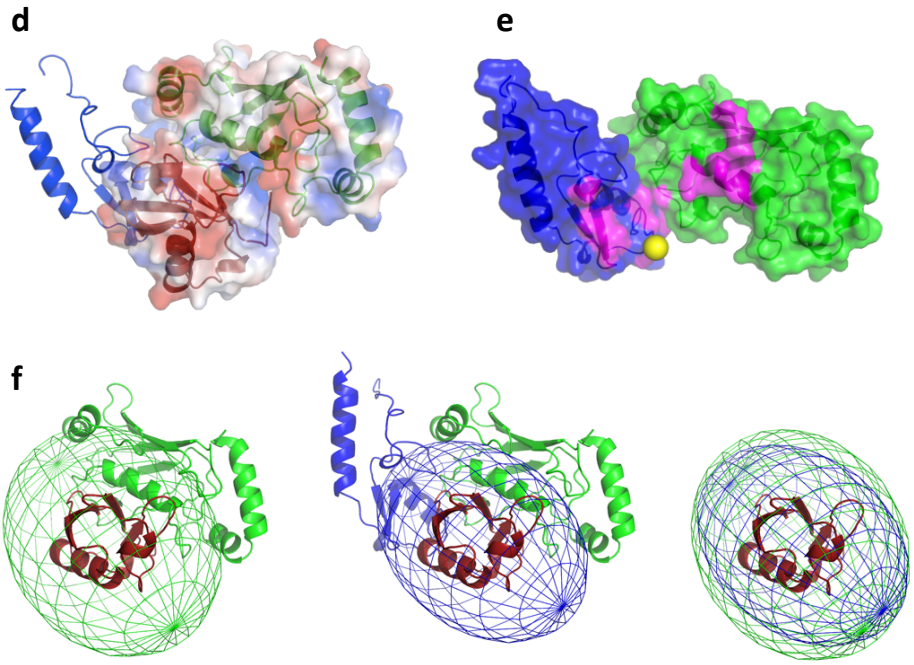

Figure 1. **d)** An electrostatic surface is shown for a representative E4BU:UbcH5c~Ub structure within the top-scored HADDOCK cluster. Note the expansive interaction between an acidic patch on UbcH5c and a basic region on Ub. **e)** Regions affected by the spin-labeled conjugate (i.e., Ub-K11SL) are painted in magenta (> 1.5 sd from the mean I_{act}/I_{red}); the alpha carbon of Ub residue 11 from one member of the ensemble is shown as a yellow sphere for reference. **f)** Mesh representation of the axially symmetric rotational diffusion tensors for Ub from the UbcH5c-O~Ub conjugate (left, green) and the ternary complex with E4BU (middle, blue), and aligned and superimposed (right).

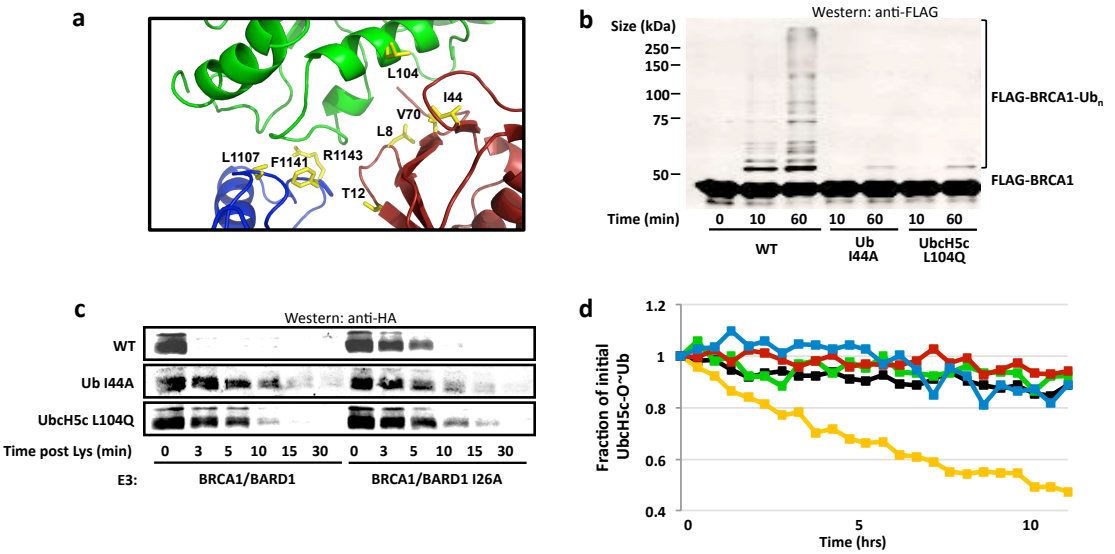

Figure 2. Mutations that disable RING/U-box E3-mediated UbcH5c~Ub conformational change disrupt activity. a) Close-up of protein-protein interactions within the ternary complex model. Residues chosen for mutation (yellow sticks) include E4BU F1141 and R1143, UbcH5c L104, and Ub L8, I44, V70, and T12. E4BU L1107 (mutation to Ala disrupts E3:E2 interaction) is shown for reference. **b)** Auto-ubiquitination activity assays with BC_{304}/BD_{327} and UbcH5c, as monitored by Western analysis following FLAG-BRCA1. Reaction components are WT except when indicated. c) Lysine reactivity assays with BC_{112}/BD_{140} and UbcH5c. Reaction components are WT except when indicated. Western blot for HA-Ub(K0) to monitor decay of the UbcH5c~HA-Ub(K0) conjugate is shown. Two reaction time courses are shown for each E2~Ub: on the left, time course in the presence of WT BC_{112}/BD_{140} and on the right, time course in the presence of I26A-BC_{112}/BD_{140}, which does not bind to UbcH5 (Brzovic et al., 2003). **d)** Time course of the hydrolysis of UbcH5c oxyesters in the presence and absence of E4BU, as followed by 1-D NMR. The y-axis shows the fraction of oxy-ester remaining, as measured by integration of the UbcH5c Asn77 resonance at its conjugated position. Curves for UbcH5c-O~Ub and E4BU:UbcH5c-O~Ub samples are presented in black and yellow, respectively. Replacement of WT components in the E4BU:UbcH5c-O~Ub complex with Ub^{I44A}, $UbcH5c^{L104Q}$, or $E4BU^{R1143A}$ are colored in red, green, and blue, respectively.

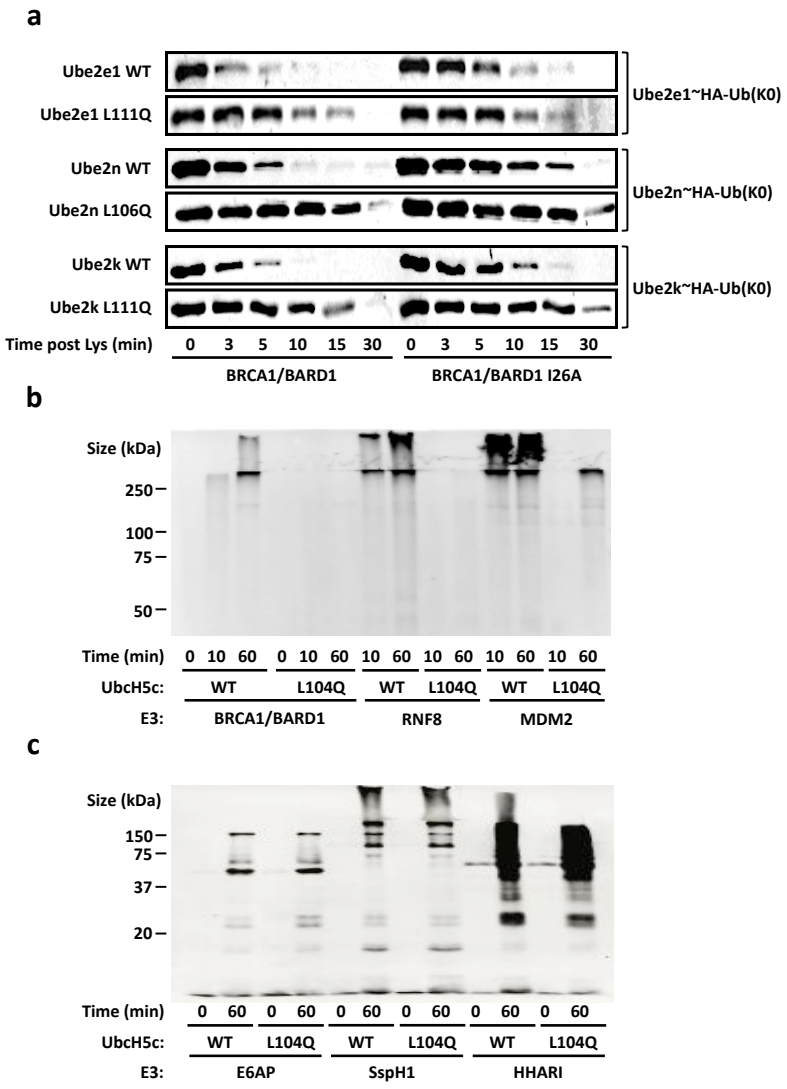

Figure 3. Conformational activation of the E2~Ub conjugate is required for RING/U-box E3 activity. a) Lysine reactivity assays for Ube2e1, Ube2n, and Ube2k with BC_{112}/BD_{140}. E2 identity is listed in column at left. Western blot for HA-Ub(K0) to follow decay of the E2~HA-Ub(K0) conjugate is shown. **b)** Auto-ubiquitination assays of RING/U-box E3s with UbcH5c^{WT} and UbcH5c^{L104Q}. Western blot following HA-Ub is shown. **c)** As in b), but with HECT-type E3s, as indicated.

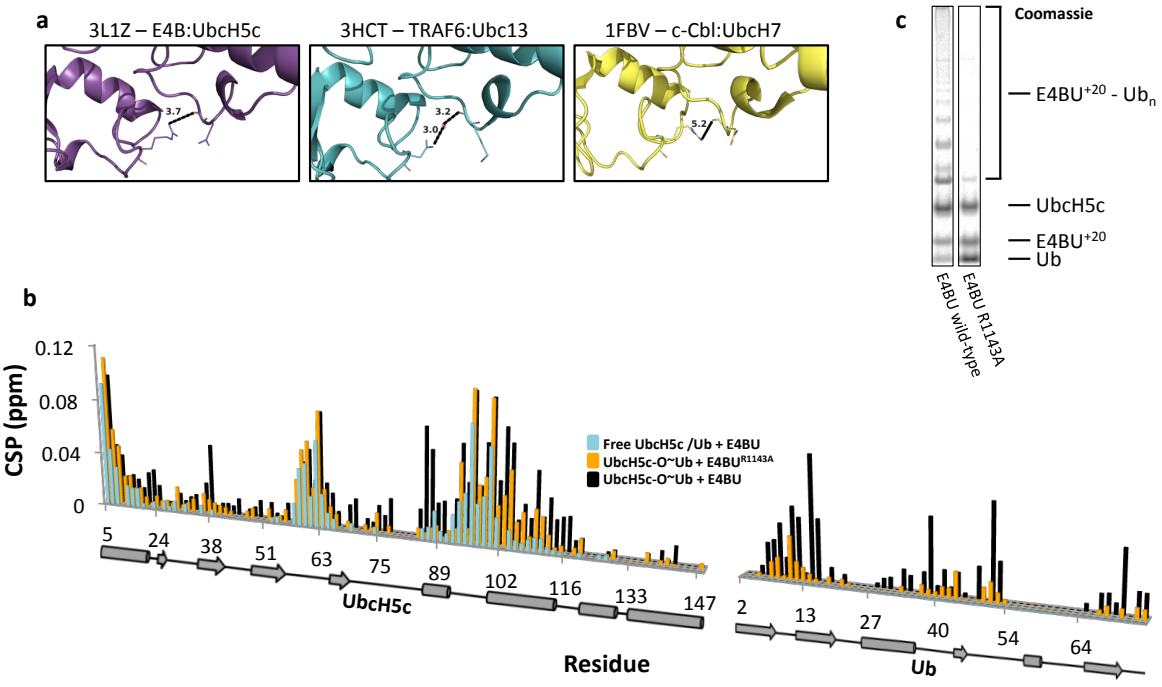

Figure 4. A conserved E3:E2 hydrogen bond is required for E3-mediated Ub transfer. a) Examples of RING/U-box E3:E2 interactions observed in deposited crystal structures include E4B:UbcH5c (3L1Z, left), TRAF6:Ubc13 (3HCT, center), and c-Cbl:UbcH7 (1FBV, right). 3L1Z represents the common case in which a conserved E3 basic residue directly hydrogen bonds the E2 backbone. TRAF6, which lacks the conserved basic residue, maintains this interaction through an ordered water molecule. In contrast, no hydrogen bond is observed in the c-Cbl:UbcH7 complex, which is in fact an inactive pair. **b)** Addition of 0.5 molar eq. of $E4BU^{R1143A}$ to ^{15}N-UbcH5c-O~^{15}N-Ub (orange) results in CSPs plotted in the histogram. 0.5 molar eq. titration points of $E4BU^{WT}$ into free ^{15}N-UbcH5c/Ub (cyan) and ^{15}N-UbcH5c-O~^{15}N-Ub (black) are shown for reference. **c)** $E4BU^{+20}$ auto-ubiquitination assays show that the $E4B^{R1143A}$ mutant is deficient in Ub transfer activity. Gel slices taken from figure S4B.

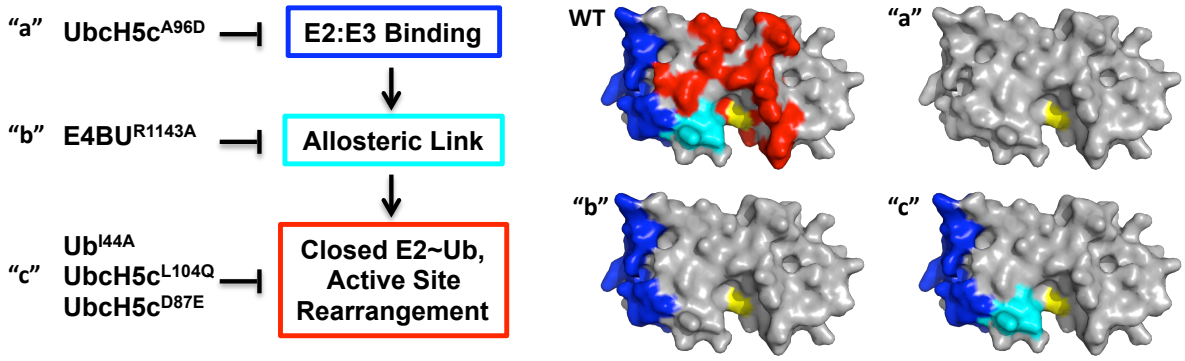

Figure 5. Allosteric activation by RING/U-Box E3s involves three discrete structural requirements. Formation of an active E3:E2~Ub complex depends on three structural requirements: 1) A consensus E3:E2 interaction at E2 Helix 1, Loop 4, and Loop 7 (reported by CSPs highlighted in dark blue), 2) Formation of an intermolecular E3:E2 hydrogen bond that causes secondary effects permeating through the E2 3_{10} helix (reported by CSPs highlighted in cyan), and 3) Overpopulation of closed E2~Ub conformations that result in additional changes surrounding the active site (reported by CSPs highlighted in red). Each requirement can be targeted with specific point mutations. Class "a" mutations such as UbcH5c Loop 7 A96D disrupt formation of the consensus E3:E2 interaction. The essential intermolecular hydrogen bond can be disrupted via a class "b" mutation such as E4B R1143A. Finally, formation of closed E2~Ub conformations can be blocked with class "c" mutations such as UbcH5c D87E, UbcH5c L104Q, or Ub I44A.

From To	UbcH5c	Ub	E4BU
UbcH5c	X	19, 20, 41, 42, 87, 91, 94, 98, 101, 104, 108, 111, 112, 114, 115, 116, 117, 119	4, 5, 7, 8, 11, 12,14, 15, 58, 59, 62, 63, 64, 94, 96, 98, 101
Ub	2, 8, 9, 10, 11, 12, 14, 16, 33, 35, 46, 47, 48, 49, 51, 66, 70, 72	X	2, 8, 9, 10, 11, 12, 14, 16, 33, 35, 46, 47, 48, 49, 51, 66, 70, 72
E4BU	18, 19, 20, 21, 22, 39, 42, 43, 46, 47, 49, 53, 55	18, 19, 32, 33, 34, 46, 47, 53, 54, 55, 56, 57	X

Supplemental Table 1. Ambiguous interaction restraints used as input for the modeling program HADDOCK are listed for each interacting surface within the E4BU:UbcH5c~Ub ternary complex. Affected regions of Ub were allowed to contact perturbed areas of either UbcH5c or E4BU without bias.

Sample	Ub τc (ns)	Dpar/Dper	theta	phi
UbcH5c-O~Ub	13.2 ± 0.2	1.29	1.0	0.34
E4BU:UbcH5c-O~Ub	14.4 ± 0.2	1.54	0.99	0.57

Supplemental Table 2. Axially symmetric rotational diffusion tensors for Ub. Parameters are presented for the diffusion tensors calculated with respect to a Ub model oriented to the inertial mass tensor for the protein.

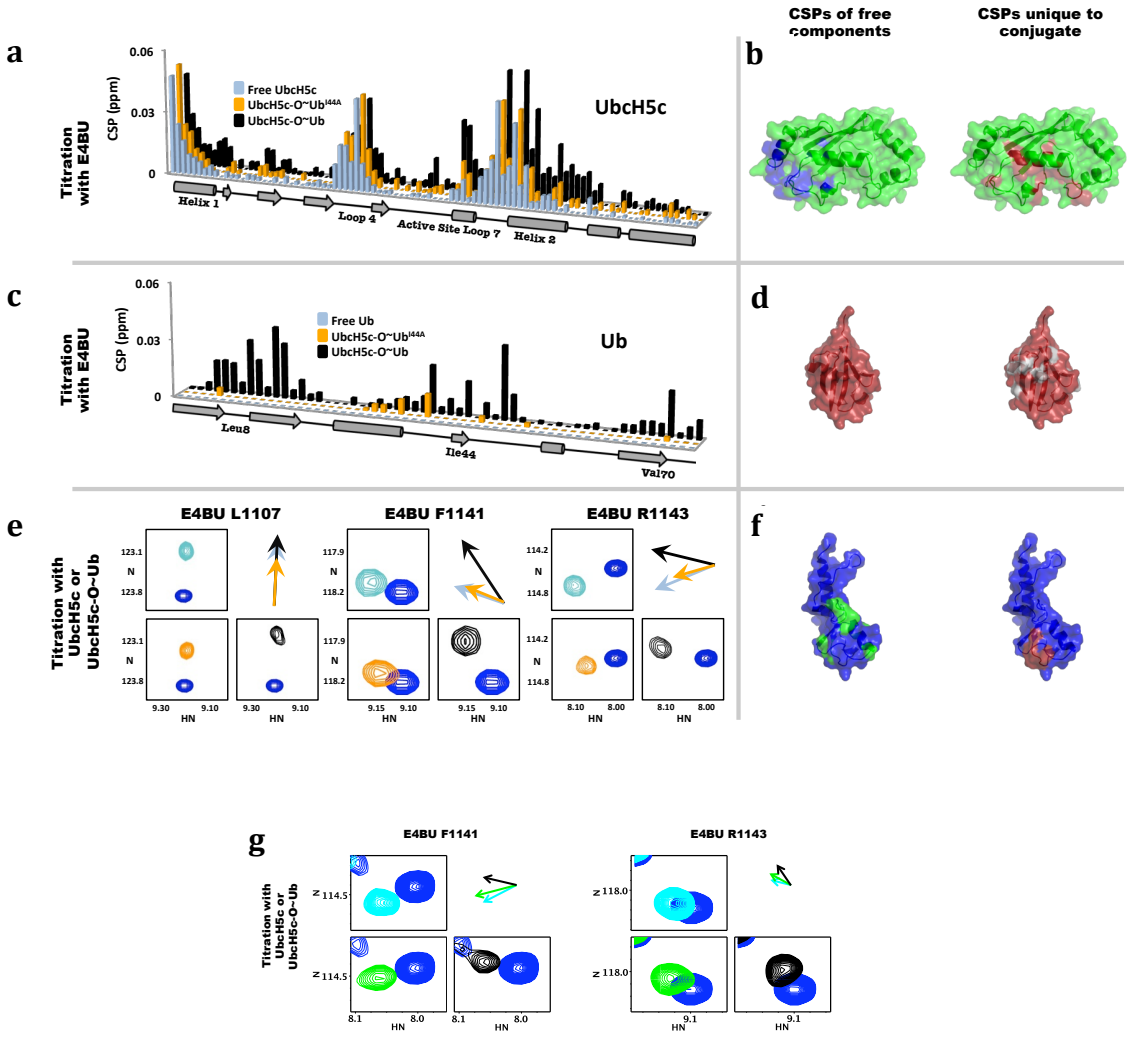

Supplemental Figure 1. NMR titration analyses reveal novel UbcH5c:Ub and E4BU:Ub interactions, related to Figure 1. Binding surfaces are colored based on the interacting partner, i.e. E4BU (blue) binds UbcH5c (green) at blue surface. Ub is colored in red. **a)** CSPs observed for titration of 0.25 molar eq. of E4BU into ^{15}N-UbcH5c (cyan), ^{15}N-UbcH5c-O~Ub (black), or ^{15}N-UbcH5c-O~Ub^{I44A} (orange) are plotted as histograms. **b)** Significant CSPs (> 1 sd from mean) arising from E4BU binding are mapped onto a cartoon/surface representation of UbcH5c (left). CSPs unique to the UbcH5c-O~Ub conjugate are mapped at right. **c)** As in a), for ^{15}N-Ub titrations. **d)** As in b), for ^{15}N-Ub. The interaction surface in the right panel is colored in grey, as perturbations could have arisen either from UbcH5c or E4BU contacts. **e)** CSP trajectories of representative E4BU residues upon titration with UbcH5c (cyan), UbcH5c-O~Ub (black), or UbcH5c-O~Ub^{I44A} (orange). Spectra are presented in sets of three; arrows indicate CSP vectors. E4BU L1107 is analogous to residue BRCA1 I26 and CHIP I235, located in Loop 1. E4BU F1141 and R1143 are located in Loop 2. **f)** Surfaces of E4BU affected by free UbcH5c and Ub are shown at left and right, respectively. **g)** As in e), for UbcH5c^{L104Q}~Ub (green).

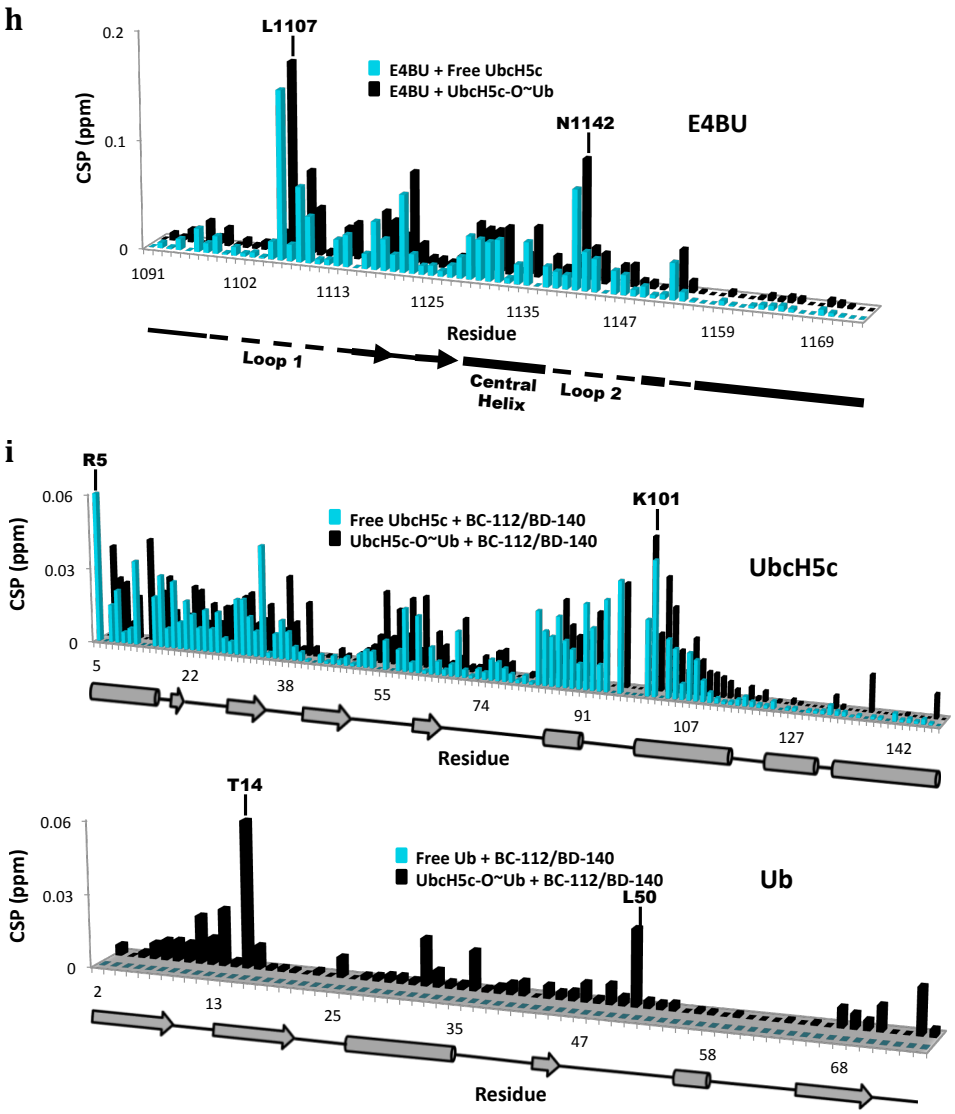

Supplemental Figure 1. h) CSPs observed for addition of 0.25 molar eq. of free UbcH5c (cyan) or UbcH5c-O~Ub (black) into ^{15}N-E4BU are shown in the histogram. The magnitude of CSPs are very similar, while different CSP trajectories are observed for E4BU Loop 2 residues, as presented in Fig. S1E. **i)** Residue-level histograms displaying CSP data observed upon addition of 0.5 molar eq. of BC_{112}/BD_{140} into ^{15}N-UbcH5c-O~^{15}N-Ub (black) are shown. CSP data for BC_{112}/BD_{140} is shown for addition of 0.5 molar eq. because addition of BC_{112}/BD_{140} results in less dramatic perturbation of UbcH5c resonances than addition of E4BU. Compared to equivalent data for free ^{15}N-UbcH5c and ^{15}N-Ub components (cyan), small shifts specific to the conjugate are observed in Helix 2 of UbcH5c (above) and throughout the Ile44 hydrophobic surface of Ub (below).

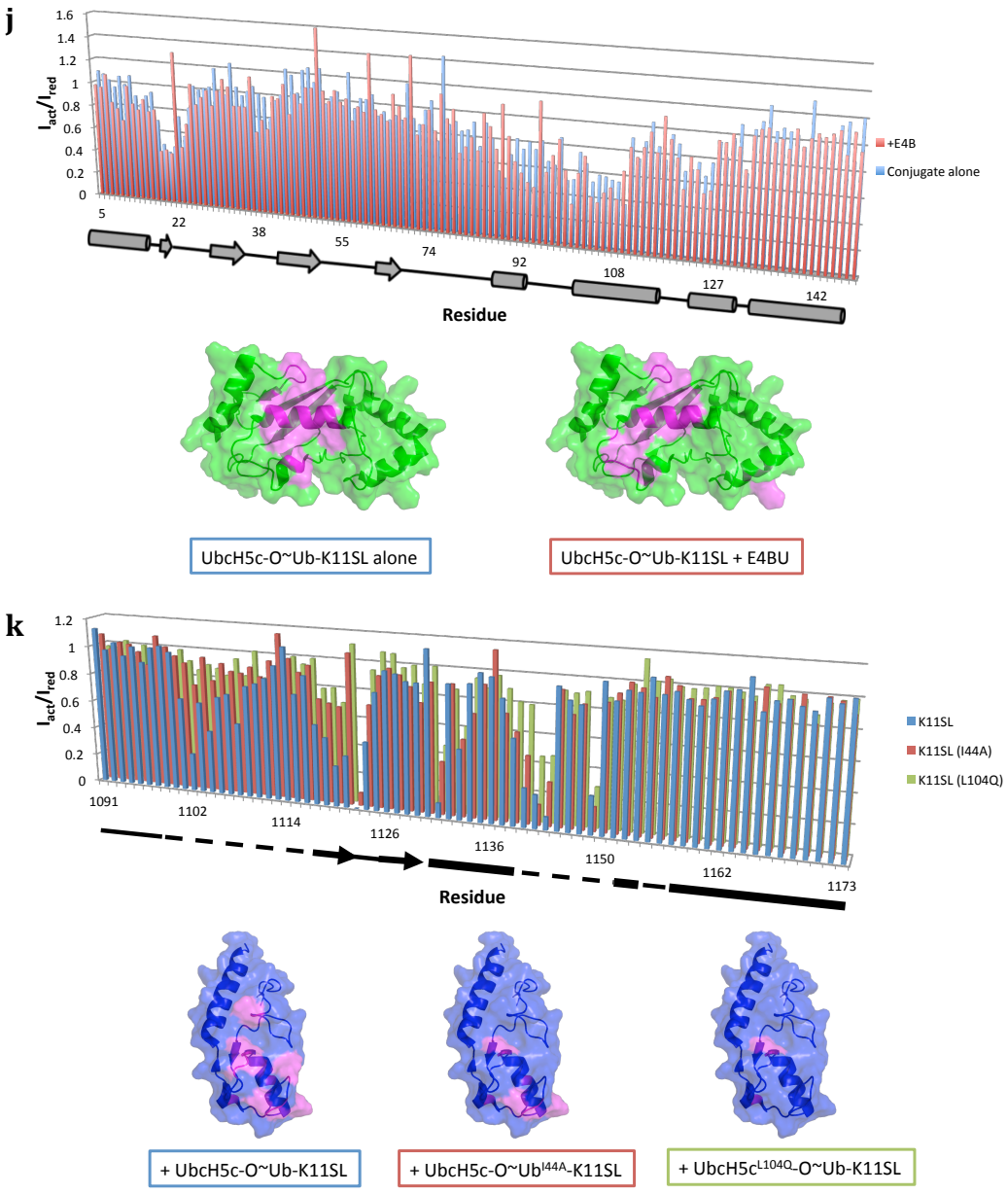

Supplemental Figure 1. j) I_{act}/I_{red} ratios are presented in residue-level histograms for ^{15}N-UbcH5c-O~Ub-K11SL in the absence (blue) and presence (red) of 0.5 molar eq. of E4BU. In complex with E4BU, the UbcH5c surface affected by the ~Ub-K11SL is slightly shifted toward Loop 7 (see structures below), consistent with the HADDOCK model. Residues in Loop 7 display an I_{act}/I_{red} ratio near 0.4, suggesting they are in close proximity to the paramagnetic probe. **k)** I_{act}/I_{red} ratios are presented in residue-level histograms for ^{15}N-E4BU in the presence of 0.5 molar eq. of UbcH5c-O~Ub-K11SL (blue). In the wild-type complex, paramagnetic effects encompassing E4BU Loop 1, the β1/β2 turn, Helix 1, and Loop 2 are observed. In matched experiments, replacement of wild-type components with Ub^{I44A} or $UbcH5c^{L104Q}$ resulted in I_{act}/I_{red} ratios plotted in red and green, respectively; paramagnetic effects in these samples are largely limited to E4BU Loop 2.

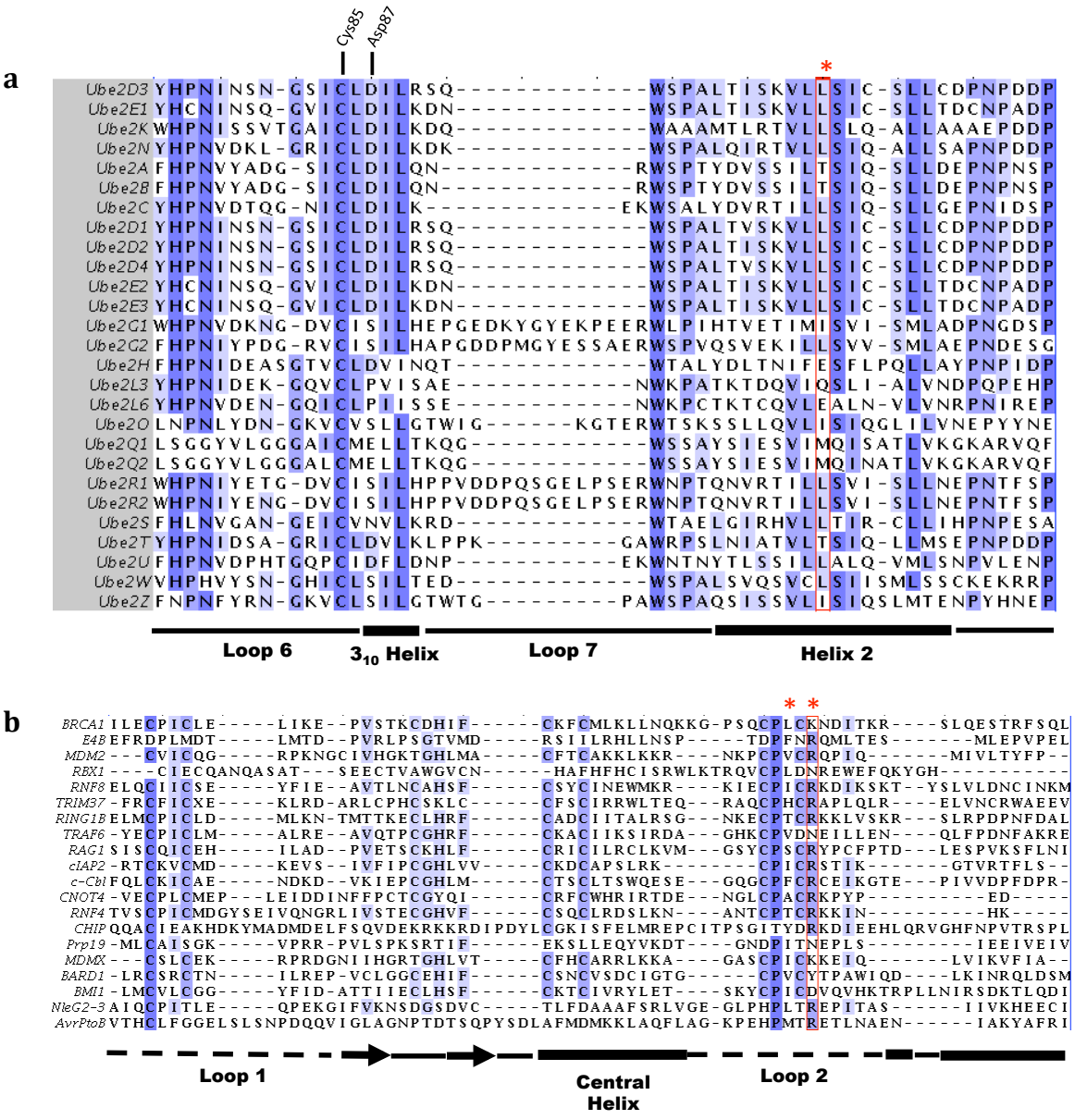

Supplemental Figure 2. Residues required for E3-mediated activation of E2~Ub conjugates are conserved, related to Figures 2 and 3. a) Sequence alignment of 27 human E2s based upon UbcH5c residues 74-118. The UbcH5c Leu104 position is denoted by a red asterisk. Other positions are marked with UbcH5c residue numbering. Notable exceptions to the conservation at UbcH5c position 104 are Ube2L3 and Ube2L6, neither of which have been shown to be active with RING/U-box E3 ligases. **b)** Sequence alignment of 20 well-characterized and functionally diverse RING/U-box domains. The highly conserved Φ-x-(K/R) motif is highlighted, with BRCA1 positions 63 and 65 denoted by red asterisks. Notable exceptions to the conservation are BARD1 and Bmi1, which are reported to be inactive partners within heterodimeric E3 ligases. Additional conservation in the bacterial effector U-boxes NleG and AvrPtoB suggest convergent evolution of this loop.

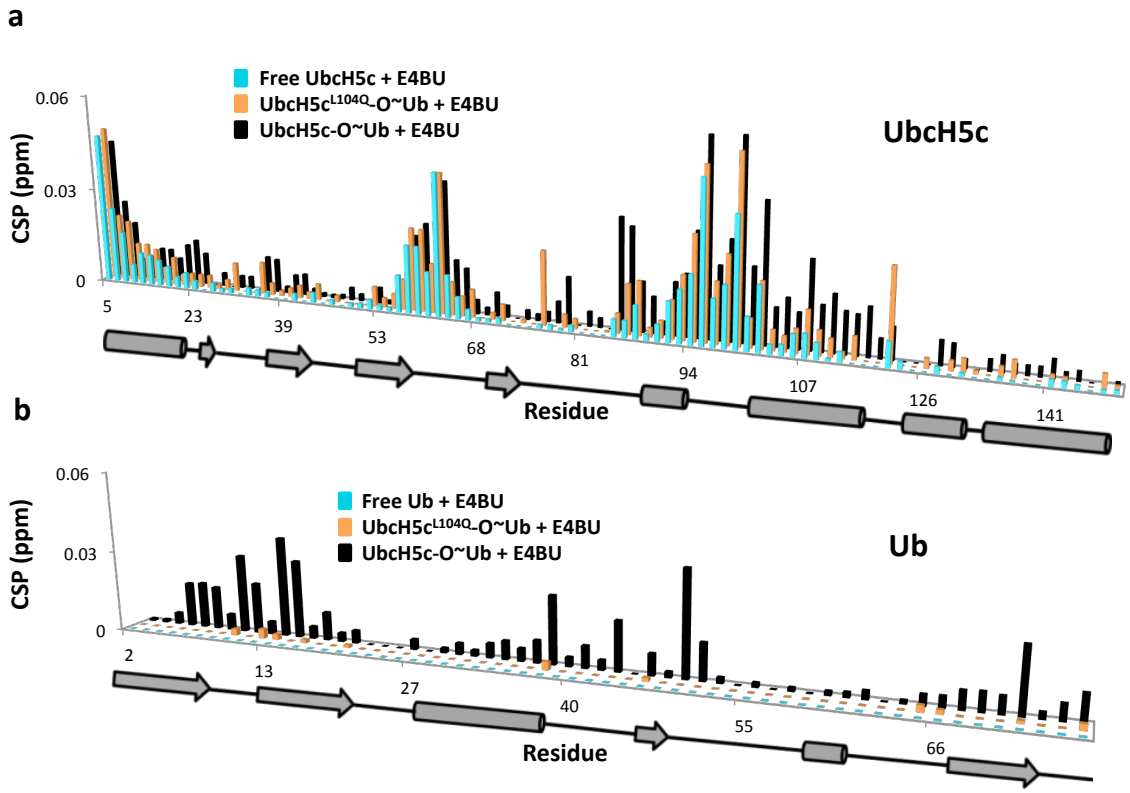

Supplemental Figure 3. **Titration of E4BU into UbcH5c^{L104Q}-O~Ub does not elicit CSPs in UbcH5c Helix 2 or in the Ub Ile44 surface, related to Figure 2.** Residue-level histograms of CSPs observed upon addition of 0.25 molar eq. of E4BU to the ^{15}N-UbcH5c^{L104Q}-O~^{15}N-Ub conjugate (orange) are more similar to free UbcH5c and Ub components (cyan) than to the wild-type conjugate (Fig. 1a). **a)** CSPs for ^{15}N-UbcH5c. **b)** CSPs for ^{15}N-Ub.

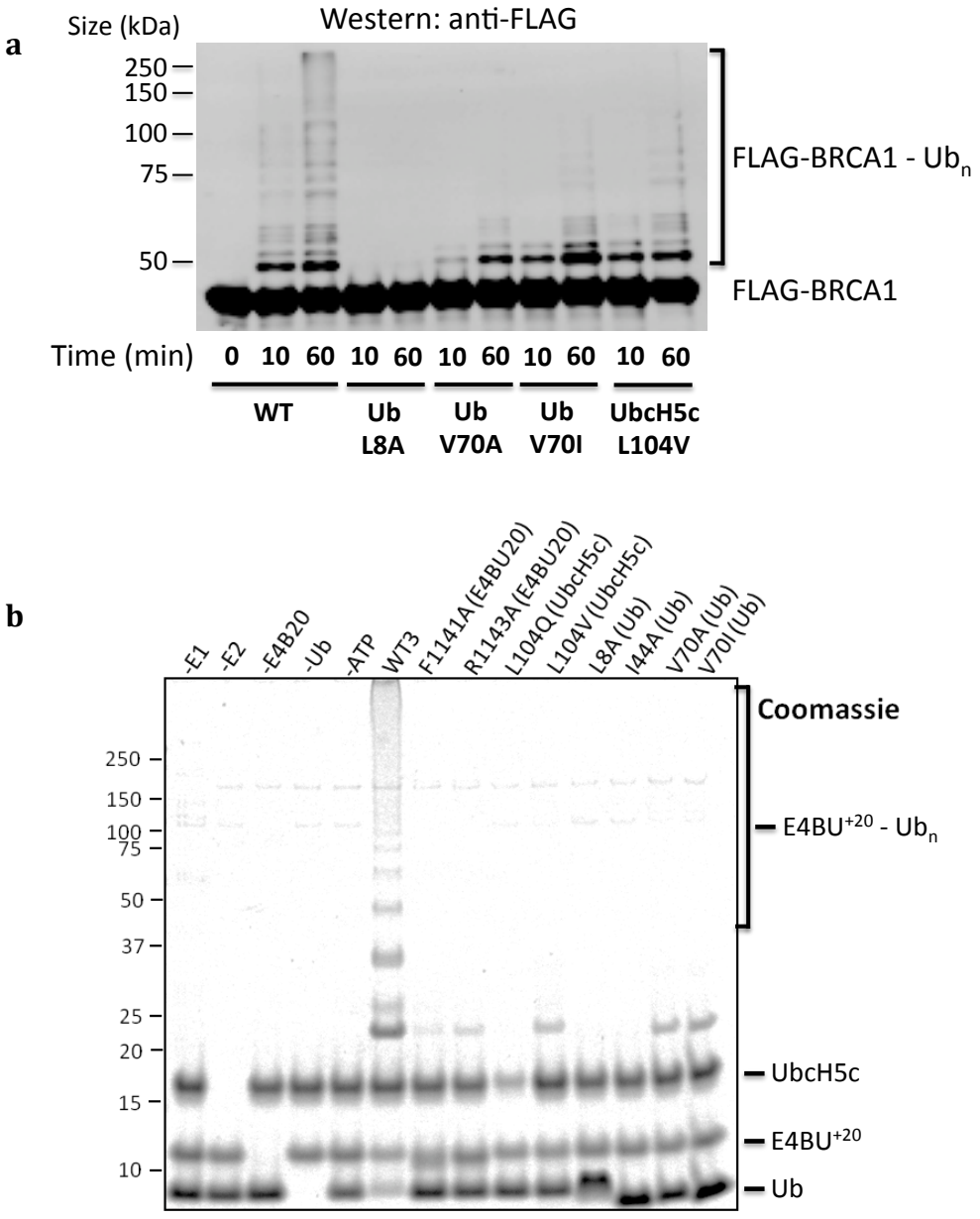

Supplemental Figure 4. Structure-based mutations disrupt E3-mediated Ub transfer, related to Figure 3. a) Mutations within the Ub Ile44 hydrophobic surface (L8A and V70A) result in low or absent BC_{304}/BD_{327} auto-ubiquitination, as detected by Western blotting for the BRCA1-FLAG tag. The more conservative mutations Ub V70I and UbcH5c L104V show intermediate levels of ubiquitin transfer activity. **b)** Ub and UbcH5c point mutants that disrupt BC_{304}/BD_{327} auto-ubiquitination show similar effects with E4BU^{+20}. Specifically, Ub -L8A, -I44A, UbcH5c -L104Q, and E4BU^{+20} -F1141A, -R1143A abrogate E4BU^{+20} auto-ubiquitination activity. Ub -V70A, -V70I, and UbcH5c -L104V show varying levels of intermediate activity.

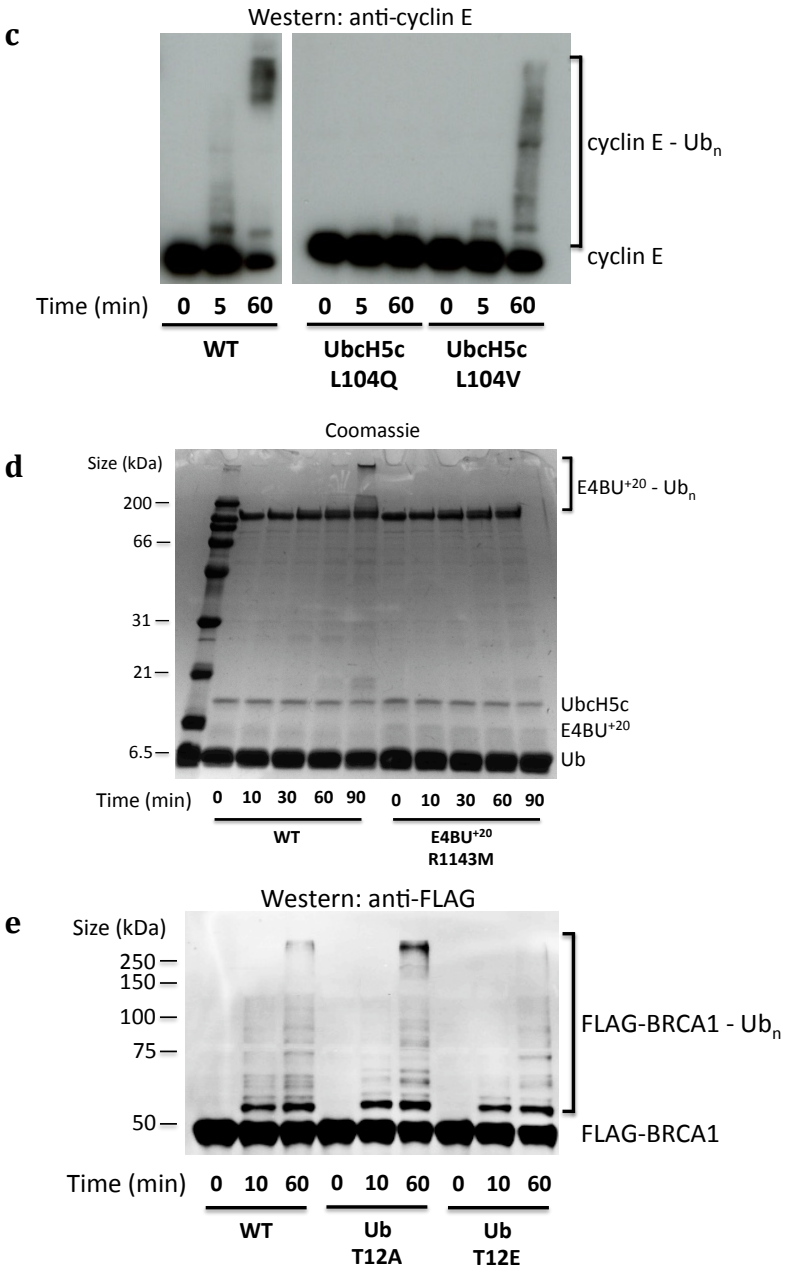

Supplemental Figure 4. c) SCF^{Fbw7} ubiquitination of cyclin E is dependent upon formation of UbcH5c~Ub closed conformations. Briefly, Myc-tagged Cyclin E generated in 293A cells was incubated with 1μM Nedd-CR1, 134nM Fbw7, 770nM GST-E1, 190nM UbcH5c, 75μM Ub, 2mM ATP, 10mM $MgCl_2$, and 50nM Velcade. Reaction samples were separated by SDS-PAGE and probed for Myc-tagged Cyclin E using 9E10 antibody. *In vitro*, the UbcH5c L104Q mutation abrogates SCF^{Fbw7}-dependent ubiquitination of substrate cyclin E. The more conservative mutation L104V displays an intermediate level of ubiquitin transfer activity. **d)** Mutation of the hydrogen bond donor residue $E4BU^{+20}$ Arg1143 to Met results in a loss of Ub transfer activity. **e)** Ubiquitin mutations Thr12Ala and Thr12Glu had no effect on BC_{304}/BD_{327} Ub transfer activity, despite the proximity of Ub Thr12 to E4BU Loop 2 within the ternary complex model.

a

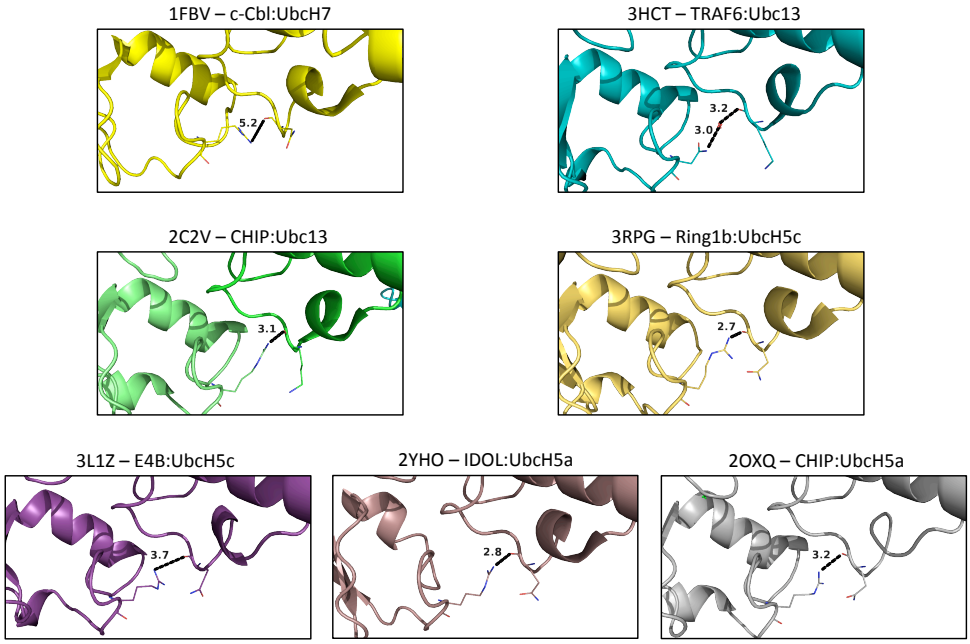

b

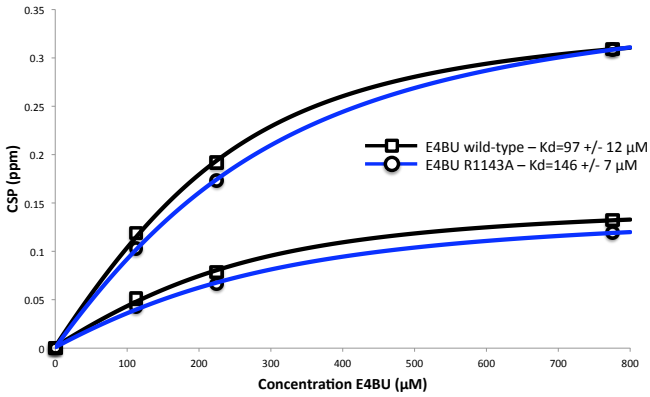

Supplemental Figure 5. RING/U-box E3:E2 crystal structures reveal a conserved hydrogen bond interaction, related to Figures 4 and 5. a) Cartoon representations are shown for the 1FBV (2.90Å resolution), 3HCT (2.10Å), 2C2V (2.90Å), 3RPG (2.65Å), 3L1Z (3.17Å), 2YHO (2.10Å), and 2OXQ (2.90Å) crystal structures. In each structure, a conserved E3 residue at the third position of the Φ-x-(K/R) motif serves as a hydrogen bond donor to a backbone carbonyl in Loop 7 of the E2 (shown as sticks). TRAF6 carries a shorter Asn side chain at this position and the hydrogen bond is mediated through an ordered water molecule. Notably, the conserved Arg in the inactive c-Cbl:UbcH7 complex is too far from the E2 to form a hydrogen bond. **b)** E4BU$^{wild\text{-}type}$ and E4BU^{R1143A} were independently titrated into ^{15}N-UbcH5c (C85S S22R) to saturation. Kd values were calculated for the complex using NMRViewJ to fit quadratic equations to the binding curves of at least ten resonances from each dataset. The quadratic equation used is: f = A+(C-A)*(((p+x+10^B)-((p+x+10^B)^2-4*p*x)^0.5))/(2*p), where p is the concentration of UbcH5c. Representative data and fits are shown for two titrating UbcH5c peaks. Error is reported as the average standard deviation determined from the quadratic fits.

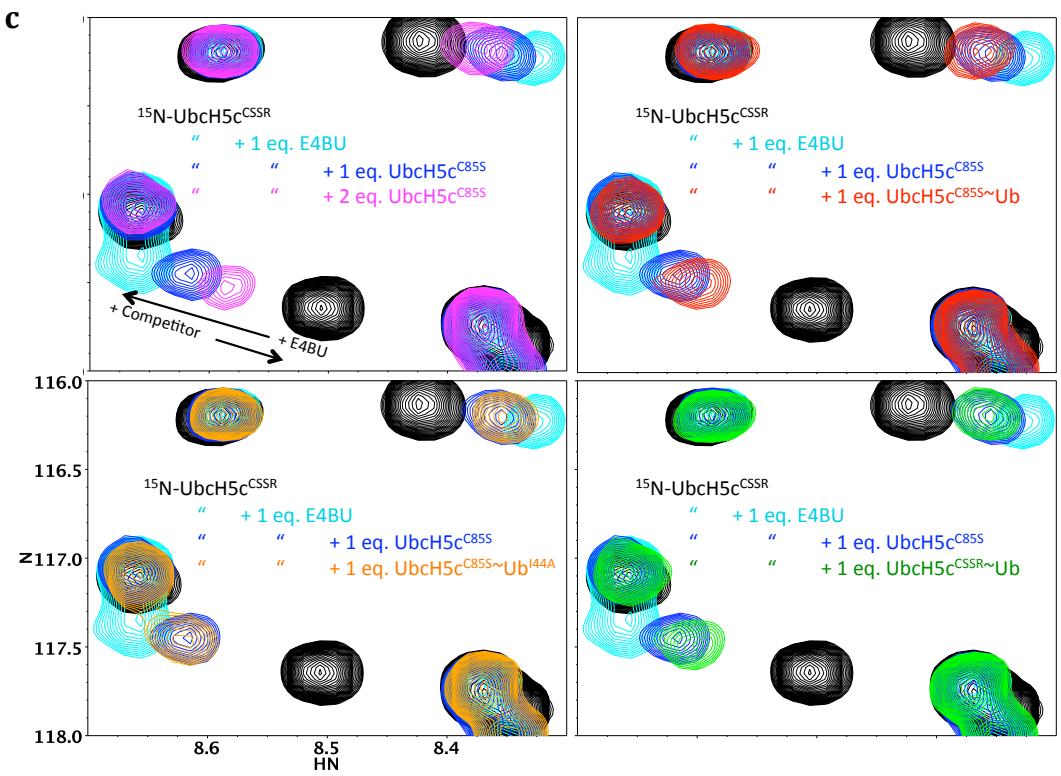

Supplemental Figure 5. c) In lieu of performing traditional NMR titration experiments to determine a Kd for E4BU binding the UbcH5c-O~Ub conjugate (which undergoes significant hydrolysis at high concentrations of E4BU), competition assays were performed to compare the affinity relative to free UbcH5c. Select resonances of ^{15}N-UbcH5c^{CSSR} (black) undergo large CSPs upon addition of 1 molar equivalent of E4BU (cyan). Further addition of 1 (blue) or 2 (magenta) equivalencies of unlabeled UbcH5c^{C85S} results in a "back-titration" of resonances as the ^{15}N-labeled and natural abundance UbcH5c molecules compete for E4BU binding. Addition of 1 equivalent of either UbcH5c^{C85S}~Ub (red), UbcH5c^{C85S}~Ub^{I44A} (orange), or UbcH5c^{CSSR}~Ub (green) conjugates result in similar levels of competition to free UbcH5c^{C85S}, indicating comparable binding affinities.

Chapter IV - Activity-enhancing mutations in an E3 ubiquitin ligase that increase E2 binding affinity or allosteric activation

Starita, L. M.*, **Pruneda, J. N.***, Lo, R. S., Fowler, D. M., Hiatt, J. B., Shendure, J., Brzovic, P. S., Fields, S., and Klevit, R. E.

*These authors contributed equally

Author Contributions

L.M.S. performed phage, auto-ubiquitination, and cell-based experiments with the assistance of R.S.L. J.N.P. performed NMR and structure-based analyses, in addition to the lysine reactivity assays. D.M.F. assisted with analysis of the deep mutational scan. J.B.H. and J.S. provided subassembly algorithms and assisted with sequencing analysis. L.M.S., S.F., J.N.P., P.S.B. and R.E.K. designed and interpreted experiments and wrote the manuscript.

Abbreviations: Ub, ubiquitin; E2, ubiquitin-conjugating enzyme; E3, ubiquitin ligase; E1, ubiquitin-activating enzyme; RING, Really Interesting New Gene; HECT, Homologous to E6AP Carboxy Terminus; NMR, nuclear magnetic resonance; CSP, chemical shift perturbation.

Introduction

Covalent modification of proteins by ubiquitin (Ub) impacts nearly all of eukaryotic cell biology. Attachment of Ub onto a substrate lysine is accomplished by three enzymes: an E1 Ub-activating enzyme, E2 Ub-conjugating enzyme, and an E3 Ub ligase[1]. Minimally, E3s consist of an E2-binding domain and a substrate-recognition domain. The majority of E3s use either a RING domain or a related U-box domain to bind to a cognate E2. E3s are thought to facilitate Ub transfer by juxtaposing a substrate and an E2~Ub conjugate. An additional allosteric role has been recently demonstrated for RING/U-box domains in the activation of E2~Ub conjugates for transfer[2,3]. Allosteric activation relies on a conserved intermolecular hydrogen bond between a conserved E3 side chain and an E2 backbone carbonyl that promotes the catalytically active "closed conformations" of the E2~Ub complex[2]. Despite conservation of the intermolecular hydrogen bond among E3:E2 co-crystal structures, E3 ligases display large differences in Ub transfer activity even when working with the same E2. Such differences raise the question: what other structural features of an E3 ligase dictate its ability to enhance Ub transfer?

Traditional approaches that involve detailed structural studies and targeted mutational analyses are limited by the number of mutants that can be analyzed. Typically, the mutations that are made disrupt activity and are often restricted to protein:protein interfaces, thereby missing much of possible sequence space. These limitations prompted us to employ a high-throughput method, known as "deep mutational scanning"[4,5], that can assess the effects of over 10^5 sequence variants of a single protein. We applied this method to generate a sequence-function map of the murine U-box E3 ligase Ube4b. The U-box domain of Ube4b is an ideal candidate for this approach because it functions as a monomer, its structure has been solved both in isolation and in complex with an E2, and it exhibits auto-ubiquitination activity *in vitro*[6,7]. *In*

vivo, the human homolog UBE4B polyubiquitinates the tumor suppressor p53 to target it for degradation by the proteasome. Increased expression of UBE4B and amplification of the genomic locus of *UBE4B* have been found in patient-derived medulloblastoma tumors that also have lower levels of p53[8], suggesting that increased UBE4B activity might be oncogenic via its ability to reduce p53 abundance.

We assessed the Ub ligase activity of nearly 100,000 unique protein variants of the U-box domain, over 900 of which contained single amino acid substitutions. Although most single mutations reduced enzymatic activity, a few mutations greatly increased activity, both in *in vitro* auto-ubiquitination reactions and in promoting the degradation of p53 in a human cell line. We used NMR to characterize activity-enhancing mutations, and found two classes: one class enhances E2~Ub catalysis by increasing E3:E2 binding affinity and the other augments the allosteric capacity of the U-box to promote catalytically active E2~Ub conformational states. These two classes of mutations are distinct and mutations from both classes can be combined to enhance activity even further. The Ube4b-activating mutations further define the molecular basis for E3-induced E2~Ub allosteric activation and provide tools for future structural and functional studies of E3 ligases.

Results

Sequence–function map of the Ube4b U-box domain

Deep mutational scanning uses a protein display format in which a large library of protein variants is placed under selection for the activity of interest, and their identity and frequency in the population before and after selection is determined by high throughput DNA sequencing. To perform a deep mutational scan of an E3 ligase domain, we fused the carboxy-terminal U-box

domain (102 amino acids) of Ube4b, termed longE4BU, to T7 bacteriophage coat protein for display. This U-box domain was chosen because it folds independently (Fig. 1a) and is sufficient in the presence of an E1, E2, and Ub for auto-ubiquitination activity. *In vitro* auto-ubiquitination assays confirmed that longE4BU fused to the carboxy-terminus of the T7 bacteriophage coat protein is an active Ub ligase (Fig. 1b, lane 1 and Figs. S1a and S1b), and that mutation of a residue that is critical for E3 function (L1107A)[9] abrogates activity with UbcH5c (Figs. 1b). As a proof of principle, we found that wild type T7-longE4BU phage were preferentially selected over their L1107A counterparts when immunoprecipitated with an antibody against tagged ubiquitin, and that this selection was E2-dependent (Fig. S1c).

We created and sequenced[10] a library of phage that express longE4BU variants containing on average two nucleotide mutations per variant (Figs. S2a and S2b). Using 163,829 unique protein variants identified from sequencing, we performed successive rounds of selection for Ub ligase activity. Each round of selection consisted of *in vitro* phage auto-ubiquitination reactions with an E1, the E2 UbcH5c, and Flag-Ub, followed by enrichment on anti-Flag agarose beads and reamplification in *E. coli* (Fig. 1c). We determined the frequency at which each variant was present in the starting population and in the population after 3 rounds of selection. The ratio of the selected frequency of each variant versus its starting frequency, called here "enrichment ratio" or *E*, provides a measure of the performance of each variant during the selection for E3 function.

We were able to calculate enrichment ratios for 98,289 unique protein variants after three rounds of selection. These included 932 with one mutation, 54,507 with two, and 42,850 with three or more. The $\log_2$-transformed enrichment ratio for each single variant is represented in a sequence–function map (Fig. 2a). Mutations in loops 1 and 2 and helix 1 of the E4BU structure

were more likely to be deleterious than mutations in other portions of the domain, whereas residues near either the amino- or carboxy-terminus of longE4BU were more tolerant to mutation (Mann-Whitney U test, p = 2.2 x10-16). The importance of Ube4b positions L1107 (buried in the E3:E2 interface) and R1143 (forms the hydrogen bond necessary for activation of the E2) was recapitulated in this screen, as illustrated by their sensitivity to mutation.

Positions with high variance in *E* indicate that both enriching and depleting mutations occur at the same site (Fig. 2b). High variances suggest that the mutations with the highest enrichment ratios are specific because these mutations occur at positions that are not tolerant to random amino acid changes. The highest variance occurs at M1124 followed by S1097, L1107, T1122, D1139, and N1142. The functional importance of some of these residues was further illustrated by the ability of enriched mutations at these positions (M1124L, M1124I, M1124V, D1139N, F1141Y and N1142T) to rescue detrimental mutations when an enriched and detrimental substitution combined in the same variant (Fig. S2c).

Highly enriched mutants are more active E3 ubiquitin ligases

To characterize the functional importance of mutations in highly enriched variants, we expressed and purified variant longE4BU domains and examined their ability to catalyze auto-ubiquitination *in vitro*. Equal concentrations of wild type and mutant U-boxes (Fig. S3a) were incubated with E1, UbcH5c, ATP/Mg, and Flag-tagged Ub over a time course from 1 to 30 minutes. For wild type longE4BU, high-molecular weight proteins bearing Flag-tagged Ub were visible after 7 minutes. The L1107A mutant, which was depleted in the phage assay, had no observable auto-ubiquitination activity (Fig. 3a). In contrast, almost all the variants that were enriched relative to wild type in the phage assay also exhibited enhanced ubiquitination activity

in vitro. The longE4BU variants L1107I, M1124V, D1139N, F1141Y, and N1142T all produced high-molecular weight ubiquitinated species within 3 minutes (Fig. 3a). The disappearance of Ub during the course of the assay was detected by Coomassie staining and quantified by densitometry to calculate approximate half-lives for each of the ubiquitination reactions (Fig. S3b). Approximate half-lives calculated for the *in vitro* auto-ubiquitination reactions correlated with *E* values determined from the phage assay, with the exception of the L1077R and Q1144A variants (Fig. 3a). Although the L1077R and Q1144A variants showed no improvement in ligase activity despite their high *E* scores in the phage assay, these mutations occur at positions that were tolerant to many amino acid changes, as judged by low variance values compared to their activating counterparts (Fig. 2b). The L1077R mutation also could not rescue deleterious mutations (Fig. S2c). Although the high *E* scores for the single mutants were predictive of high *in vitro* activity for 5 of 7 variants tested, the combined information gleaned from *E* values, variance, and rescue scores more accurately predicted the effect of mutations on protein function.

As activity-enhancing variants are generated by conservative amino acid changes, we sought to determine if the same mutations have arisen in the Ube4b U-box domain throughout evolution. Analysis of multiple sequence alignments of Ube4b across species shows that substitutions equivalent to L1107I, M1124V, D1139N, and N1142T all exist in metazoans[11]. To determine if these amino acids occur at the same position in other U-box domains, we compared an alignment of the seven murine U-box containing proteins. Ube4a contains the equivalent of the L1107I and M1124V mutations; Cyc4 the equivalent of the D1139N mutation; and CHIP, Cyc4, Uip5, and Wdsub1 the equivalent of the N1142T mutation (Fig. 3b). Thus, the positions of mutations that enhance the activity of Ube4b may represent sites at which E3 activity has been fine-tuned through evolutionary history. The positions of the L1107I, M1124V, D1139N, and

N1142T mutations are highlighted on the structure of E4BU bound to UbcH5c (Fig. 3c): L1107 is in loop 1 and directly contacts the E2, M1124 is buried behind loops 1 and 2 and helix 1, and D1139 and N1142 are located in loop 2, away from the E2 interface.

To further assess the activating effects of the M1124V, L1107I, D1139N, and N1142T mutations, we used a simplified assay to test the ability of E4BU mutants to activate UbcH5c for Ub transfer. A shorter E4BU domain, which lacks the residues in longE4BU that allow auto-ubiquitination of the E3, was incubated with pre-formed UbcH5c~Ub and the free amino acid lysine. In the absence of an E3, the UbcH5c~Ub conjugate reacted slowly with lysine, with conjugate still observed after a 15-minute incubation. Addition of wild type E4BU significantly enhanced reactivity, with most of the ubiquitin reacted with lysine by 5 minutes (Fig. 3d). The M1124V, L1107I, D1139N, and N1142T E4BU mutants all demonstrated increased activation of the UbcH5c~Ub conjugate toward lysine compared to wild type, with most of the E2~Ub consumed by the 3-minute time point (Fig. 3d).

The effects of some E3 activating mutations are synergistic

Based on the large positive *E* scores for the double mutants M1124V/D1139N, M1124V/N1142T, and D1139N/N1142T (40.1, 106.5, and 96.3, respectively), we further characterized the activity of U-boxes that combine two activating mutations. *In vitro* auto-ubiquitination assays revealed that combining the M1124V mutation with either the D1139N or N1142T mutation resulted in more rapid Ub transfer activity than any of these single mutations on their own. Combining the D1139N and N1142T mutations also enhanced ligase activity, with high-molecular weight poly-Ub products visible after only 1 minute of incubation (Fig. 4). Quantitation of the free Ub band in Coomassie-stained gels as a function of reaction time

show Ub was consumed with a half-life of approximately one minute by both the M1124V/N1142T and D1139N/N1142T double mutants--considerably faster than the nearly 22 minute half-time of the reaction catalyzed by wild type E4BU (Fig. 3a). The rate enhancement observed for the M1124V/N1142T and D1139N/N1142T mutants (i.e., $k_{obs}(E4BU_{mutant})/k_{obs}(E4BU_{wild\ type})$) corresponds to a $\Delta\Delta G^{\ddagger}$ of ~2 kcal/mol. For comparison, the rate enhancement for addition of wild type E4BU to an otherwise uncatalyzed UbcH5c~Ub hydrolysis reaction corresponds to a $\Delta\Delta G^{\ddagger}$ of approximately 1 kcal/mol[2]. The rate enhancements observed for double mutants incorporating M1124V, D1139N, or N1142T correspond to more than the sum of the individual mutations' rate enhancements ($\Delta\Delta G^{\ddagger}$ values ranging from 0.5 to 1 kcal/mol), indicating that these mutations work in synergy. However, not all combinations of enhancing mutations further increase activity. The L1107I/M1124V double mutant exhibited activity below the level observed for the L1107I mutant alone (Fig. 4). Therefore, some but not all combinations of mutations are synergistic.

Classification of activating mutations that enhance E4BU ligase activity

We sought to determine the structural bases for the enhancements in ligase activity due to the activating mutations. Circular dichroism (CD) spectra of purified wild type E4BU and the four mutants showed similar secondary structure (Fig. S4a) and stability toward thermal denaturation (Fig. S4b). L1107, D1139, and N1142 are positioned in and around the E2-binding site, raising the likely possibility that mutations at these positions would alter this interaction. An NMR-HSQC spectrum of E4BU with the most buried mutation, M1124V, showed a number of changes centered around the site of the mutation that map to E4BU loops 1 and 2, suggesting a potentially altered E2-binding interface (Fig. S4c). The capacity of each

E4BU variant to bind UbcH5c was assessed using ^{1}H, ^{15}N HSQC-TROSY experiments in which increasing quantities of E4BU were titrated into ^{15}N-UbcH5c. The spectra confirm that each E4BU variant binds to the same E2 surface comprised of residues in helix 1, loop 4, and loop 7 of UbcH5c (Fig. 5a). However, the magnitude and character of the chemical shift perturbations (CSPs) differed among E4BU mutants. While the D1139N and N1142T mutants exhibited fast exchange behavior similar to wild type E4BU, both the L1107I and M1124V mutants had shifted toward the intermediate exchange regime, indicating a longer lifetime of the E4BU:UbcH5c complex (Fig. 5b).

To quantify the differences, we fit CSPs of a minimum of ten resonances from each titration to quadratic binding equations to calculate K_d values (Fig. S5a). Wild type E4BU and the D1139N and N1142T mutants bind UbcH5c with similar affinity (K_d ~99, 98, and 70 μM, respectively) whereas the L1107I and M1124V mutants bind with higher affinity (K_d ~14 and 17 μM, respectively) (Fig. 5c). Therefore, we classify the L1107I and M1124V variants as enhanced E2-binding mutants. Combination of these two mutations, L1107I/M1124V, had no additional effect on binding (K_d ~21 μM) as compared to the individual mutations. Similarly, the double mutant D1139N/N1142T had an E2 binding affinity that was unchanged from either single mutant (Kd ~100 μM) (Fig. 5a). Combining the E2-binding mutation M1124V with D1139N, which did not affect binding, yielded a double mutant that binds UbcH5c with an intermediate affinity relative to the two single mutants (K_d ~77 μM), suggesting that mutation of the buried Met side chain may have a complicated effect on loops 1 and 2 of the E2 binding interface, as might be expected from the widespread changes observed in the HSQC NMR spectrum of such a mutant (Fig. S4c).

As enhanced binding affinity for the E2 *per se* does not provide an explanation for the activity enhancement of some E4B mutants, we asked whether the variants have altered interactions with the E2~Ub conjugate. NMR experiments with the UbcH5c~Ub conjugate can provide a direct observation of interactions involved in Ub transfer but are complicated by the reactivity of the UbcH5c~Ub thioester bond. We used the active site cysteine-to-serine mutation to create the more stable oxyester-linked UbcH5c-O~Ub conjugate[12]. A subset of resonances in the UbcH5c-O~Ub spectrum serve as indicators for assembly of an active E4BU:UbcH5c~Ub ternary complex. These indicators correspond to residues within the closed UbcH5c-O~Ub interface (Ub V70 and UbcH5c D112) and a residue within the E2 active site (UbcH5c N77), all of which undergo CSPs upon addition of E4BU[2]. Addition of 0.25 molar equivalents of each E4BU variant (L1107I, M1124V, D1139N, and N1142T) to ^{15}N-UbcH5c-O~Ub increased the magnitude of CSPs in these resonances beyond those observed for addition of wild type E4BU (Fig. 5d, 5e). In contrast, addition of the R1143A mutant, in which the hydrogen bond required for allosteric activation of UbcH5c~Ub is lost, failed to elicit CSPs in the indicators of an active E3:E2~Ub conformation (Fig. 5d, 5e).

Each of the four mutants showed increased formation of closed, active E2~Ub conformations, with the D1139N and N1142T mutants exhibiting the strongest induction of these states (Fig. 5e). Larger closed-state-specific CSPs observed upon addition of sub-stoichiometric amounts of the D1139N and N1142T mutants could arise for two reasons: 1) a higher binding affinity for the E2~Ub conjugate; or 2) more effective induction of the closed-states upon binding. To distinguish between these two possibilities, we performed NMR binding assays with the most highly active variant, the D1139N/N1142T double mutant (Fig. 4). To test if the mutant U-Box has an affinity for free ubiquitin, the E4BU double mutant was added in large

excess over free ^{15}N-Ub. No interaction was detected (Fig. S5b). In an NMR experiment in which the ability of the mutant to compete with wild-type E4B for binding to UbcH5c-O~Ub was assessed, the double mutant outperformed the wild type U-Box (Fig. S5b). The enhancement is modest, with binding simulations estimating an approximately 3-fold enhancement in binding affinity over wild type. This difference corresponds to a $\Delta\Delta G$ of less than 1 kcal/mol. Such a difference does not account for the ~25-fold increase in activity observed for this mutant, which corresponds to a $\Delta\Delta G$ for activation of ~2 kcal/mol. Thus, it appears that the D1139N and N1142T mutations activate Ub transfer by binding the E2~Ub conjugate more tightly and by more effectively inducing the active, closed conformation of the ternary complex upon binding. Altogether, results from the NMR binding studies delineate two classes of activating mutation: mutations that predominantly increase the binding affinity to the E2 itself; and mutations that primarily increase binding specifically to the E2~Ub conjugate and augment the ability of the U-box to allosterically activate the UbcH5c~Ub conjugate.

Activating E4BU mutations promote increased degradation of p53 in cell culture

Mouse Ube4b and human UBE4B have E4 activity for the tumor suppressor p53[8]. Members of the E4 group of E3 ligases polymerize Ub chains on existing mono-Ub groups; in this case, Ube4b extends Ub chains on p53 initiated by mouse Mdm2 or human HDM2. The chain extension on p53 results in degradation of p53 by the proteasome, with implications for tumorigenesis.

We hypothesized that a hyperactive UBE4B would promote increased ubiquitination and proteasome-dependent degradation of p53 in cell culture. Co-transfection of p53 and Myc-Hdm2 into the H1299 human cell line led to discrete laddering of p53 bands, likely representing

multiple modifications of p53 with single or short Ub chains, as there was no loss of steady state protein levels (Fig. 6, lanes 1 and 2). Transfection of the wild type UBE4B expression plasmid led to a decrease in p53 protein levels (Fig. 6, lane 5), in a U-box-, HDM2-, and proteasome-dependent fashion (Fig. 6, lane 10 and Figs. S6a and S6b). Transfection of a plasmid expressing UBE4B with the M1124V, L1107I, D1139N, or N1142T mutation led to a more dramatic loss of steady state p53 protein levels (Fig. 6, lanes 4 and 6-8). As with the *in vitro* auto-ubiquitination assays, the relative levels of p53 degradation upon transfection of each UBE4B mutant correlate with *E* values from the phage selection.

A single human polymorphism, P1140T, has been identified in the U-box domain of UBE4B (dbSNP identifier rs15191). This mutation is so deleterious for E4BU function that it disappeared from the round three population of the deep mutational scan. Transfection of a plasmid expressing UBE4B harboring a P1140T mutation resulted in no change in p53 degradation, validating this variant as a loss-of-function allele (Fig. 6, lane 9). The combination of results from these cell-based assays demonstrate that the activity-enhancing and activity-lowering mutations identified in the high throughput assay have similar effects in the context of the full-length protein on a relevant substrate in human cells. Additionally, our mutational scanning data provide functional data as future genome or tumor sequencing efforts identify more UBE4B mutations.

Discussion

Our deep mutational scan of Ube4b has provided the most in-depth analysis to date of U-box sequence-function relationships. Many of the most enriched variants contain a conservative mutation, suggesting that the weak interactions and catalytic functions of U-box ligases can be

specifically tuned to suit their biological roles. Despite the capacity of a single point mutation to greatly enhance ligase activity, Ube4b has evolved in mammals to function with more moderate ubiquitination activity. Two of the most activating mutations in Ube4b occur at positions D1139 and N1142, which are analogous to conserved zinc-binding cysteines in RING domains (*e.g.* C61 and C64 in BRCA1), suggesting that U-boxes may have evolved as a class of E3 ligase distinct from the RING cross-brace structure in order to enable additional modes of regulating their ligase activities. It is not obvious why the U-box class of E3 ligases requires an added mode of regulation. However, the importance of human UBE4B ligase activity in the turnover of p53[8] argues that precise levels of ubiquitination activity are critical for cellular function. Overactive ubiquitination by UBE4B would offer an opportunity for tumor cells to suppress the p53-dependent cell cycle arrest and/or apoptotic response.

Gain-of-function mutations that aid in the elucidation of enzymatic mechanisms are commonly sought but rarely discovered using conventional mutagenesis strategies. The rare nature of ligase-activating mutations emphasizes the power of the deep mutational scanning method: only 25 single mutants (2.7% of the total) exhibited 3- to 50-fold enrichment over wild type after three rounds of selection. Many of the activity-enhancing mutations are chemically similar, evolutionarily conserved, and physically distant from known protein-protein interfaces, making it unlikely that they would have been predicted even with the available high-resolution structural information. As the first set of mutations to significantly activate E3s, these provide unique tools to further the understanding of ligase function.

Longstanding models for E3 ligase function have focused on their role in scaffolding E2~Ub conjugate and substrate, thereby facilitating the direct transfer of Ub from the E2 to the substrate lysine. Further studies have defined a second role for E3 ligases in activating their

cognate E2~Ub conjugate in order to enhance this rate of transfer[2,3,13-19]. A recent crystal structure offers a glimpse of this activated state just prior to the final step of Ub transfer[3]. More subtle aspects of how E3 ligases enact Ub transfer, however, have evaded even the highest resolution studies. The activity-enhancing mutations identified in our screen offered a unique opportunity to perturb the Ub transfer reaction in order to examine structural features of the E3 that contribute to catalysis. Our NMR-based analyses illustrate that the E4BU-activating mutations fall into two classes: those that predominantly affect the binding affinity of E4BU for the E2 (L1107I and M1124V) and those that primarily affect the ability of E4BU to allosterically activate E2~Ub conjugates (D1139N and N1142T).

Because E4BU binds both the free and Ub-conjugated forms of the E2 with relatively similar affinities[2], it was unknown whether tighter binding would be beneficial or detrimental for Ub transfer. On the one hand, an extremely tight binding E2 would transfer only the first Ub before acting as an inhibitor, as it would be unable to be re-charged by the E1 Ub-activating enzyme. On the other hand, a longer-lived E3:E2~Ub complex (as is observed with the L1107I and M1124V variants) would allow more time for the formation of active E2~Ub conformations and the approach of the incoming substrate lysine. We postulate that along the continuum of E3:E2 binding affinities, a point must exist at which Ub transfer reactivity is maximized before additional binding energy inhibits the reaction, at which point the E3:E2 dissociation step becomes rate-limiting. Wild-type Ube4b must be low enough on this binding energy *versus* catalysis curve such that tighter binding can lead to enhanced Ub transfer; the hyperactive L1107I and M1124V variants showed as much as a 6-fold enhancement in binding affinity.

While the D1139N and N1142T variants showed no appreciable effect on E2 binding compared to wild-type, they demonstrated an enhanced ability to allosterically stimulate the closed, active conformations of the E2~Ub conjugate. Our recent studies on the E4BU:UbcH5c~Ub complex identified R1143 in E4BU loop 2 as the "linchpin" for the allosteric activation of Ub transfer[2]. Despite their abilities to dramatically enhance ligase activity, neither the D1139N nor the N1142T mutation could rescue an R1143 mutation in the phage assay. As the U-box equivalent to a set of zinc-binding cysteine residues in RING domains, D1139 and N1142 contribute significantly to the interactions that stabilize E4BU loop 2. We propose that the D1139N and N1142T mutations alter the structure and/or dynamics of loop 2, thereby enhancing the probability and/or longevity of the E4BU:UbcH5c intermolecular hydrogen bond and augmenting the allosteric role of the E3.

Beyond the practical applications for future studies of E3 ligases, the identification and characterization of Ube4b ligase-activating mutations has added molecular detail to the separable binding and allosteric roles of E3 ligases in facilitating Ub transfer. The insights into E3 ligase function provided by our deep mutational scans of Ube4b suggest that the mutational analysis of enzymes on a high throughput basis has promise as a general means to identify key features of enzymatic mechanisms.

Experimental Procedures

Bacteriophage library preparation. Oligonucleotides for cloning the E4BU library were synthesized with a 2% error rate by TriLink Biotechnologies, and all other oligonucleotides were from IDT. Stop codons were inserted in all three frames 3' of the coding region, followed by a degenerate 18-base barcode. Molecular cloning of the library is outlined in Fig. S1d.

T7-longE4BU ubiquitination reactions. T7-longE4BU ubiquitination reactions contained 30 nM 6xHis-E1, 100 nM UbcH5c, 1 mM Flag-Ub (Sigma), 2 mM ATP, 5 mM MgCl2 and ½ total volume bacteriophage lysate (~5 x108 pfu) in 50 ml total reaction volume. Reactions were incubated for 45 minutes at 37˚C and stopped by addition of 2 mM DTT.

Enrichment of Flag-ubiquitinated bacteriophage and reamplification. M2-agarose beads (Sigma) were equilibrated into Flag dilution buffer (20 mM Tris pH 7.5, 200 mM NaCl, 0.2 mM EDTA, 0.1% NP-40) and added to ubiquitination reactions. After a 1-hour incubation at room temperature, the beads were washed 5x with Flag wash buffer (20 mM Tris pH 7.5, 500 mM NaCl, 0.2 mM EDTA, 0.05% NP-40, 1 mM DTT) and eluted twice at 37˚C by addition of 2.5 mg/ml 3xFlag peptide (Sigma) in Flag wash buffer. Phage eluted from the M2-agarose beads were re-amplified and titered according to manufacturer's instructions to avoid bottlenecks of the population. Individual clones were monitored by plaque PCR followed by Sanger sequencing for population convergence.

Protein purification. E4BU and its variants were purified based on[7]. The human 6xHis-E1, wheat E1, and UbcH5c and were purified as previously described[20 21].

Ubiquitination reactions with purified longE4BU. 1 mM E1, 8 mM Flag-Ub, 4 mM UbcH5c, 2 mM ATP, 5 mM MgCl2 and 4 mM longE4BU were mixed in 10 mM HEPES, 60 mM NaCl, 5% glycerol, 0.5 mM EDTA, pH 7.9 buffer. The reactions were incubated at 37˚C for indicated times. Reactions were stopped with 2x LDS buffer (Invitrogen) containing 2.5% b-

mercaptoethanol. Samples were separated on a 4-12% NuPAGE gel (Invitrogen) and transferred to PVDF membrane. Membranes were probed with M2 antibody and anti-mouse-HRP (GE Healthcare).

Library preparation for tag-directed subassembly and barcode counting. Phage DNA was purified by phenol chloroform extraction and ethanol precipitation. Illumina sequencing libraries were constructed by PCR amplification to sequence the 5' end of longE4BU and the barcode. To sequence internal regions of longE4BU, nested libraries were prepared by PCR. A detailed description of the library construction can be found in Figs. S1d, S1e.

Enrichment ratios. The Enrich software package[22] was used to determine locations and identity of mutations in the assemblies, and the frequency that each variant appeared in the population. A nonspecific carryover correction factor was applied to the tally of each variant in the selected population[23]. The corrected frequencies were used to calculate enrichment ratios and wild type normalized enrichment ratios for variants found in both the input and selected populations.

Structure visualization. All structure figures were generated using the Pymol visualization software.

Multiple sequence alignment. The U-box domains of the seven U-box domain-containing proteins found in the mouse genome were aligned using T-Coffee[24] and visualized with Jalview[25]. The U-box consensus sequence was determined by aligning sequences of the 17 U-box domain Pfam seed sequences (Pfam identifier PF04564) in Jalview using the default parameters.

NMR Spectroscopy. NMR spectra were recorded on a 500 MHz Bruker Avance II (University of Washington) at 25°C in 25 mM sodium phosphate (pH 7.0), 150 mM NaCl, 10% D2O. The UbcH5c-O~Ub conjugate was prepared as previously described and incorporated the C85S mutation to improve conjugate stability and the S22R mutation to prevent "self-assembly" through noncovalent Ub:UbcH5c interactions[26]. Spectra were recorded on 225 μM 15N-labeled samples using 1H,15N-HSQC-TROSY experiments, processed with NMRPipe/NMRDraw[27], and visualized with NMRView [28] . Chemical shift perturbations were calculated using the formula Δδj = [(Δδj15N/5)2 + (Δδj1H)2]1/2. NMRView was used to fit the E4BU:UbcH5c binding data with the quadratic equation f = A+(C-A)*(((p+x+10B)-((p+x+10B)2-4*p*x)0.5))/(2*p), where p is the concentration of UbcH5c. A minimum of 10 representative titrating peaks were used to determine a Kd, and the error is reported as the average standard deviation from the quadratic fits.

Cell culture and transfections. H1299 were purchased from ATCC and cultured according to the instructions. The cells were transfected at ~90% confluency in 500 μl antibiotic-free media with 100 ng pCMV-neo-p53, 100 ng pCMV-Myc3-Hdm2, 900 ng Flag-GFP or pcDNA3_Flag-Ube4b, and 2.2 ml Lipofectamine 2000 (Invitrogen) according to manufacturer's instructions. The cells were split 6 hours after addition of transfection reagents. 24 hours after transfection, cells were washed with cold phosphate-buffered saline and lysed with 200 μl lysis buffer (50 mM Tris 8.0, 150 mM NaCl, 1% NP-40, 1 mM EDTA and protease inhibitors (Roche)) on ice. Lysates were clarified by centrifugation and quantified using Bradford reagent. 20 mg of protein was electrophoresed on 4-12% NuPAGE gels and transferred to PVDF. The blots were probed with anti-Flag antibody (M2, Sigma), anti-p53 (DO-1, Santa Cruz) and anti-HSP90 (16F1, Abcam).

References

1. Pickart, Eddins, M. J. Ubiquitin: structures, functions, mechanisms. *Biochim Biophys Acta* **1695**, 55-72 (2004).
2. Pruneda, J. N. et al. Structure of an E2:E3~Ub Complex Reveals an Allosteric Mechanism Shared among RING/U-box Ligases. *Mol. Cell* (2012).
3. Plechanovová, A., Jaffray, E. G., Tatham, M. H., Naismith, J. H. & Hay, R. T. Structure of a RING E3 ligase and ubiquitin-loaded E2 primed for catalysis. *Nature* (2012).
4. Araya, C. L. & Fowler, D. M. Deep mutational scanning: assessing protein function on a massive scale. *Trends Biotechnol.* **29**, 435-442 (2011).
5. Fowler, D. M. et al. High-resolution mapping of protein sequence-function relationships. *Nat. Methods* **7**, 741-746 (2010).
6. Benirschke, R. C. et al. Molecular basis for the association of human E4B U box ubiquitin ligase with E2-conjugating enzymes UbcH5c and Ubc4. *Structure* **18**, 955-965 (2010).
7. Nordquist, K. A. et al. Structural and functional characterization of the monomeric U-box domain from E4B. *Biochemistry* **49**, 347-355 (2010).
8. Wu, H. et al. UBE4B promotes Hdm2-mediated degradation of the tumor suppressor p53. *Nat. Medicine* **17**, 347-355 (2011).
9. Brzovic, P. S. et al. Binding and recognition in the assembly of an active BRCA1/BARD1 ubiquitin-ligase complex. *Proc. Natl. Acad. Sci. USA* **100**, 5646-5651 (2003).
10. Patwardhan, R. P. et al. Massively parallel functional dissection of mammalian enhancers in vivo. *Nat. Biotech.* **30**, 265-270 (2012).
11. Marín, I. Ancient origin of animal U-box ubiquitin ligases. *BMC Evol. Biol.* **10**, 331 (2010).
12. Levin, I. et al. Identification of an unconventional E3 binding surface on the UbcH5 ~ Ub conjugate recognized by a pathogenic bacterial E3 ligase. *Proc. Natl. Acad. Sci. USA* **107**, 2848-2853 (2010).
13. Ozkan, E., Yu, H. & Deisenhofer, J. Mechanistic insight into the allosteric activation of a ubiquitin-conjugating enzyme by RING-type ubiquitin ligases. *Proc. Natl. Acad. Sci. USA* **102**, 18890-18895 (2005).
14. Reverter, D. & Lima, C. D. Insights into E3 ligase activity revealed by a SUMO-RanGAP1-Ubc9-Nup358 complex. *Nature* **435**, 687-692 (2005).
15. Zhang, M. et al. Chaperoned ubiquitylation--crystal structures of the CHIP U box E3 ubiquitin ligase and a CHIP-Ubc13-Uev1a complex. *Mol. Cell* **20**, 525-538 (2005).
16. Song, J. et al. Stability of thioester intermediates in ubiquitin-like modifications. *Protein Sci.* **18**, 2492-2499 (2009).
17. Yin, Q. et al. E2 interaction and dimerization in the crystal structure of TRAF6. *Nat. Struct. Mol. Biol.* **16**, 658-666 (2009).

18. Saha, A., Lewis, S., Kleiger, G., Kuhlman, B. & Deshaies, R. J. Essential role for ubiquitin-ubiquitin-conjugating enzyme interaction in ubiquitin discharge from Cdc34 to substrate. *Mol. Cell* **42**, 75-83 (2011).

19. Wenzel, D. M., Lissounov, A., Brzovic, P. S. & Klevit, R. E. UBCH7 reactivity profile reveals parkin and HHARI to be RING/HECT hybrids. *Nature* **474**, 105-108 (2011).

20. Starita, L. M. et al. BRCA1-dependent ubiquitination of gamma-tubulin regulates centrosome number. *Mol. Cell. Biol.* **24**, 8457-8466 (2004).

21. Christensen, D. E., Brzovic, P. S. & Klevit, R. E. E2-BRCA1 RING interactions dictate synthesis of mono- or specific polyubiquitin chain linkages. *Nat. Struct. Mol. Biol.* **14**, 941-948 (2007).

22. Fowler, D. M., Araya, C. L., Gerard, W. & Fields, S. Enrich: software for analysis of protein function by enrichment and depletion of variants. *Bioinformatics* **27**, 3430-3431 (2011).

23. Jolma, A. et al. Multiplexed massively parallel SELEX for characterization of human transcription factor binding specificities. *Gen. Res.* **20**, 861-873 (2010).

24. Di Tommaso, P. et al. T-Coffee: a web server for the multiple sequence alignment of protein and RNA sequences using structural information and homology extension. *Nucl. Acids Res.* **39**, W13-7 (2011).

25. Waterhouse, A. M., Procter, J. B., Martin, D. M. A., Clamp, M. & Barton, G. J. Jalview Version 2--a multiple sequence alignment editor and analysis workbench. *Bioinformatics* **25**, 1189-1191 (2009).

26. Brzovic, P. S., Lissounov, A., Christensen, D. E., Hoyt, D. W. & Klevit, R. E. A UbcH5/ubiquitin noncovalent complex is required for processive BRCA1-directed ubiquitination. *Mol. Cell* **21**, 873-880 (2006).

27. Delaglio, F. et al. NMRPipe: a multidimensional spectral processing system based on UNIX pipes. *J. Biomol. NMR* **6**, 277-293 (1995).

28. Johnson, B. A. NMR View: A computer program for the visualization and analysis of NMR data. *J. Biomol. NMR* (1994).

Acknowledgements

We thank W. Chazin and N. Zheng for critical reading of the manuscript. We also thank W. Chazin, R. Leng, and R. James for plasmids. Additionally, we acknowledge C. Lee for Illumina sequencing, and A. Borst for protein purification work. This work was supported by National Institute of General Medical Sciences grants R01 GM088055 (R.E.K.), P41 GM103533 (S.F.),

and PHS NRSA 2T32 GM007270 (J.N.P.). S.F. is an investigator of the Howard Hughes Medical Institute.

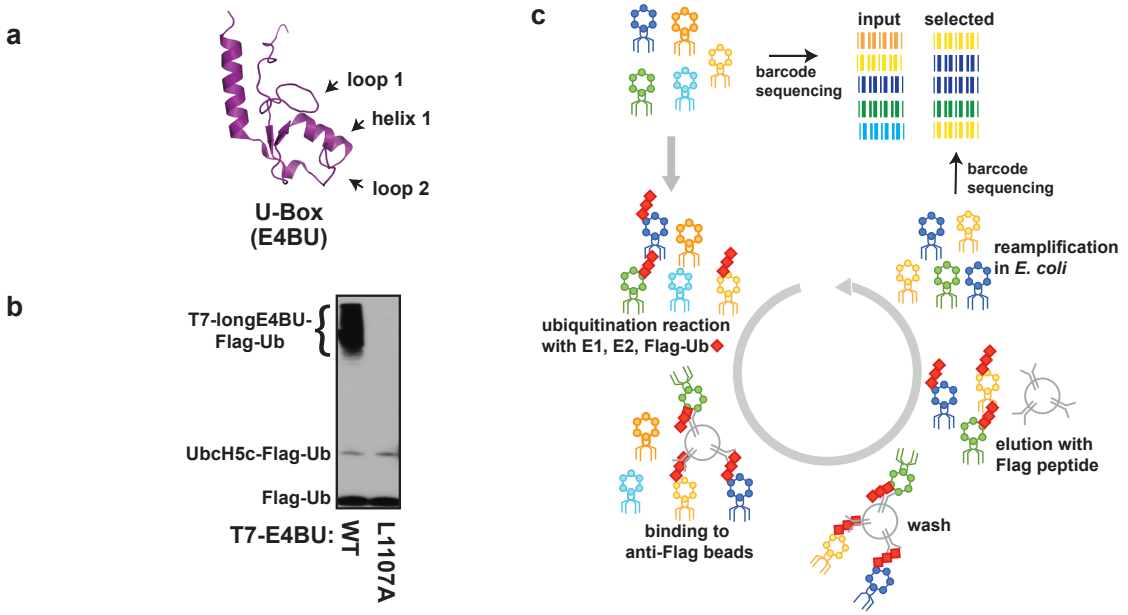

Figure 1. A highly parallel method for examining ubiquitin ligase activity. (a) Cartoon representation of the 80 amino acid E4BU solution structure (Protein Data Bank identifier 2kr4). Residues within loop 1, loop 2, and helix 1 form the E3:E2 interface. longE4BU contains an extra 20 amino-terminal residue required for autoubiquitination activity. **(b)** Western blot for Flag-Ub shows Ub ligase activity of T7-longE4BU expressed on the surface of phage. LongE4BU wild type (lane 1) or L1107A (lane 2) were fused to the coat protein of T7 bacteriophage. Amplified phage lysate was incubated with recombinant E1, UbcH5c, ATP/Mg, and Flag-Ub. The reaction was analyzed by western blot with anti-Flag to follow Flag-Ub. **(c)** A library of longE4BU sequence variants was generated from doped oligonucleotides, with a degenerate 18-base barcode inserted 3' of the stop codon. The variable region and barcode were cloned into the phage genome and displayed as a carboxy-terminal fusion with the T7 coat protein. The input library of T7-longE4BU sequence variants was subjected to multiple rounds of selection for functional Ub ligase activity. The input pool was incubated with recombinant 6xHis-E1, UbcH5c, ATP/Mg, and Flag-Ub. The ubiquitinated phages were selected on anti-Flag agarose and unbound phages were washed away. Bound Flag-ubiquitinated-T7-longE4BU variants were eluted by competition with 3xFlag peptide. Eluted phages were re-amplified and subjected to additional rounds of selection. DNA was purified from the input and selected T7-E4BU populations, Illumina libraries were constructed, and the barcodes were sequenced by 36-base single end reads.

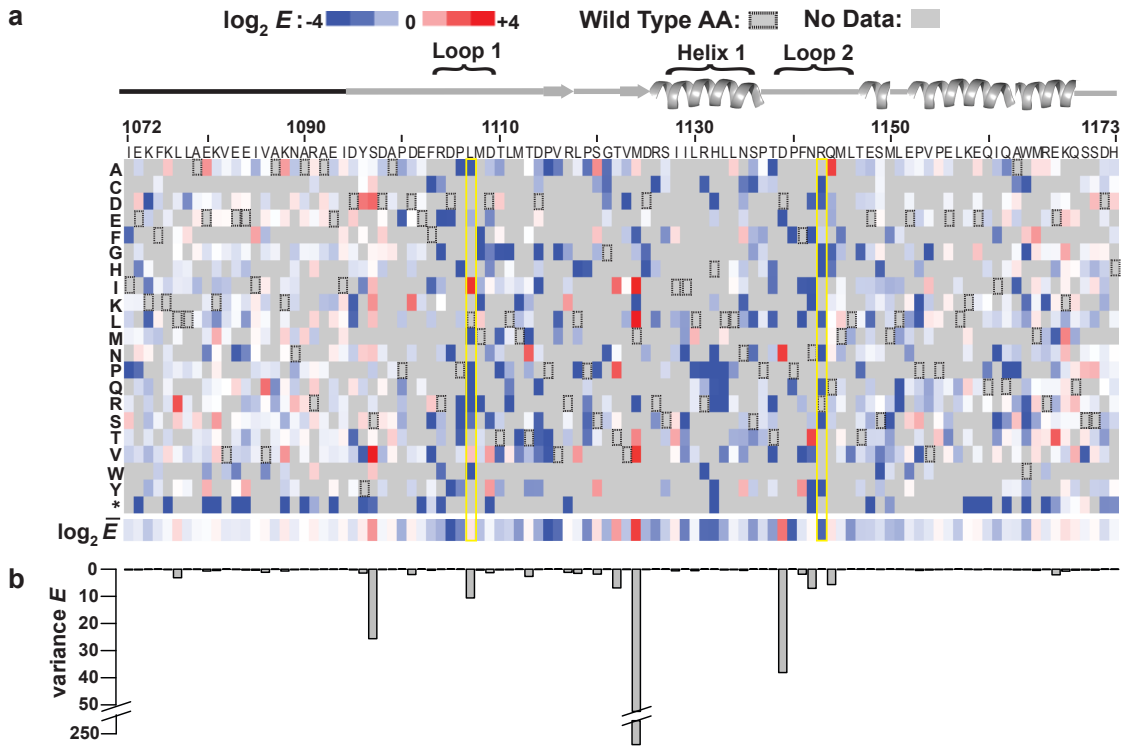

Figure 2. The effects of >900 novel mutations on E3 function are uncovered by deep mutational scanning of longE4BU. (a) A sequence-function map of log2 enrichment ratios (*E*) for 932 T7-longE4BU variants with a single amino acid change. Blue, white, and red boxes represent T7-longE4BU variants that were depleted, neutral, or enriched, respectively, during the selection process. A schematic of E4BU secondary structure is shown above. The amino-terminal 20 amino acids that were not included in either deposited structure are represented by a black line. Loop 1, loop 2, and helix 1 are indicated. The longE4BU sequence is represented on the x-axis and the possible amino acid substitutions are represented on the y-axis. Below is the position averaged *E* scores for each position in T7-longE4BU. **(b)** The variance of *E* scores for each position represented in a bar graph.

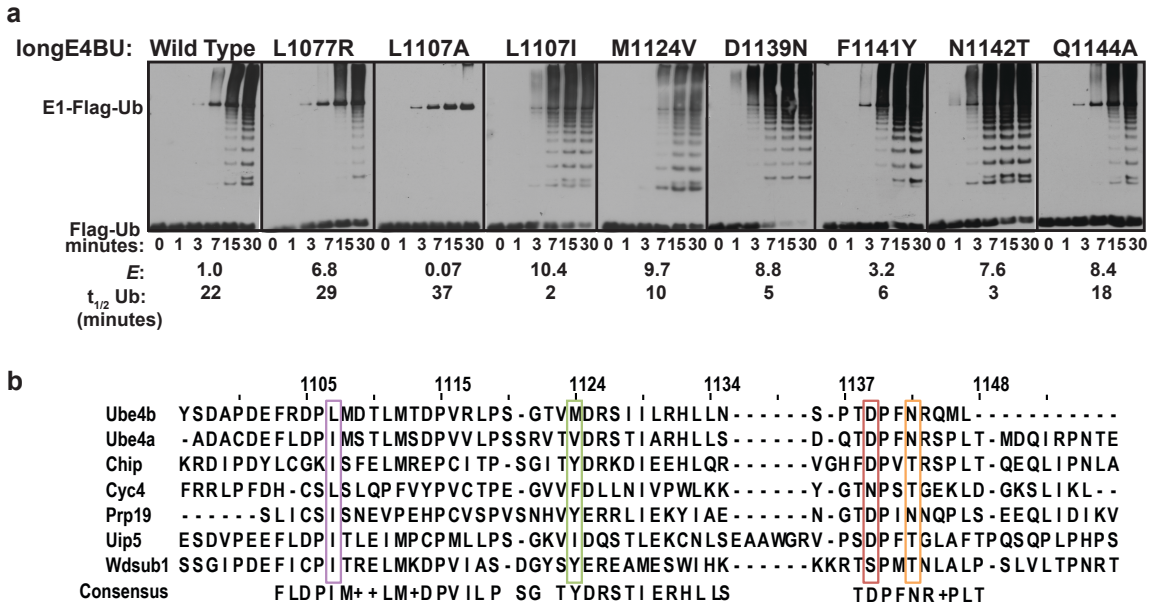

Figure 3. Enriched longE4BU variants are more active Ub ligases than the wild type protein. (a) Ubiquitination assays. Recombinant wild type longE4BU and the indicated variants were incubated with recombinant E1, UbcH5c, ATP/Mg, and Flag-Ub at 37ºC for the indicated time. Ubiquitination products were monitored by western blot to follow Flag-Ub. *E* scores and the approximate half-life of unmodified ubiquitin calculated from densitometry of Coomassie-stained reactions are indicated below (see also Supplementary Fig. 3). **(b)** A multiple sequence alignment of the U-box domains for the seven murine U-box containing proteins. Positions corresponding to E4BU L1107 (purple), M1124 (green), D1139 (red), and N1142 (orange) are indicated.

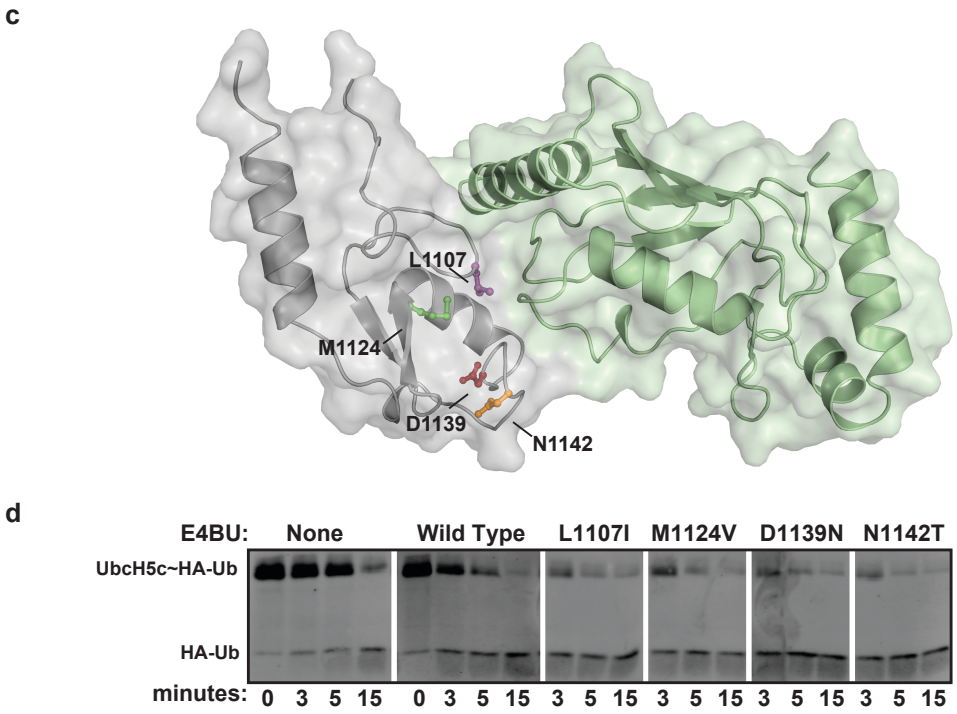

Figure 3. **(c)** Sites of mutation in highly enriched T7-longE4BU variants mapped to the E4BU:UbcH5c crystal structure (Protein Data Bank identifier 3L1Z). L1107 (purple), M1124 (green), D1139 (red) and N1142 (orange) are depicted on grey E4BU. UbcH5c is pale green. **(d)** Lysine reactivity assays. Recombinant minimal U-box domains of wild type E4BU (1092-1173) and the indicated variants were incubated with purified UbcH5c~HA-Ub and free lysine at 37ºC for times indicated. Breakdown of the UbcH5c~HA-Ub thioester linkage was monitored by western blot with anti-HA antibodies.

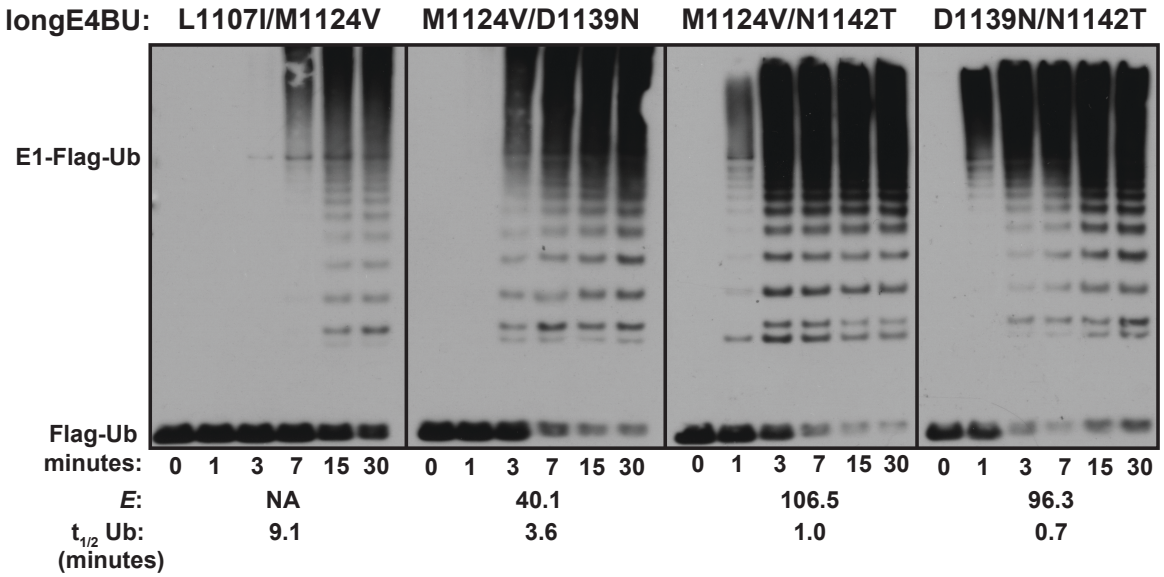

Figure 4. The effects of some activating mutations are synergistic and create hyperactive U-box domains. Ubiquitination assays. The indicated purified variants of longE4BU were incubated with recombinant E1, UbcH5c, ATP/Mg, and Flag-Ub at 37ºC for the indicated time. Ubiquitination products were monitored by western analysis to follow Flag-Ub. *E* scores and the approximate half-life of unmodified ubiquitin calculated from densitometry of Coomassie-stained reactions are indicated below (see also Supplementary Fig. 3).

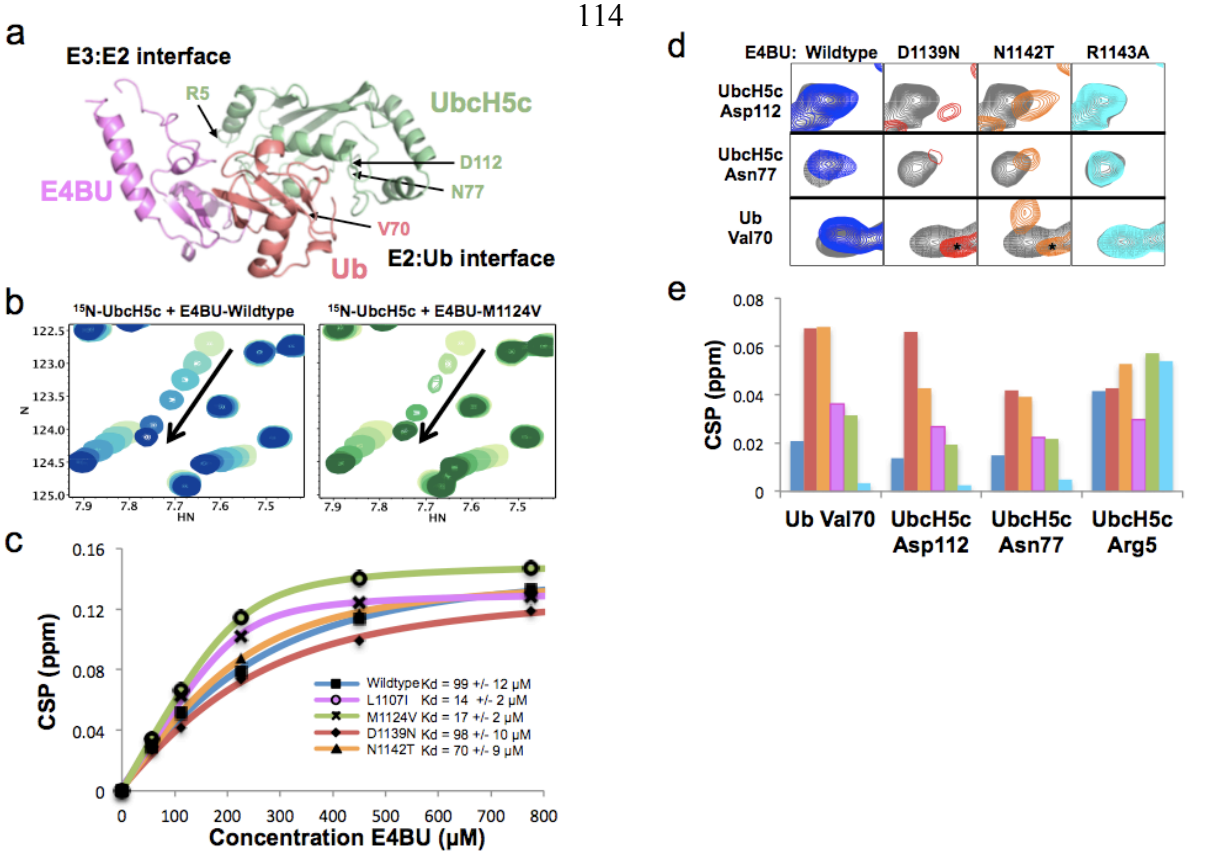

Figure 5. NMR analysis reveals that E4BU activating mutations fall into two classes. **(a)** One member from the E4BU:UbcH5c~Ub HADDOCK model[2] is shown for reference with the E3:E2 and E2:Ub interfaces annotated. **(b)** A representative portion of the UbcH5c HSQC spectrum showing chemical shift perturbations upon addition of 0.25, 0.5, 1, 2, and 3.4 equivalents of E4BU wild type (left, blue) or M1124V (right, green) to 225 μM 15N-UbcH5c. The M1124V mutant exhibits binding phenomena that approach intermediate exchange, as illustrated by linewidth broadening at early titration points. **(c)** Chemical shift perturbation values fit with quadratic binding equations using NMRView. Kd values were determined for wild type (blue, 99 +/- 12 μM), L1107I (magenta, 14 +/- 2 μM), M1124V (green, 17 +/- 2 μM), D1139N (red, 98 +/- 10 μM), and N1142T (orange, 70 +/- 9 μM) E4BU titrated into 15N-UbcH5c. **(d)** Resonances corresponding to D112 in UbcH5c Helix 2, N77 near the UbcH5c active site, and V70 within the Ub hydrophobic surface act as indicators for the promotion of closed, active UbcH5c~Ub conformations upon E4BU binding. Compared to the addition of 0.25 molar equivalences of wild type E4BU (blue) to 225 μM 15N-UbcH5c-O~15N-Ub, both the D1139N (red) and N1142T (orange) mutants induce further overpopulation of closed UbcH5c~Ub conformations. We could not collect NMR data at higher additions of E4BU due to the catalyzed hydrolysis of the oxyester effected by the E3. Addition of the catalytically inactive E4BU mutant R1143A (cyan) is shown for reference. Signal arising from small quantities of free, hydrolyzed Ub is marked by asterisks. **(e)** Chemical shift perturbations shown in (d) are quantified and shown in histogram format for the addition of 0.25 molar equivalencies of wild type (blue), D1139N (red), N1142T (orange), L1107I (magenta), M1124V (green), and R1143A (cyan) E4BU to 225 μM 15N-UbcH5c-O~15N-Ub. Perturbations corresponding to E3:E2 binding are largely unaffected, as shown by UbcH5c residue R5.

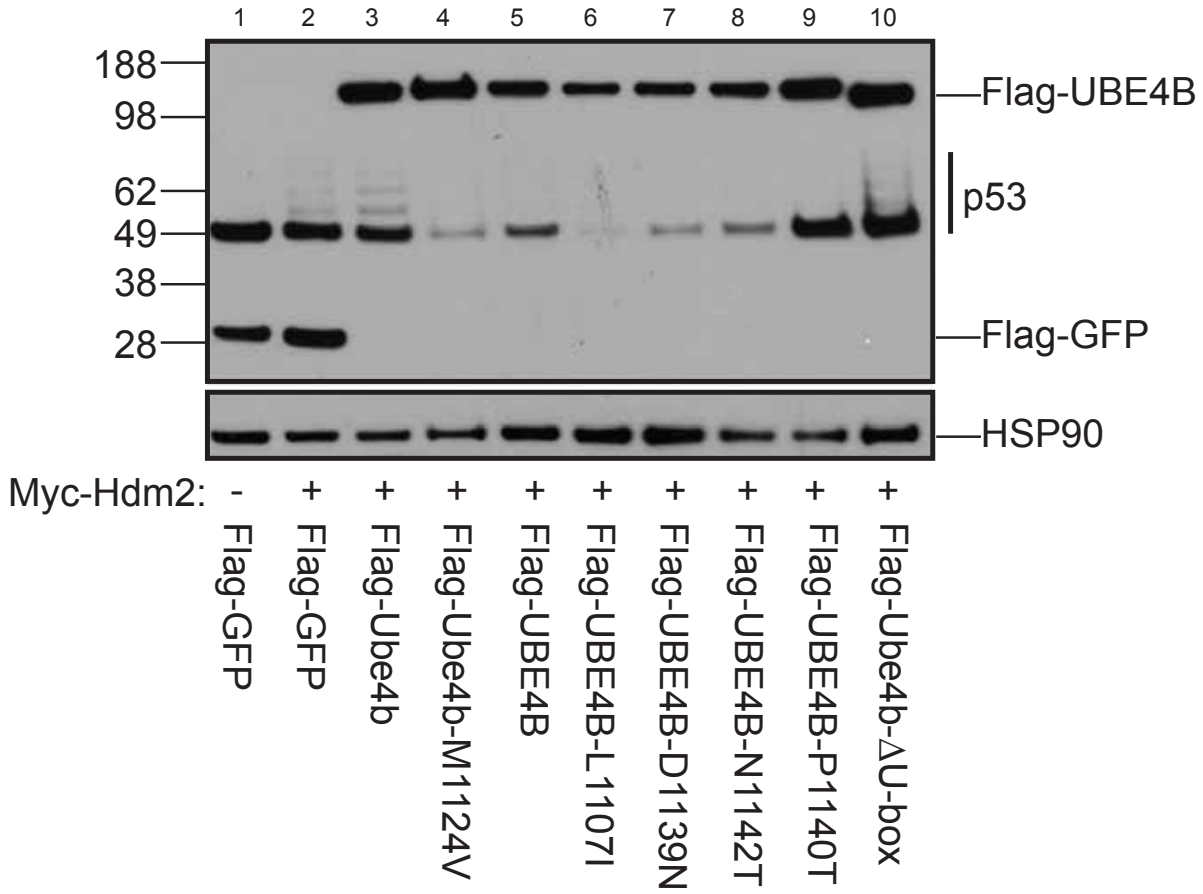

Figure 6. Activating mutants in the context of full length UBE4B promote degradation of p53 in tissue culture. H1299 cells were transfected with pCMV-neo-p53, cells in lanes 2-8 were transfected with pCMV-Myc-Hdm2. Flag-tagged, full length mouse Ube4b or human UBE4B constructs were transfected as indicated. Blots were probed for p53 and the Flag epitope. Endogenous HSP90 was used as a protein loading control.

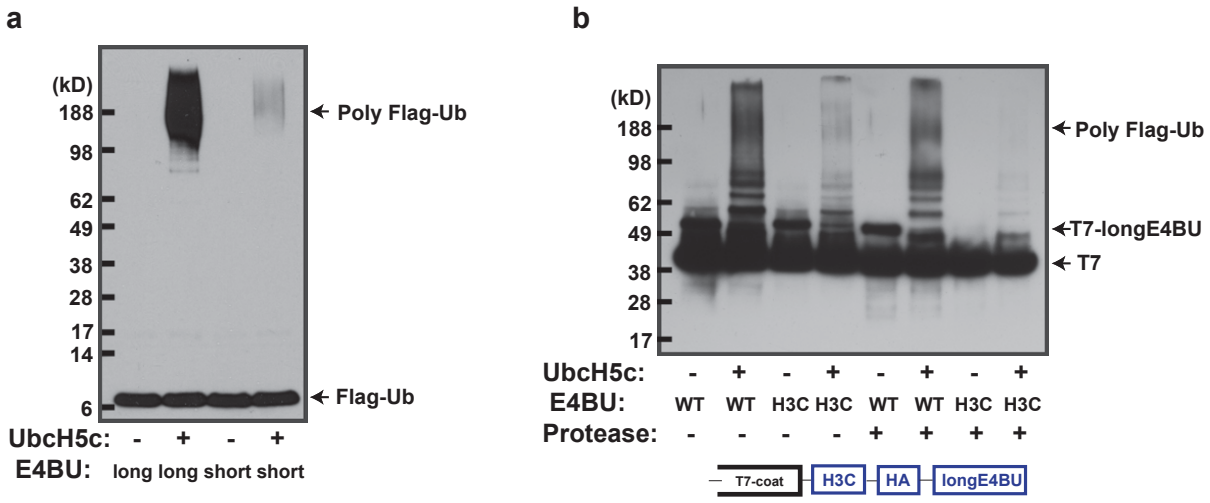

Supplemental Figure 1. Control reactions and cloning details. (a) The minimal U-box of E4BU does not support robust ubiquitin polymerization. longE4BU (1072-1173) or minimal E4BU (1092-1173) were fused to the coat protein of T7 bacteriophage. The minimal E4BU is lacking 4 lysine residues that are the presumed auto-ubiquitination targets (Nordquist et al., 2010). Amplified phage lysate was incubated with purified E1, UbcH5c, ATP and Flag-ubiquitin. The reaction was resolved by SDS-PAGE, transferred to PVDF membrane and probed with anti-Flag antibodies. **(b)** Protease cleavage between the U-box and T7 coat protein reduces high-molecular weight species. longE4BU in addition to an HA tag and an H3C protease cleavage site were fused to T7 coat protein as diagrammed. Amplified wild type or H3C-HA-E4BU phage lysates were incubated with purified E1, UbcH5c, ATP and Flag-ubiquitin. Following the ubiquitination reaction, the mixture was incubated with GST-H3C protease. The reaction was resolved by SDS-PAGE, transferred to PVDF membrane and probed with monoclonal anti-T7 antibodies. E4BU and H3C cleavage as indicated.

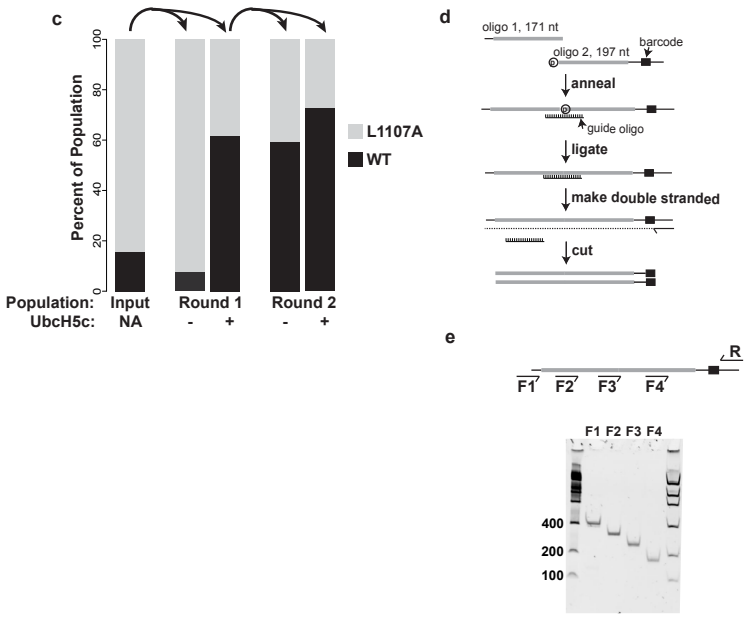

Supplemental Figure 1. (c) Wild type T7-E4BU is enriched after selection for ubiquitinated T7 bacteriophage. For round 1 of selection amplified phage lysates from wild type and the L1107A variant of T7-longE4BU were mixed 1:5 (Input) and were incubated with purified E1, ATP, and Flag-ubiquitin with or without UbcH5c as indicated. Flag-ubiquitinated phages were purified with anti-Flag agarose and eluted with Flag peptide. Eluates were re-amplified in *E. coli*. The longE4BU inserts were amplified by PCR from the phage lysate and Sanger sequenced. The ratio of the mixed bases coding for the mutant position were quantified using the PeakPicker algorithm and is represented in the bar graphs (Ge et al., 2005). The eluate from ubiquitination reaction with UbcH5c from round 1 of selection was used as the input for round 2 of selection as indicated by the arrows. **(d)** Diagram of T7-E4BU variant cloning. Since the longest oligonucleotide we were able to purchase was 200 bases we spread features of the library across two oligonucleotides, lengths are indicated. longE4BU is represented as grey boxes and was synthesized with a mutation rate of 2 mutations per 306 nucleotides encoding the 102 amino acids of longE4BU. Oligo 2 was synthesized with a 5' phosphate. Oligo 2 also codes for a stop codon in all three frames 3' of the E4BU open reading frame, an 18-base degenerate barcode (black box) and a common sequence. The oligos were annealed to a guide oligo synthesized with a 3' dideoxy nucleotide to prevent polymerase extension and ligated together with T4 DNA ligase. This construct was made double-stranded by annealing a short oligo to a common sequence 3' of the barcode and extending that oligo with the strand displacing polymerase phi29. The double stranded construct was cut with EcoRI and HindIII and ligated into T7-Select 10-3b bacteriophage arms in the purchased T7Select Cloning Kit. **(e)** Nested amplicons for tag-directed subassembly. Oligonucleotides for amplification of nested amplicons are represented by arrows. The 101-base sequences the forward read of each amplicon were designed to overlap by 10 nucleotides. The first 18 bases of reverse sequencing read comprise the barcode. Each amplicon was separated on a 10% TBE gel and stained with SYBR gold. See Supplementary Table 1 for sequencing and subassembly statistics.

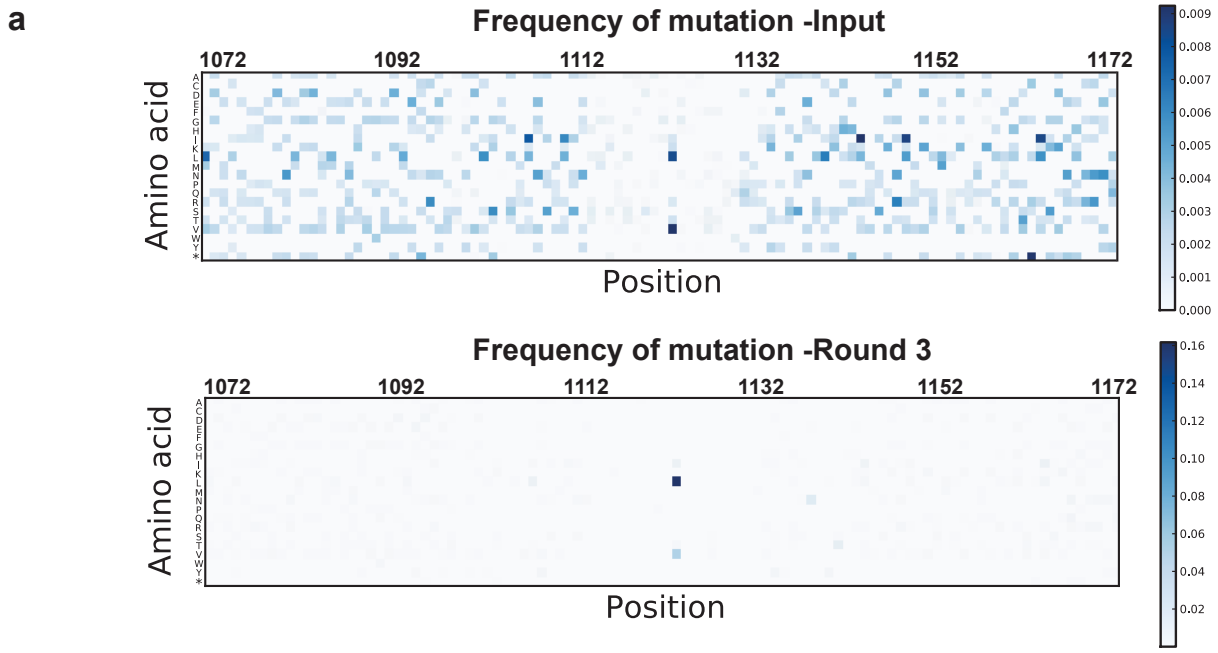

Supplemental Figure 2. Mutation frequency and selection statistics. (a) Mutations within longE4BU are distributed throughout the protein. The frequency of occurrence of each amino acid substitution in the input (top) and round 3 (bottom) populations are plotted as a heat map with the position of longE4BU across the horizontal axis and each possible amino acid change on the vertical axis. Scales are on the right. Note: the mutations in the input library are not completely random. 1) Mutations are depleted between amino acid positions 42 and 60. We believe that this occurred because the nucleotides that code for these positions annealed to the guide oligonucleotide used in the ligation step (Supplementary Figure 2a). Some mutations in this region may have caused inefficient annealing and ligation and would therefore be depleted in the library. 2) As expected from random mutagenesis, changes to amino acids that required more than one nucleotide change are less common. For example, an amino acid change to W, which is encoded by only a single codon, occurred only once throughout the whole domain.

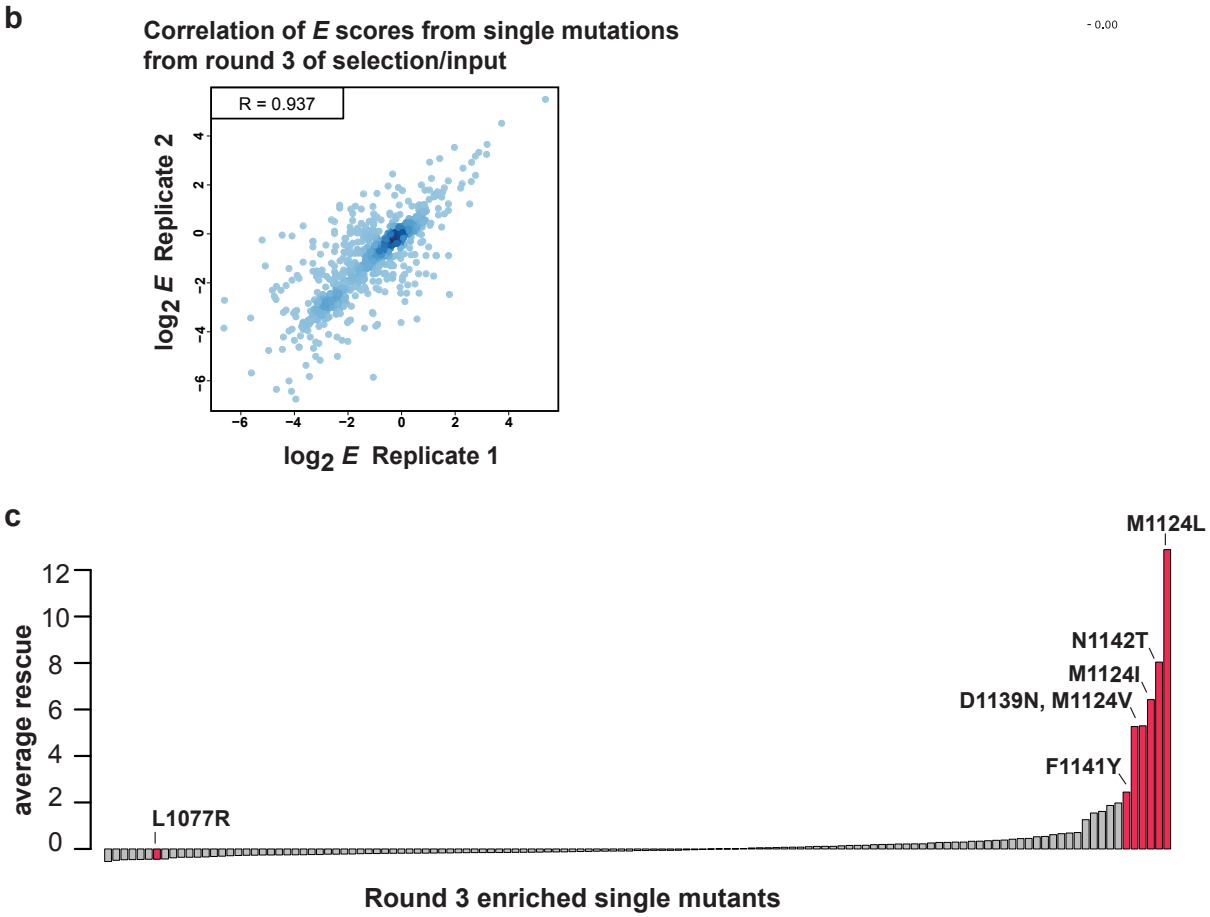

Supplemental Figure 2. **(b)** *E* scores for technical replicates of the longE4BU deep mutational scan are highly concordant. Correlation of *E* scores of variants containing a single mutation from two experimental replicates of selection. A Pearson correlation coefficient of 0.93 was calculated for the two datasets. **(c)** Mutations found in highly enriched variants can rescue most other mutations. To assess the functional importance of enriched mutations we evaluated their ability to rescue detrimental mutations when the two are paired. To this end, we calculated an average rescue score ($\overline{R}$) for variants with E >1 by the following steps. To calculate R for a mutation X (where E_X >1), we identified all double mutants that contain X and another mutation Y. We excluded single mutations found in fewer than 50 doubly mutated variants. Next, we subtracted E_Y from $E_{X,Y}$ and averaged all of these remainders to determine $\overline{R}$. For 120 of the 132 mutations for which we could calculate an average rescue score, $\overline{R}$ was near zero, indicating that they did not rescue second site mutations. Average rescue score ($\overline{R}$) for variants with an E score >1 that were observed in combination with ≥50 secondary mutations are shown. Select mutations are indicated.

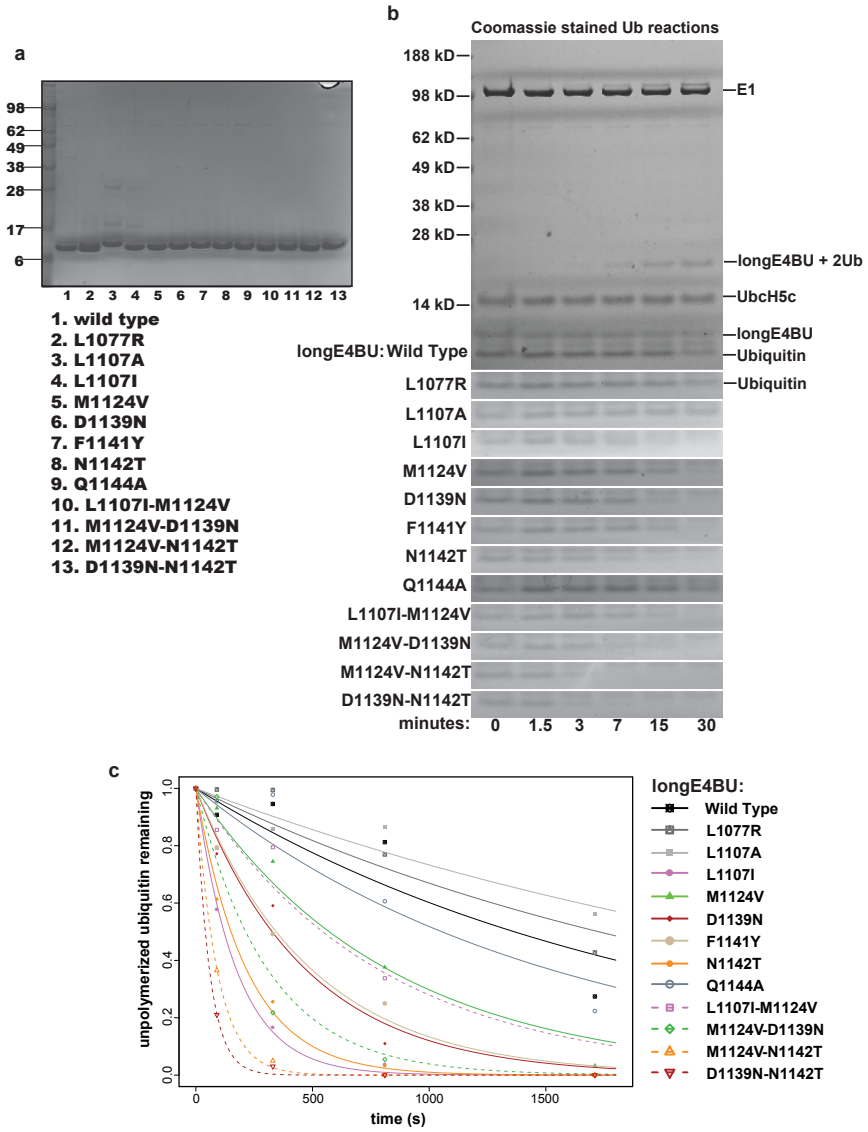

Supplemental Figure 3. Quantification of ubiquitination activity assays. (a) Equal concentrations of longE4BU variants were used in *in vitro* ubiquitination assays. 200 pmol of each longE4BU variant was electrophoresed on a 4-12% gel and visualized with Coomassie stain. Variants as indicated. **(b)** Ubiquitination assays. The purified variants of longE4BU were incubated with recombinant E1, UbcH5c, ATP/Mg, and Flag-Ub at 37ºC for the indicated time. Ubiquitination products were separated by SDS-PAGE and visualized by Coomassie staining. The full-size gel for the wild type longE4BU reaction is shown along with only the ubiquitin band for all the indicated variants. The intensities of these bands were quantified by ImageJ to estimate the rate of disappearance of unmodified ubiquitin. **(c)** Decay curves for the loss of the unmodified ubiquitin band. Intensities from the unmodified ubiquitin bands were normalized to the 1.5 minute time point due to the fuzzy nature of the T = 0 ubiquitin bands. The normalized band intensities were used to estimate the rate (k) at which the ubiquitin was lost by fitting the data to a first order rate law equation $[A] = [A_o]e^{kt}$.

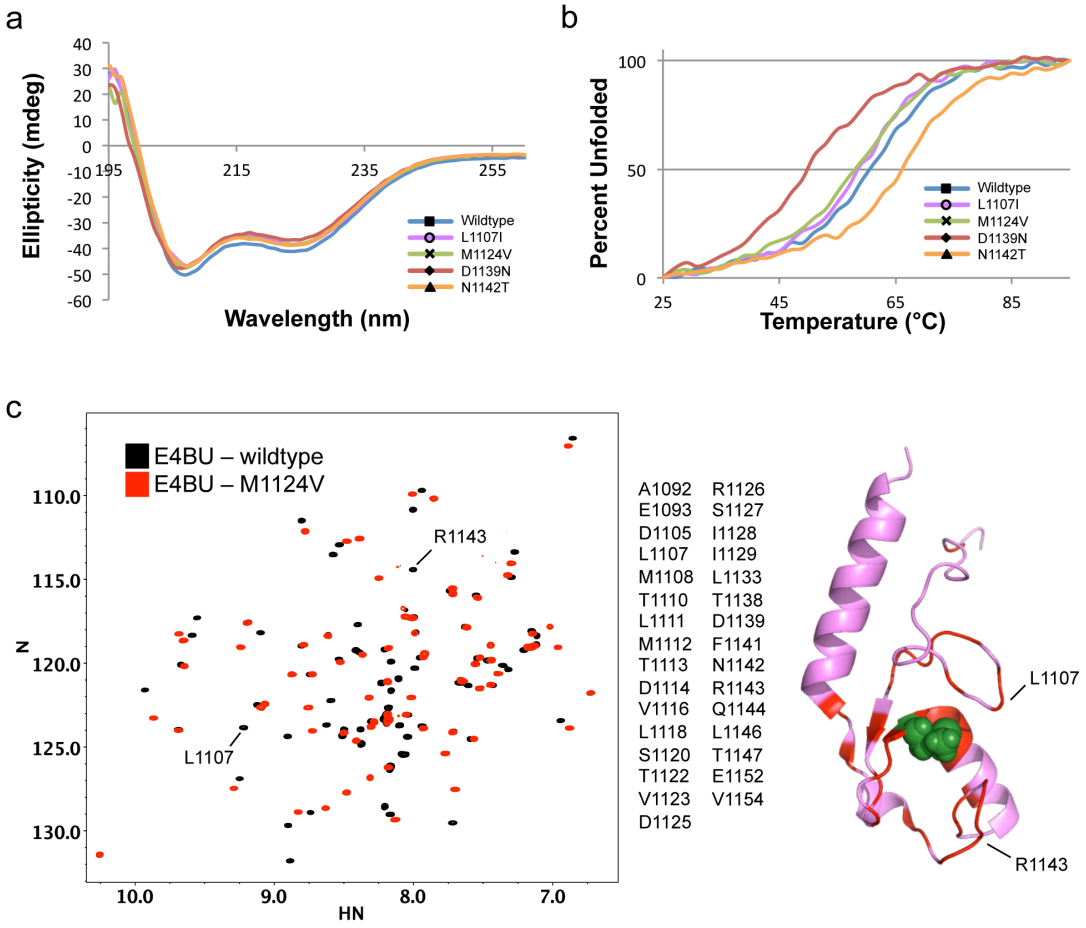

Supplemental Figure 4. Activity enhancing mutations do not cause significant structural or stability changes. (a) Circular dichroism wavelength scans from 195-260 nm are shown for 50 µM samples of E4BU WT (blue), L1107I (magenta), M1124V (green), D1139N (red), and N1142T (orange). **(b)** Thermal melts following CD signal at 220 nm were used to determine Tm values for E4BU WT (61°C), L1107I (59°C), M1124V (57°C), D1139N (50°C), and N1142T (66°C). Color scheme follows as in (a). All ellipticity data was normalized to 0 and 100% unfolded using the first and last datapoints, respectively. **(c)** ^{1}H, ^{15}N HSQC-TROSY overlay of wild type (black) and M1124V E4BU (red). E4BU M1124V resonances that have shifted off of the peak in the wild type spectrum are listed and mapped onto the E4BU structure in red. The M1124 position is shown in green spheres. Assignments of select resonances that show large perturbations are labeled and their positions in the structure are marked.

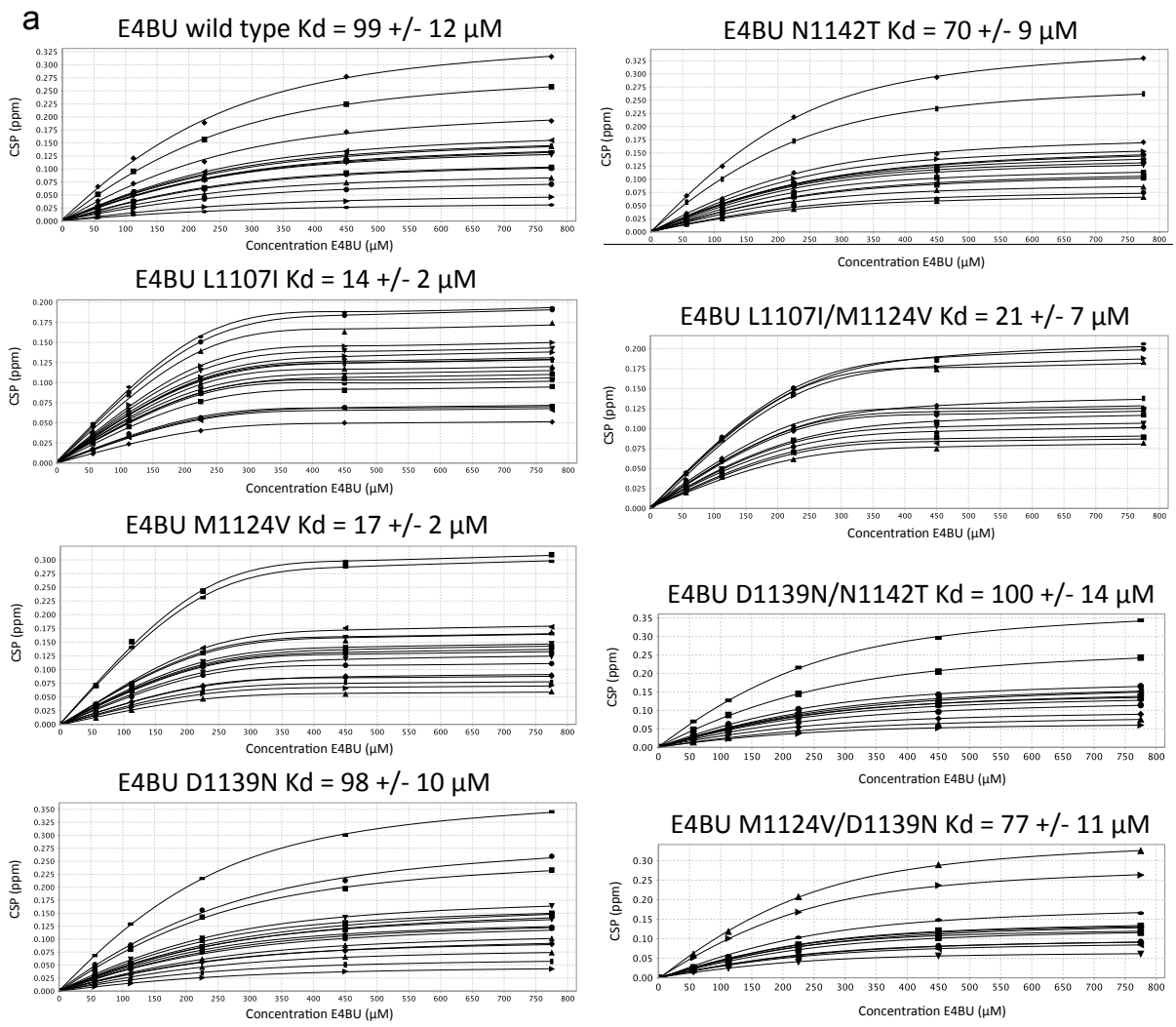

Supplemental Figure 5. NMR analyses of interactions with activity enhancing mutants. **(a)** Individual binding curves for titrations of E4BU variants into 225 mM ^{15}N-labeled UbcH5c. NMRView was used to fit the E4BU:UbcH5c binding data with the quadratic equation $f = A+(C-A)*(((p+x+10^{B})-((p+x+10^{B})^{2}-4*p*x)^{0.5}))/(2*p)$, where p is the concentration of UbcH5c. A minimum of 10 representative titrating peaks were used to determine a K_d, and the error is reported as the average standard deviation from the quadratic fits. Variants as indicated.

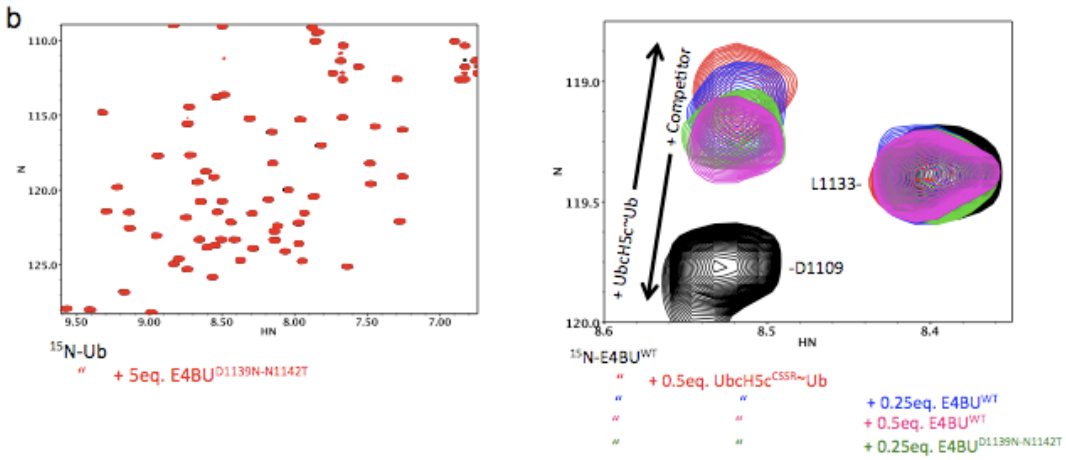

Supplemental Figure 5. (b) Left, Comparison of HSQC-spectra collected on ^{15}N-Ub in isolation (black) and in the presence of 5 molar equivalences of E4BU$^{D1139N/N1142T}$ (red) showed no observable interaction. Right, Because the UbcH5c~Ub conjugate undergoes appreciable hydrolysis in the presence of E4BU, competition experiments were used in place of traditional NMR titrations to compare the binding of wild type and D1139N/N1142T E4BU. Select resonances of ^{15}N-E4BU^{WT} (black) undergo large chemical shift perturbations upon addition of 0.5 molar equivalencies of UbcH5c^{CSSR}~Ub (red). Further addition of 0.25 (blue) or 0.5 (magenta) equivalencies of unlabeled E4BU^{WT} result in a backward titration as the ^{15}N-labeled and natural abundance E4BU compete for UbcH5c~Ub binding. Addition of 0.25 equivalencies of unlabeled E4BU$^{D1139N/N1142T}$ resulted in levels of competition similar to wild type, indicated comparable binding affinities. Fresh samples were prepared for each of the HSQC spectra.

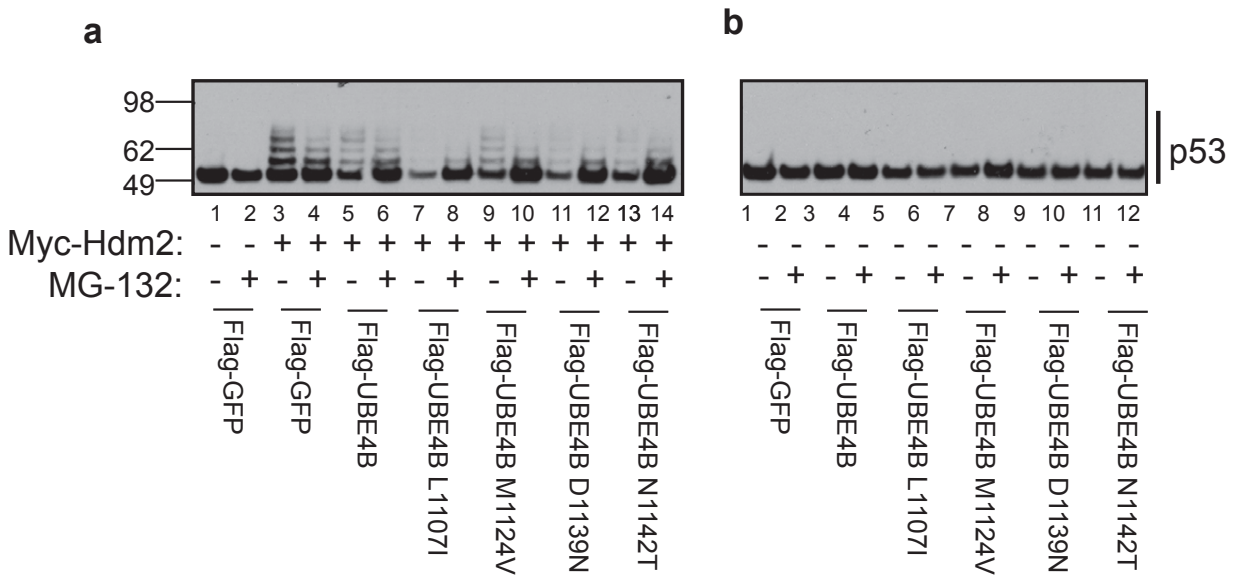

Supplemental Figure 6. UBE4B induced degradation of p53 is proteasome- and Hdm2-dependent. (a) H1299 cells were transfected with pCMV-neo-p53, cells in lanes 3-14 were transfected with pCMV-Myc-Hdm2. Flag-tagged, full-length human UBE4B constructs were transfected as indicated. 25 μM MG132 or DMSO was added 5 hours prior to cell lysis. Protein concentration was quantified by Bradford assay and 10 μg of protein was separated by SDS-PAGE and transferred to PVDF membrane. Blots were probed for p53. **(b)** H1299 cells were transfected with pCMV-neo-p53 and UBE4B in the absence of Hdm2. 25 μM MG132 or DMSO was added 5 hours prior to cell lysis. Protein concentration was quantified by Bradford assay and 10 μg of protein was separated by SDS-PAGE and transferred to PVDF membrane. Blots were probed for p53.

Chapter V – Activation of *Shigella* effector OspG requires binding to host ubiquitination machinery

Pruneda, J. N., Smith, F. D., Swaney, D. L., Villén, J., Scott, J. D., Klevit, R. E., and Brzovic, P. S.

Author Contributions

J.N.P. performed all experiments with the exception of tissue culture and kinase activity assays performed by F.D.S, and mass spectrometry performed by D.L.S. J.N.P., P.S.B., and R.E.K. designed the overall study.

Abbreviations: Ub, ubiquitin; E2, ubiquitin-conjugating enzyme; E3, ubiquitin ligase; E1, ubiquitin-activating enzyme; RING, Really Interesting New Gene; LPS, lipopolysaccharides; PG, peptidoglycan; NF-κB, nuclear factor κB; MAPK, mitogen-activated protein kinase; NMR, nuclear magnetic resonance.

Introduction

The human immune system is a complex, well-oiled machine. Inflammation, leukocytes, and lymphocytes orchestrate a formidable defense against foreign invasion. Despite all of these intricacies, pathogenic bacteria have developed a number of tricks to evade our responses. *Shigella* spp. and other intracellular pathogens elude much of the immune response by penetrating and replicating within the confines of the host cell. To accomplish this, pathogenic bacteria have developed a toolkit of effector proteins that, when delivered by the Type III secretion system, enact an array of functions within the host cell that favor bacterial survival. The ~35 secreted effectors can be roughly divided into two waves: the first wave to be secreted enacts cytoskeletal rearrangements within the host cell that allow bacterial invasion, and the second wave functions to dampen the host inflammatory responses triggered by detection of bacterial lipopolysaccharides (LPS) and peptidoglycans (PG)[1].

Recognition of bacterial LPS and PG by host Toll-like and NOD receptors (respectively) activate both the nuclear factor-kB (NF-kB) and mitogen-activated protein kinase (MAPK) pathways, ultimately leading to the upregulation of immune-response genes including cell adhesion factors and pro-inflammatory cytokines. Typical of eukaryotic signaling cascades, the NF-kB and MAPK pathways rely heavily upon post-translational phosphorylation and ubiquitination modifications. Preempting the inflammatory response by blocking the required signaling events within the NF-kB and MAPK pathways is critical for bacterial propagation.

Phosphorylation is responsible for much of the signal amplification in response to the detection of LPS. A cascade of tightly controlled kinases that, depending on the site of modification, can be activated or repressed by phosphorylation initiates both the NF-kB and MAPK pathways. Though critical for proper signaling, the sensitivity of this cascade to

modifications makes it an enticing target for effector proteins. The *Shigella flexneri* effector OspF uses a phosphate elimination reaction to irreversibly deactivate MAP kinases[2,3]. YopJ, an effector protein from *Yersinia pestis*, subverts both the NF-kB and MAPK pathways by acetylating Ser/Thr residues within a group of MAPK kinases, thereby blocking the phosphorylation necessary for pathway activation[4].

Post-translational modifications with the small signaling protein ubiquitin (Ub) are also essential within the NF-kB pathway. Ubiquitination proceeds through a three-enzyme pathway; E1-E2-E3. The E1 enzyme activates and transfers Ub onto the E2 active site cysteine to form the E2~Ub conjugate, which then interacts with an E3 ligase to transfer Ub onto a substrate lysine. At an early stage in the NF-kB response, the E3 ligase TRAF6 polymerizes chains of Ub that are thought to recruit downstream components. To subvert this process, the *Shigella flexneri* effector OspI deamidates the relevant E2, Ubc13, at a position that renders it incompetent for Ub transfer[5]. Later in the NF-kB response, inhibitor protein IkB is phosphorylated and subsequently ubiquitinated to signal for its proteasomal degradation, thereby releasing NF-kB and allowing for its nuclear translocation. A *Shigella flexneri* effector termed OspG was proposed to circumvent this process by binding to the E2~Ub conjugate intermediate. Interestingly, OspG itself demonstrates kinase activity, suggesting a potential interplay between phosphorylation and ubiquitination signaling[6].

We find that OspG can interact *in vitro* with a minimum of 10 different E2 enzymes that function in diverse cellular processes. To identify the details of one such OspG:E2~Ub complex, we determined a 2.7Å crystal structure of OspG bound to the UbcH5c~Ub conjugate. Formation of the complex appears to have direct structural ramifications on both OspG and the UbcH5c~Ub conjugate. In the structure, OspG holds UbcH5c~Ub in an extended conformation by contacting

both subunits of the E2~Ub conjugate. Conversely, the kinase architecture of OspG is held in a conformation primed for catalysis. Consistent with the structure, both ATP-binding and OspG kinase activity against the proxy substrate Histone H1 are dramatically enhanced while in complex with UbcH5c~Ub. These results demonstrate a previously unappreciated role for E2~Ub conjugates in governing OspG activity and identify a catalytic function OspG may serve in the inhibition of the inflammatory response during *Shigella* invasion.

Results

OspG binds a cohort of E2s

From a bacterial effector standpoint, the critical position upheld by E2s within the ubiquitination pathway likely makes them enticing targets; beyond OspG, *Shigella flexneri* secretes OspI (as mentioned above) in addition to its own set of E3 ligases that use host ubiquitination machinery to target new substrates. While it is not uncommon for E2s to mediate multiple protein-protein interactions (for a review, see Wenzel *et al.*[7]), interactions with proteins outside of the ubiquitination pathway have been rarely observed and even more rarely characterized in molecular detail. Building a comprehensive list of E2s that are able to interact with OspG can not only identify molecular determinants for binding but also offer perspective on what cellular processes might be intersected by OspG during infection. In early work by Kim *et al.*, OspG was shown by yeast 2-hybrid to interact with a small set of E2s, including members of the Ube2D, Ube2E, and Ube2L families. To confirm and expand upon this list, we performed a series of immunoprecipitation and pulldown experiments followed by mass spectrometry to identify interacting E2s.

In the first experiment, YFP-tagged OspG was transiently transfected into HeLa cells under control of the CMV promoter. Expression of OspG appeared diffuse, though similar transfection experiments of 293T cells showed localization to puncta of unknown origin (Fig. S1). YFP-immunoprecipitation followed by mass spectrometry identified a list of interacting E2s that were not present in the YFP control, including UbcH5b, UbcH5c, Ube2E1, Ube2E2, Ube2L3, and Ube2L6. In a second approach, cell extracts were prepared from Caco-2 intestinal epithelium cells and incubated with recombinant GST-tagged OspG. After washing, OspG-interacting proteins were eluted and analyzed by mass spectrometry. This approach identified UbcH5b, UbcH5c, Ube2E1, Ube2E2, Ube2K, and Ube2L3 as interacting E2s that were not present in the GST control. To confirm these interactions *in vitro*, GST-OspG pulldown experiments were performed with a panel of E2s in their free and Ub-conjugated states. To test for interactions with free versus Ub-loaded E2s, each E2 was pre-incubated with E1, Ub, and $MgCl_2$ in the absence or presence of ATP before being subjected to GST-OspG pulldowns. As shown by SDS-PAGE and Coomassie staining, OspG only binds the E2~Ub conjugate with a strong enough affinity for a pulldown, as neither the isolated E2 nor Ub are detected (Fig. 1a, compare open and closed circles). OspG interacts with numerous Ub-conjugated E2s to varying degrees, including all E2s identified by yeast 2-hybrid[6], immunoprecipitation, and pulldown experiments in addition to the highly similar UbcH5a and Ubc13 (Figs. 1a and S2a). Members from this set of E2s are diffusely expressed and carry out highly diverse cellular functions. Therefore, if OspG function or localization is dependent upon one specific E2, it is difficult to predict which E2 is the most relevant. Primary sequence analysis of the OspG-interacting E2s identified from cellular experiments highlights a number of highly conserved regions, including Helix 1, Loop 4, and the region surrounding the active site (Fig. 1b). A Consurf analysis of these

E2s highlights the active site and E3-binding region (comprised of Helix 1, Loop 4, and Loop 7) as the most highly conserved areas in the structure (Fig. 1c). As elements of the active site are common among all E2 Ub-conjugating enzymes, it is likely that OspG recognizes the only other highly conserved region – the E3 binding site.

OspG binds isolated UbcH5c and Ub with very low affinity

Because pulldown experiments require relatively high affinity interactions that are not characteristic of the eukaryotic ubiquitination machinery[7], NMR was used to look for low-level interactions between OspG and E2/Ub. As the HSQC spectra of UbcH5c and Ub are assigned, any interactions detected upon addition of OspG can be mapped onto the structures to determine the binding regions. Addition of OspG to UbcH5c and Ub resulted in significant perturbations in the Ub spectrum and only minor effects in the UbcH5c spectrum (Fig. 2a, compare black and red). The majority of Ub resonances exhibited linewidth broadening, the most severe of which mapped to regions surrounding I44 and V70, a region commonly involved Ub interactions. The UbcH5c spectrum was significantly less perturbed upon addition of OspG, consistent with an even weaker interaction. The perturbed resonances in the UbcH5c spectrum map to portions of Helix 1, Loop 4, and Loop 7, a region that is conserved among all OspG-interacting E2s (Fig. 1c). Interactions with the UbcH5c-O~Ub conjugate can also be examined by NMR, however, addition of OspG caused severe linewith broadening (the UbcH5c-O~Ub carries the UbcH5c C85S and S22R mutations to allow for a stable, monomeric conjugate[8] (Fig. 2b). This spectroscopic phenotype is consistent with a tight interaction and offers stark contrast to the weak interactions observed with the free UbcH5c and Ub components (compare Figs. 2a and 2b).

X-ray crystal structure of the OspG:UbcH5c~Ub complex

To determine the molecular details of the OspG:UbcH5c~Ub interaction, we crystallized the complex and determined its structure to 2.70Å (Fig. 3 and Table 1). OspG was co-purified with the UbcH5c-O~Ub conjugate by size exclusion and crystallized in the $P6_322$ spacegroup. The phase information was obtained by molecular replacement of the UbcH5c and Ub structures. As evident by the electron density, the oxyester linkage between UbcH5c S85 and the carboxy-terminus of Ub was maintained in the structure. OspG contacts both the UbcH5c and Ub components of the conjugate, resulting in an extended conformation of Ub with respect to UbcH5c. On their own, UbcH5c and Ub show no major structural changes resulting from binding OspG. As predicted by the sequence conservation among OspG-interacting E2s, OspG contacts UbcH5c at Helix 1 (K4, K8, and R5), Loop 4 (D59, F62, K63), and Loop 7 (S91, Q92, W93, P95, and A96) (Fig. 3b). OspG contacts Ub with an extensive interface centered around the L8-I44-V70 hydrophobic patch for a buried surface area of 907Å (Fig. 3c). Both binding regions are consistent with the NMR studies. While the extended conformation is populated to some extent by UbcH5c~Ub conjugate in solution, it is in contrast to the closed conformations promoted upon binding of an E3 ligase[9,10]. Recent studies on the activation of E2~Ub conjugates by E3 ligases within the RING family have suggested that, in addition to providing increased accessibility to the active site, formation of closed E2~Ub conformations alters the active site and primes the thioester linkage for transfer[10-12]. Among the interactions believed to be important in the activation of the thioester is a hydrogen bond between a conserved E2 asparagine (N77 in UbcH5c) and the carbonyl of the Ub carboxy-terminus. Although UbcH5c~Ub is not in a closed conformation in our structure, a 3.2Å hydrogen bond between UbcH5c N77 and the Ub G76 carbonyl is present (Fig. 3d). Given the unique opportunity to

lock the UbcH5c~Ub conjugate into an extended conformation, we measured the reactivity of the thioester toward lysine in the free and OspG-bound states. By this measure, we found that the UbcH5c~Ub conjugate is stabilized in the context of the OspG complex, thereby confirming the connection between closed conformations and increased catalysis but raising question as to what side chain rearrangements in the active site are required for Ub transfer (Fig. S3a). Minimally, E3-catalyzed Ub transfer depends upon E2:E3 binding and the ability of the E2~Ub conjugate to form closed conformations. Because OspG effectively blocks both of these requirements, it could potentially be an effective inhibitor of ubiquitination, as proposed in the original model of OspG function[6]. However, purified OspG:UbcH5c~Ub complex is still functional in *in vitro* ubiquitination reactions, suggesting that the interaction may not be strong enough to prevent all encounters with an E3 ligase (Fig. S3b).

OspG is part of a family of similar bacterial effector kinases that includes YpkA from *Yersinia pestis* and NleH1 and NleH2 from enterohemorrhagic *Escherichia coli*. Because of their similarity, observations from one family member are often related and/or applied to the others. Primary sequence analysis of these family members with specific focus on the UbcH5c~Ub binding interface revealed that, while YpkA is 100% conserved at the interface (92% identical throughout the kinase domain), NleH1 and NleH2 are much more divergent (13% identical in the interface, 22% throughout the kinase domain for NleH1) (Fig. S4). High sequence conservation would predict that *Yersinia* YpkA would also bind E2~Ub conjugate, but the low sequence conservation of NleH1 and NleH2 necessitated experimentation. We cloned NleH1 and NleH2 from O157:H7 *Escherichia coli* and expressed the proteins as GST fusions for use in pulldown assays. Based on these assays, we found that NleH1 and NleH2 do not interact

with the UbcH5c~Ub conjugate (Fig. S2b). This result suggests that future comparisons between OspG and NleH1/2 function should be made with caution.

OspG itself displays a bilobal α/β structure typical of kinase domains (Fig. 3a). Contacts to the UbcH5c and Ub are made through both lobes of the domain. The structure is complete with the exception of 25 residues at the N-terminus, which likely encode the signal sequence for secretion. Like many bacterial kinases, OspG encodes a very minimalistic kinase domain that only loosely follows sequence motifs established from eukaryotic kinases. The "P-loop" that caps the ATP binding pocket in eukaryotic kinases typically contains large, aromatic residues that close in around the gamma-phosphate group. OspG lacks these aromatic residues and, as such, may utilize some other means to secure ATP within the binding pocket (Fig. 4a, compare CDK2 to OspG). Many eukaryotic kinases contain a large "activation loop" that, when phosphorylated, undergoes a large conformational change that ultimately orients the active site for catalysis. OspG likely relies upon some other type of regulation as it lacks this activation loop entirely (Fig. 4b, compare PKA to OspG). Extensive crystallographic studies on eukaryotic kinases have identified structural determinants for activity that can be used as indicators for the active or inactive states. Proper coordination of ATP/Mg^{2+} requires a number of salt bridge contacts that rely upon proper orientation of an α-helix in the N-terminal lobe. The orientation of this helix is controlled by a nearby conserved phenylalanine, the position of which is indicative of the active (Fig. 4c, CDK2-magenta) and inactive states (Fig. 4c, CDK2-yellow). Analysis of the crystal structure indicates that, within the complex with UbcH5c-O~Ub, OspG shows all of the hallmarks of the active conformation, including the phenylalanine-helix contact (Fig 4c, compare CDK2 and OspG).

OspG is activated upon binding UbcH5c~Ub

The observation that OspG is in the active conformation raises the interesting possibility that binding to E2~Ub conjugates regulates OspG kinase activity. Attempts to crystallize OspG in isolation, however, were unsuccessful due to an increased propensity for aggregation. An NMR HSQC spectrum of OspG shows a high degree of heterogeneity in peak shapes and intensities, consistent with significant conformational exchange (Fig. S5) To assess the activity state of OspG in isolation, we monitored binding to nonhydrolyzable ATP-γ-S by isothermal calorimetry. Addition of concentrated ATP-γ-S to OspG produced only minor heats, though clearly above the control (Fig. 5, compare left and center). Addition of ATP-γ-S to the OspG:UbcH5c~Ub complex, however, produced significantly higher heats of binding (Fig. 5, compare center and right). Although the interaction was not strong enough to obtain a full titration curve, the difference between OspG in complex and in isolation is clear.

To measure OspG activity directly, we used γ32P-ATP and autoradiography to detect levels of phosphorylation. As previously reported[6], GST-OspG displays low levels of autophosphorylation activity (Fig 6, lane 1). Low levels of activity toward proxy substrate Histone H1 can also be detected (Fig 6, lane 1). Formation of the OspG:UbcH5c~Ub complex dramatically increases both auto- and Histone phosphorylation (Fig 6, lane 2). This increase in kinase activity is largely dependent upon the covalent linkage between UbcH5c and Ub, as substitution with the isolated proteins results in lower levels of phosphorylation (Fig. 6, lane 3). Additionally, mutation of the OspG active site (K53M) or the Ub-binding interface (C127R) both result in decreased activity (Fig. 6, lanes 4 and 5). As OspG can also phosphorylate free GST, it is likely that the autophosphorylation observed with the GST-OspG fusion protein occurs on the GST tag, and not within the kinase domain itself (Fig. 6, lanes 6-8). Altogether, the ATP-

binding and kinase activity experiments are consistent with a model in which the OspG kinase domain is activated upon binding to the UbcH5c~Ub conjugate.

Discussion

After invasion of the host cell and subsequent escape from the endocytic pathway, it is imperative that *Shigella flexneri* and other pathogenic bacteria manipulate eukaryotic signaling pathways in order to hide from the innate immune response. To that end, pathogens have evolved sets of effector proteins that target multiple steps within the NF-kB and MAPK signaling cascades. Although these effectors all suppress the NF-kB and MAPK responses from different angles, the commonality lies in the ability of effector proteins to target critical components of the pathway with crippling post-translational modifications. As they are likely secreted into the host cell in low copy numbers, effector proteins that fulfill enzymatic roles carry the highest potential for impacting cellular function. Deamidation, acetylation, ubiquitination, phosphorylation, and proteolysis are only a few examples of activities carried out by effector proteins. The *Shigella flexneri* effector OspG targets host cell pathways at an interesting crossroad between ubiquitination and phosphorylation.

OspG, itself a kinase, interrupts host cell NF-kB signaling through binding to what is commonly regarded as an intermediary within the ubiquitination pathway, the E2~Ub conjugate. Though it isn't the only *Shigella* effector thought to target the NF-kB pathway, infection of rabbit ileal loops with a *Δospg* mutant strain results in significantly more inflammation and tissue destruction compared to the wild type strain[6]. Although OspG's critical role in controlling inflammation has been established, the connection between this large impact on cellular function and the ability to bind E2~Ub conjugates was largely unknown. We found that OspG can

interact with a minimum of 10 E2 enzymes in a cellular context, all of which carry out diverse roles in various cellular compartments making it difficult to predict how OspG might localize to a specific area or pathway within the cell. In fact, outside of the active site, these E2s only show a small amount of sequence conservation that maps to a region of the structure typically known to interact with E3 ligases. NMR titration experiments showed that OspG does interact with the isolated E2 and Ub components, albeit with low affinity. In its conjugated form, however, UbcH5c~Ub copurifies with OspG, a phenomenon not usually observed among the weak and transient interactions that are typical in the ubiquitination pathway. With an interest in how OspG is affecting the UbcH5c~Ub conjugate and vice versa, we determined the crystal structure of the OspG:UbcH5c-O~Ub complex to 2.70Å.

Serendipitously, the OspG:UbcH5c~Ub complex offered a unique opportunity to study the mechanics of Ub transfer. A number of recent studies have described a link between closed E2~Ub conformations and enhanced activities for Ub transfer. In complex with OspG, UbcH5c~Ub is locked into an extended conformation that is, in fact, stabilized and slower to react with a substrate lysine. This observation nicely agrees with previous studies. A source of controversy, however, lies in the contacts made by critical residues in the E2 active site. Past structural and biochemical studies of the E2 active site have defined a model in which a conserved asparagine stabilizes the oxyanion intermediate through hydrogen bonding while the position of a conserved aspartate suppresses the pKa of the incoming lysine (UbcH5c residues N77 and D117, respectively). The UbcH5c~Ub conjugate in our structure meets both of these modeled requirements, yet the active site is apparently not primed for catalysis. This would imply that there is a requirement not present in our structure but fulfilled in closed E2~Ub conformations that has remained unidentified in previous studies of Ub transfer.

Although OspG would make a good inhibitor of ubiquitination based upon the structure, our assays for *in vitro* ubiquitination activity suggest that the interaction is not long-lived enough to effectively block interactions with an E3 ligase. In search of some other source of OspG function, we turned to focus on the OspG kinase domain itself. OspG had been previously shown to possess weak kinase activity that was at least partially responsible for the suppression of the NF-kB transcriptional response[6]. Our structure indicated that the OspG kinase domain is in the active conformation while bound to UbcH5c~Ub. Follow-up studies that examined the capacity of OspG to bind ATP and phosphorylate a proxy substrate both indicated that the activity of OspG is regulated through binding to an E2~Ub conjugate. This represents a novel role for E2~Ub conjugates, which are typically thought to only function within the ubiquitination pathway.

Eukaryotic kinases utilize phosphorylation, localization, and regulatory proteins or domains to carefully limit their activity, so it is reasonable that OspG would also rely upon some type of regulation to enact its function in a precise, targeted manner. The lack of sequence conservation among OspG-interacting E2s outside of the binding region would imply that the localization of OspG to a region/pathway relies upon the Ub or some other potential interaction, and that the role of E2 binding is strictly regulatory. Because most E2s are thought to be Ub-conjugated within the cell[13], it is interesting to speculate that OspG might use E2~Ub conjugates as sensors in the host cell that regulate the switch in kinase activity. The identification of a substrate for OspG kinase activity and how this relates to E2~Ub conjugates will prove to be an interesting avenue of research and will, perhaps, complete the story of how OspG controls the host inflammatory response.

Experimental Procedures

OspG transfections. HEK293 or HeLa cells were grown in DMEM (Gibco) supplemented with 10% FBS (or 5% NCS for HeLa) and penicillin/streptomycin. HEK293 cells were transfected with 4 - 8 μg plasmid DNA per dish using TransIT LT1 (Mirus) and incubated a further 24-36 hours. HeLa cells were transfected with Lipofectamine 2000 (Invitrogen) for 4 hours before media was changed and cells incubated 24-36 hours.

Cell Staining. HEK293 cells were plated on poly-L-lysine coated glass coverslips (BD Biosciences) in 6 well dishes, and incubated overnight at 37˚C under 5% CO2. Cells were then transfected with 1 μg plasmid DNA/well using TransIT LT1 (Mirus) and incubated a further 24-36 hours. HeLa cells were grown on fibronectin coated coverslips (BD Biosciences) and transfected using Lipofectamine 2000 (Invitrogen) for 4 hours before media was changed and cells incubated 24-36 hours. Cells were fixed with 4% (v/v) paraformaldehyde in PBS for 20 min at room temperature, permeabilized in PBS supplemented with 0.2% BSA and 0.1% Triton X-100 for 10 min, and stained with the appropriate primary antibodies for 4 hours at 4°C. Cells were washed three times in PBS and incubated with Alexa Fluor conjugated secondary antibodies (1:500) for 2 h at room temperature. Cells were washed again and mounted on glass slides using ProLong antifade media (Invitrogen). Tubulin was detected using an anti-tubulin monoclonal antibody (Sigma T5168) at a 1:2500 dilution. Actin was labeled by incubation with Texas Red-phalloidin. Nuclei were stained with DRAQ5 or DAPI (4',6-diamidino-2-phenylindole) in the final step before mounting. Cells were imaged with a Zeiss LSM 510 META confocal microscope.

Immunoprecipitation. HeLa cells in 100 mm dishes were transfected as above with DNA encoding N-terminally YFP-tagged OspG in the pDEST6.2 vector. After ~48 hours, cells were harvested in 20 mM HEPES pH 7.4, 150 mM NaCl, 1 mM EDTA, 1% Triton X-100 containing complete-Mini protease inhibitor (Roche). Lysates were centrifuged at 13,000 x g for 20 minutes at 4˚C. The clarified lysates were incubated with GFP-Trap-M magnetic beads (ChromoTek) for 1 hour at 4˚C with rocking. Beads were washed 4 x 1 mL lysis buffer using a handheld magnet (Invitrogen) for bead capture. Protein was eluted by incubation of beads with 0.2 M glycine, pH 2.5 for 10 minutes. Supernatant was removed and quenched with 2 M Tris pH 8.8, then further processed for mass analysis.

Plasmids, protein expression, and purification. Plasmid constructs, expression, and purification of E1, E2s, and Ub were as previously described[14]. For crystallography, OspG was expressed from the pet16 vector at 16˚C for 16 hours with 0.2mM IPTG. OspG was harvested from inclusion bodies with 8M urea, 25mM Tris (pH 7.6), 200 mM NaCl, 10mM NH_4Cl, and refolded through serial 2-fold dilutions of the urea with intermittent centrifugation to remove aggregated protein. The final 1M-0M urea dilution was performed by dialyisis. The protein was then concentrated and purified further by SDX75 size exclusion chromatography into 25mM sodium phosphate (pH 7.0), 150mM NaCl. For all other experiments, OspG was expressed as a GST-fusion protein from the pGEX-4T-2 vector and purified using GSH resin according to the manufacturer's protocol and SDX75 size exclusion chromatography into 25mM sodium phosphate (pH 7.0), 150mM NaCl.

OspG pulldowns from cell extract. Caco-2 cells were grown to confluency and lysed in 50mM Tris (pH 7.6), 150mM NaCl, 1mM EDTA, and 1% NP-40 with protease (Sigma) and phosphatase (Roche) inhibitor cocktails. 30 µL of GSH resin (Invitrogen) was pre-loaded with 30 µL of 50µM protein (GST-OspG, GST-OspG:UbcH5c^{C85S}~Ub, or GST alone) and washed 3X with 500 µL cold 50mM Tris (pH 7.6) 150mM NaCl buffer. Pre-loaded resin was incubated with 100 µL of 1mg/mL cell extract on ice for 30 minutes, then washed 7X with 500 µL cold Tris/NaCl buffer. Resin was eluted with 50 µL of Tris/NaCl + 10mM GSH and processed for mass analysis.

Mass Spectrometry. After tryptic digest, each sample was separated by nanoflow reversed-phase chromatography and directly eluted into a Velos Orbitrap mass spectrometer. Injected peptides were fragmented via collision-activated dissociation and detected in the linear ion trap of the mass spectrometer. Resulting mass spectra were searched against the human IPI database, to which the OspG protein sequence has been added. Identified peptides were filtered to a 1% false-discovery rate. Only those proteins from peptides found exclusively in the OspG containing samples (i.e. not the GST or YFP tag control) were considered to be binding partners of OspG.

OspG pulldowns of E2 panel. Prior to addition of GST-OspG, 35 µL of 10µM E2, 1µM human E1, 20µM Ub, and 5mM $MgCl_2$ were pre-incubated at 37˚C for 15 minutes with or without the addition of 2.5mM ATP. After a 10 µL gel sample was collected (input), 10 µL of GSH resin pre-loaded with 12.5 µL of 25µM GST-tagged protein was added and the mixture was incubated on ice for 30 minutes. After washing 2X with 250 µL cold 25mM sodium phosphate (pH 7.0),

150mM NaCl, the resin was eluted with addition of 35 µL load dye. For samples that were pre-incubated with ATP, non-reducing load dye was used to preserve the E2~Ub thioester.

NMR Spectroscopy. NMR spectra were recorded on a 500 MHz Bruker Avance II (University of Washington). UbcH5c-O~Ub was prepared as previously described using the active site C85S mutation in UbcH5c to improve conjugate stability, and the S22R mutation to prevent self-assembly of the conjugated species (Levin et al., 2010). Spectra were recorded at 25°C in 25mM sodium phosphate (pH 7.0) 150mM NaCl 10% D_2O. $^{1}H,^{15}N$-HSQC-TROSY experiments were collected of 200µM labeled protein with or without the addition of 1 molar equivalent of unlabeled GST-OspG. Datasets were processed using NMRPipe/NMRDraw[15], and visualized with NMRView[16].

Crystallization and Data Collection. The OspG:UbcH5c-O~Ub complex was purified over SDX75 size exclusion chromatography into 50mM HEPES (pH 7.5), 100mM NaCl and concentrated to 200µM. Crystals were grown by sitting drop vapor diffusion at 4˚C in a 2 µL drop (1 µL protein, 1 µL reservoir solution). The optimal condition for crystal growth was 0.1M Tris (pH 8.5), 20% EtOH as a part of the Hampton Research Crystal Screen 2 kit. Crystals were cryoprotected in paraffin oil and shipped to the Stanford Synchrotron Radiation Lightsource for data collection on beamline 9-2. 180 frames at 1˚ intervals were collected at 100K using a MAR325 detector with a crystal distance of 350mm. The X-ray wavelength was 0.9795Å. The datasets were processed using DENZO and SCALEPACK[17].

Structure solution and refinement. Phases were calculated by molecular replacement using the PHASER[18] program within the CCP4 software suite[19] and the UbcH5c structure (PDB ID 1X23) followed by residues 1-72 of the Ub structure (1UBQ). A single solution was found in spacegroup $P6_322$ with one OspG:UbcH5c-O~Ub complex in the asymmetric unit. Parrot[20] and Buccaneer[21] were used for density modification and automated model building of OspG. The model was subjected to iterative refinement with REFMAC5[22] and manipulation in COOT[23]. Molprobity[24] and TLSMD[25] were used during and after refinement. All structure figures were prepared using PyMOL[26]. The atomic coordinates and structure factors have been deposited into the Protein Data Bank (code XXXX).

Isothermal Calorimetry. Measurements were made on a MicroCal ITC-200 calorimeter with freshly prepared proteins at 25˚C. Protein and ATPγS were made up in 25mM HEPES (pH 7.0), 150mM NaCl, 5mM $MgCl_2$, quantified by absorbance (with an ε_{260} of 15.4 for ATP), and degassed under vacuum before use. A range of concentrations and conditions were tested, but the most binding information was obtained with 1.5 µL additions of 1mM ATPγS at 3-minute intervals into 50µM protein (GST, GST-OspG, or GST-OspG:UbcH5c-O~Ub). Reverse titrations of 100µM protein (GST-OspG or GST-OspG:UbcH5c-O~Ub) into 1mM ATPγS were also performed to approximate the total enthalpy of binding.

Kinase Assays. Kinase assays were performed with purified proteins and Histone H1 (Sigma) as a proxy substrate. OspG alone, OspG mutants or OspG-conjugate complexes (~6.7 µM final) were incubated in 25 mM Tris-HCl pH 7.5, 10 mM MgCl2, 100 µM ATP with 5 µg histone and 0.5 µCi γ32P-ATP for 20 minutes at 30˚C with shaking. Reactions were stopped by addition of

5X Laemlli sample buffer and boiling for 5 minutes. Kinase reactions were separated by SDS-PAGE on 4-12% gradient gels (Invitrogen). After transfer to nitrocellulose, membranes were washed 3 x 5 minutes in PBS + 0.3% Tween-20 and stained with 0.2% india ink in the same buffer. Membranes were dried and exposed to autoradiographic film.

References

1. Parsot, C. *Shigella* type III secretion effectors: how, where, when, for what purposes? *Curr. Opin. Microbiol.* **12**, 110-116 (2009).
2. Brennan, D.F. & Barford, D. Elimination: a post-translational modification catalyzed by phosphothreonine lyases. *Trends Biochem. Sci.* **34**, 108-114 (2009).
3. Li, H. *et al.* The phosphothreonine lyase activity of a bacterial type III effector family. *Science*. **315**, 1000-1003 (2007).
4. Mukherjee, S. *et al. Yersinia* YopJ acetylates and inhibits kinase activation by blocking phosphorylation. *Science*. **312**, 1211-1214 (2006).
5. Sanada, T. *et al.* The *Shigella flexneri* effector OspI deamidates UBC13 to dampen the inflammatory response. *Nature*. **483**, 623-626 (2012).
6. Kim, D.W. *et al.* The *Shigella flexneri* effector OspG interferes with innate immune responses by targeting ubiquitin-conjugating enzymes. *Proc. Natl. Acad. Sci. USA*. **102**, 14046-14051 (2005).
7. Wenzel, D.W., Stoll, K.E., & Klevit, R.E. E2s: Structurally economical and functionally replete. *Biochem. J.* **433**, 31-42 (2010).
8. Levin, I. *et al.* Identification of an unconventional E3 binding surface on the UbcH5~Ub conjugate recognized by a pathogenic bacterial E3 ligase. *Proc. Natl. Acad. Sci. USA*. **107**, 2848-2853 (2010).
9. Pruneda, J.N., Stoll, K.E., Bolton, L.J., Brzovic, P.S., & Klevit, R.E. Ubiquitin in motion: Structural studies of the E2~Ub conjugate. *Biochemistry*. **50**, 1624-1633 (2011).
10. Pruneda, J.N. *et al.* Structure of an E3:E2~Ub complex reveals an allosteric mechanism shared among RING/U-box ligases. *Mol. Cell*. **47**, 933-942 (2012).
11. Plechanovová, A., Jaffray, E.G., Tatham, M.H., Naismith, J.H., & Hay, R.T. Structure of a RING E3 ligase and ubiquitin-loaded E2 primed for catalysis. *Nature*. **489**, 115-120 (2012).
12. Dou, H., Buetow, L., Sibbet, G.J., Cameron, K., & Huang, D.T. BIRC7-E2 ubiquitin conjugate structure reveals the mechanism of ubiquitin transfer by a RING dimer. *Nat. Struct. Mol. Biol.* **19**, 876-883 (2012).
13. Haas, A.L. & Rose, I.A. The mechanism of ubiquitin activating enzyme. A kinetic and equilibrium analysis. *J. Biol. Chem.* **257**, 10329-10337 (1982).

14. Christensen, D.E., Brzovic, P.S., & Klevit, R.E. E2-BRCA1 RING interactions dictate synthesis of mono- or specific polyubiquitin chain linkages. *Nat. Struct. Mol. Biol.* **14**, 941-948 (2007).

15. Delaglio, F. *et al*. NMRPipe: A multidimensional spectral processing system based on UNIX pipes. *J. Biomol. NMR.* **6**, 277-293 (1994).

16. Johnson, B. A. & Blevins, R. A. NMRView: a computer program for the visualization and analysis of NMR data. *J. Biomol. NMR.* **4**, 603-614 (1994).

17. Otwinowski, Z. & Minor, W. Denzo and Scalepack. *Methods Enzymol*. **276**, 307-326 (1997).

18. McCoy, A.J. *et al.* PHASER crystallographic software. *J. Appl. Cryst.* **40**, 658-674 (2007).

19. Winn, M.D. *et al.* Overview of the CCP4 suite and current developments. *Acta Crystallogr. D Biol. Crystallogr.* **67**, 235-242 (2011).

20. Cowtan, K. Recent developments in classical density modification. *Acta Crystallogr. D Biol. Crystallogr.* **66**, 470-478 (2010).

21. Cowtan, K. The Buccaneer software for automated model building. 1. Tracing protein chains. *Acta Crystallogr. D Biol. Crystallogr.* **62**, 1002-1011 (2006).

22. Murshudov, G.N. *et al.* REFMAC5 for the refinement of macromolecular crystal structure. *Acta Crystallogr. D Biol. Crystallogr.* **67**, 355-367 (2011).

23. Emsley, P., Lohkamp, B., Scott, W.G., & Cowtan, K. Features and development of Coot. *Acta Crystallogr. D Biol. Crystallogr.* **66**, 486-501 (2010).

24. Chen, V.B. *et al.* MolProbity: all-atom structure validation for macromolecular crystallography. *Acta Crystallogr. D Biol. Crystallogr.* **66**, 12-21 (2010).

25. Painter, J. & Merritt, E.A. Optimal description of a protein structure in terms of multiple groups undergoing TLS motion. *Acta Crystallogr. D Biol. Crystallogr.* **62**, 439-450 (2006).

26. The PyMOL Molecular Graphics System, Version 1.5.0.4 Schrödinger, LLC.

27. Ashkenazy, H., Erez, E., Martz, E., Pupko, T., & Ben-Tal, N. ConSurf 2010: calculating evolutionary conservation in sequence and structure of proteins and nucleic acids. *Nucl. Acids Res.* **38**, 529-533 (2010).

Acknowledgements

We thank I. Le Trong and R. Stenkamp for their assistance with X-ray data collection and their guidance with structure solution and refinement. This work was supported by National Institutes of Health Grants R01 GM088055 (R.E.K.), the U.S. Public Health Service Grant NRSA 2T32 GM007270 from the National Institute of General Medical Sciences (J.N.P.), and the Northwest Regional Center of Excellence.

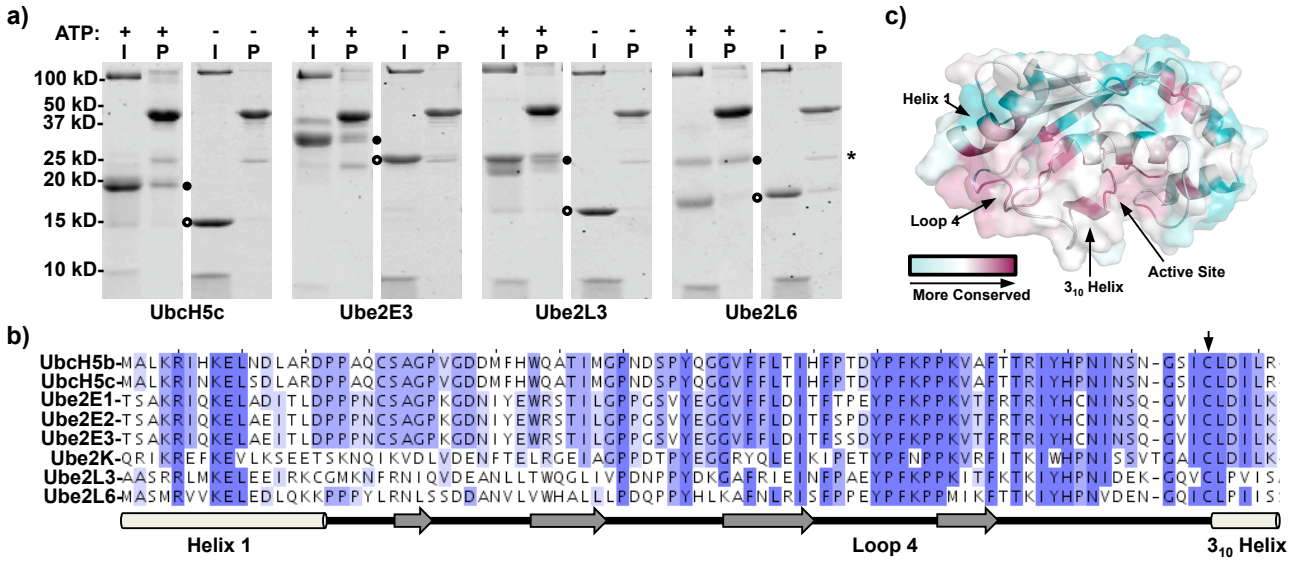

Figure 1. OspG binds a cohort of E2s. a) Representative *in vitro* GST-OspG pulldowns of E2 and E2~Ub conjugates (see Supplementary Fig. 1 for whole gels). Samples pre-incubated with ATP were loaded in non-reducing load dye to preserve the thioester linkage. Closed and open circles denote the migration of the Ub-conjugated and isolated forms of each E2, respectively. Input (I) samples represent a 100% potential for the Pulldown (P) sample. A small amount of free GST contaminant in the GST-OspG prep is denoted with an asterisk. **b)** Primary sequence alignment of all OspG-interacting E2s identified by yeast 2-hybrid[6] or mass spectrometry experiments and confirmed by *in vitro* pulldown experiments. The active site cysteine is marked with an arrow. Residues are colored by conservation. **c)** ConSurf[27] analysis of the E2s shown in part b), colored onto the UbcH5c solution structure (PDB 2FUH). Structural features are marked. The active site and E3-binding interface (magenta) are the most conserved regions among all OspG-interacting E2s.

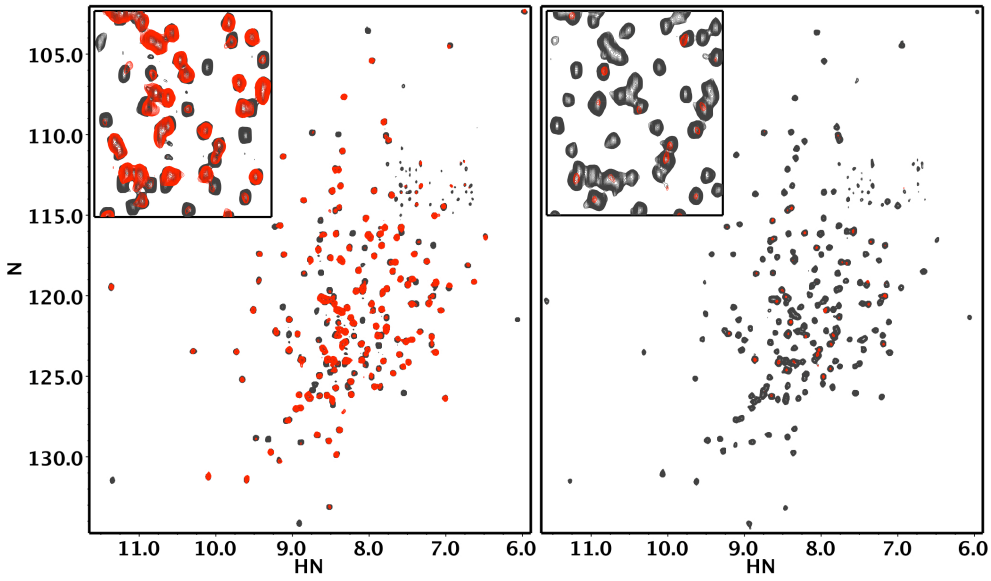

Figure 2. OspG weakly interacts with isolated UbcH5c and Ub. ^{1}H, ^{15}N-HSQC-TROSY experiments of isolated UbcH5c + Ub (left) and the UbcH5c-O~Ub conjugate (right) before and after addition of 1 molar equivalent of GST-OspG (grey and red, respectively). An enlarged region of the center (inset) shows severe linewidth broadening in the UbcH5c-O~Ub spectrum after addition of OspG, illustrating the significant difference in affinity attained through conjugation of the two molecules. By comparision, OspG shows weaker interactions with the isolated components, mapping to the E3-binding interface of UbcH5c and I44 hydrophobic patch of Ub.

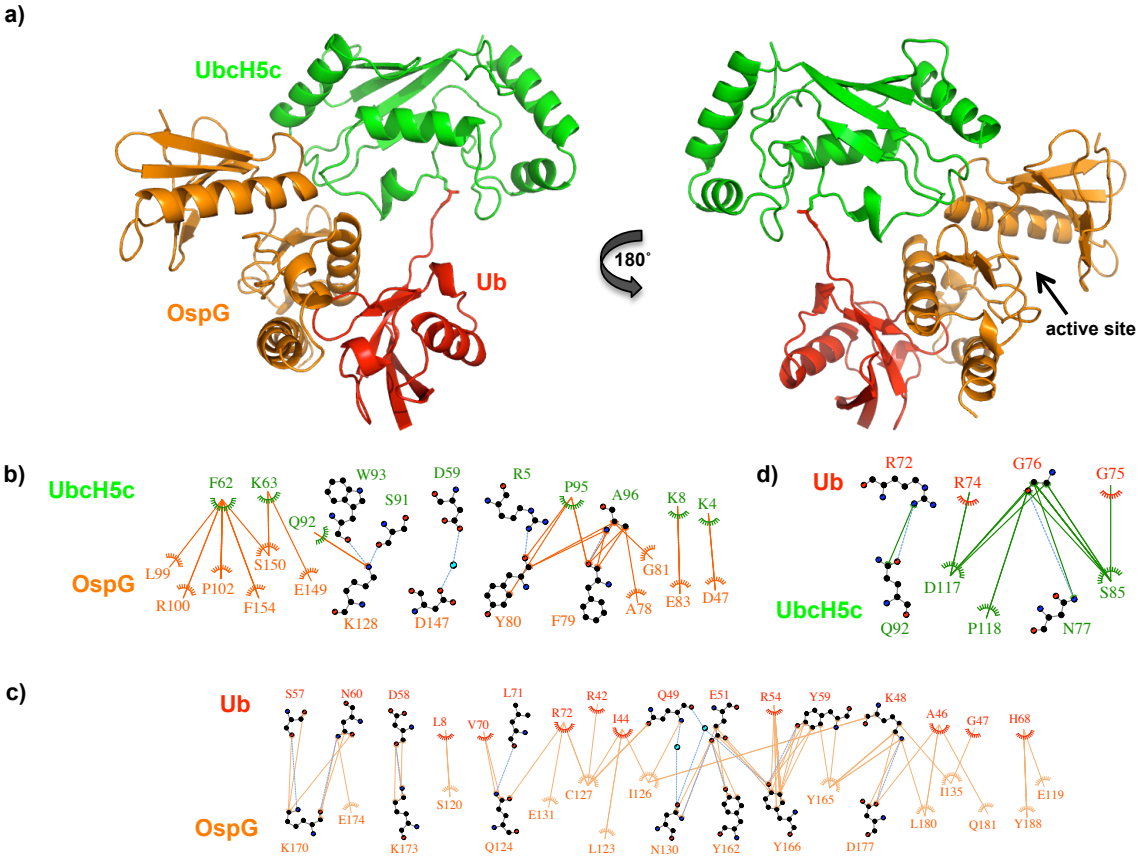

Figure 3. Crystal structure of the OspG:UbcH5c~Ub complex. a) Ribbon representation of the OspG:UbcH5c-O~Ub crystal structure at 2.70Å. UbcH5c (green) is covalently linked to Ub (red) and locked into an extended conformation by OspG (orange). The OspG active site is marked and faces away from the UbcH5c~Ub conjugate. Detailed schematics are shown for the **b)** UbcH5c:OspG, **c)** Ub:OspG, and **d)** Ub:UbcH5c interfaces.

Table 1 Data collection and refinement statistics

	OspG:UbcH5c-O~Ub
Data collection	
Space group	$P6_322$
Cell dimensions	
a, *b*, *c* (Å)	183.87, 183.87, 63.97
α, β, γ (°)	90, 90, 120
Resolution (Å)	50-2.70 (2.80-2.70)
R_{sym}	0.202 (1.0)
$I / \sigma I$	16.39 (2.58)
Completeness (%)	99.90 (99.72)
Redundancy	19.1 (11.2)
Refinement	
Resolution (Å)	44.16-2.70
No. reflections	17031
R_{work} / R_{free}	0.200 / 0.266
No. atoms	3256
Protein	3165
Ligand/ion	0
Water	91
B-factors	
Protein	18.70
Water	18.50
R.m.s. deviations	
Bond lengths (Å)	0.009
Bond angles (°)	1.18

*Values in parentheses are for highest-resolution shell.

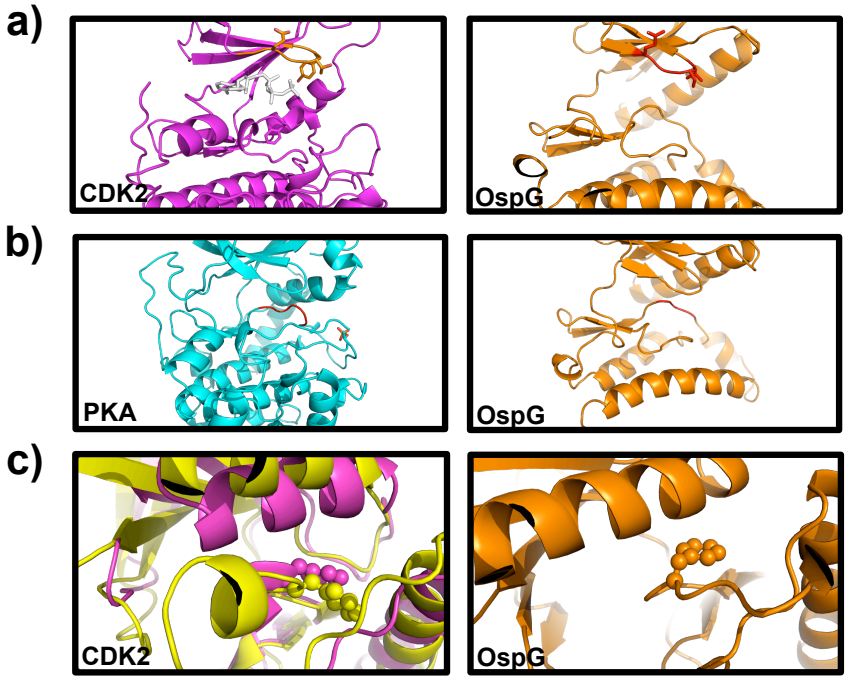

Figure 4. Structural comparisons to eukaryotic kinases. **a)** Left, the role of the P-loop (orange) in capping the ATP-binding pocket is shown for CDK2 (PDB 1FIN). Right, by comparison, the analogous loop in OspG (red) encodes smaller side chains and is likely less efficient at holding ATP in place. **b)** Left, the catalytic loop (red) of eukaryotic kinases is often properly oriented by a nearby phosphorylation event (sticks), as shown for PKA (PDB 2CPK). Right, the structure of OspG lacks the regulatory region of the activation loop (red), suggesting that it must be regulated by some other means. **c)** Left, the CDK2 Phe-Helix αC contact is shown as a hallmark of the inactive (yellow, PDB 1HCL) and active (magenta, PDB 1FIN) kinase states. Right, the OspG Phe-Helix αC contact is shown. This, along with other hallmarks of active kinases, demonstrates that OspG is in the active state while in complex with the UbcH5c~Ub conjugate.

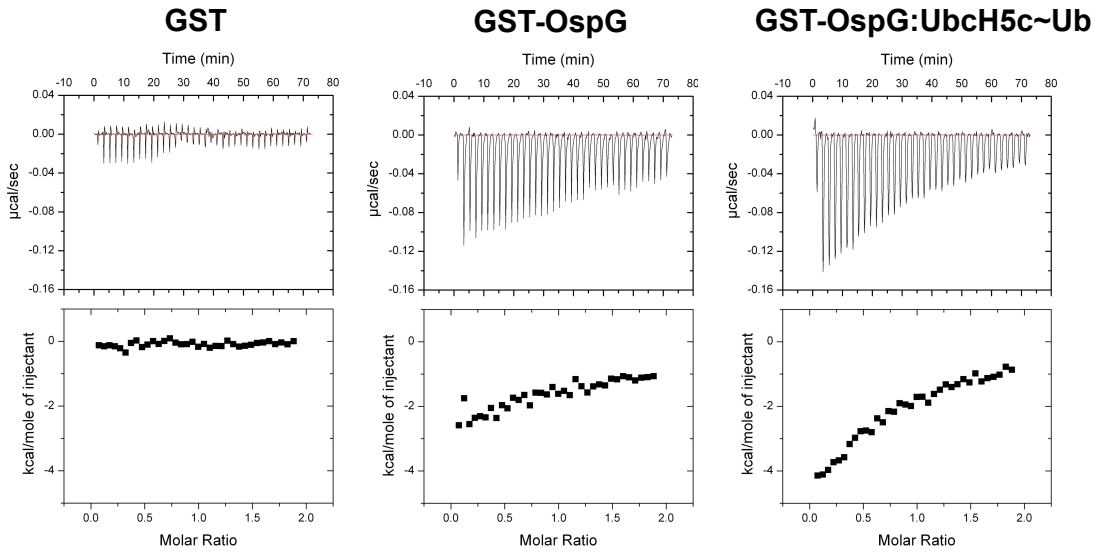

Figure 5. OspG binds ATP with higher affinity in the context of the OspG:UbcH5c~Ub complex. Raw heat outputs and integrated isotherms for titration of 1mM ATPγS into 50µM GST (left), GST-OspG (center), or GST-OspG:UbcH5c-O~Ub complex (right).

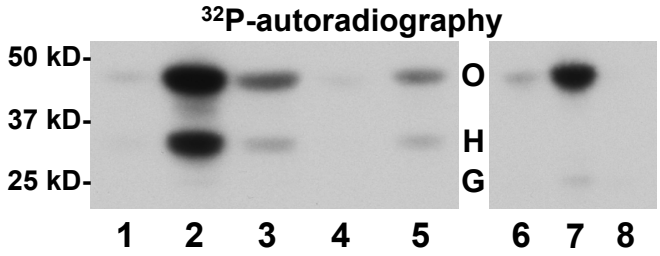

Figure 6. OspG kinase activity is elevated in the context of the OspG:UbcH5c~Ub complex. (1-5) γ32P-ATP kinase assay measuring activity against GST-OspG itself (O) and Histone H1 (H). Kinase samples were premixed with E2/Ub (or buffer) at a 1:1.2 molar ratio. **1)** OspG alone, **2)** premixed OspG + UbcH5c^{C85S}~Ub, **3)** premixed OspG + UbcH5c + Ub (unconjugated), **4)** premixed OspG^{K53M} + UbcH5c^{C85S}~Ub, **5)** premixed OspG^{C127R} + UbcH5c^{C85S}~Ub. **(6-8)** γ32P-ATP kinase assay measuring activity against GST-OspG itself (O) and GST (G) control. **6)** OspG alone, **7)** purified OspG:UbcH5c^{C85S}~Ub complex, **8)** purified OspG^{K53M}:UbcH5c^{C85S}~Ub complex.

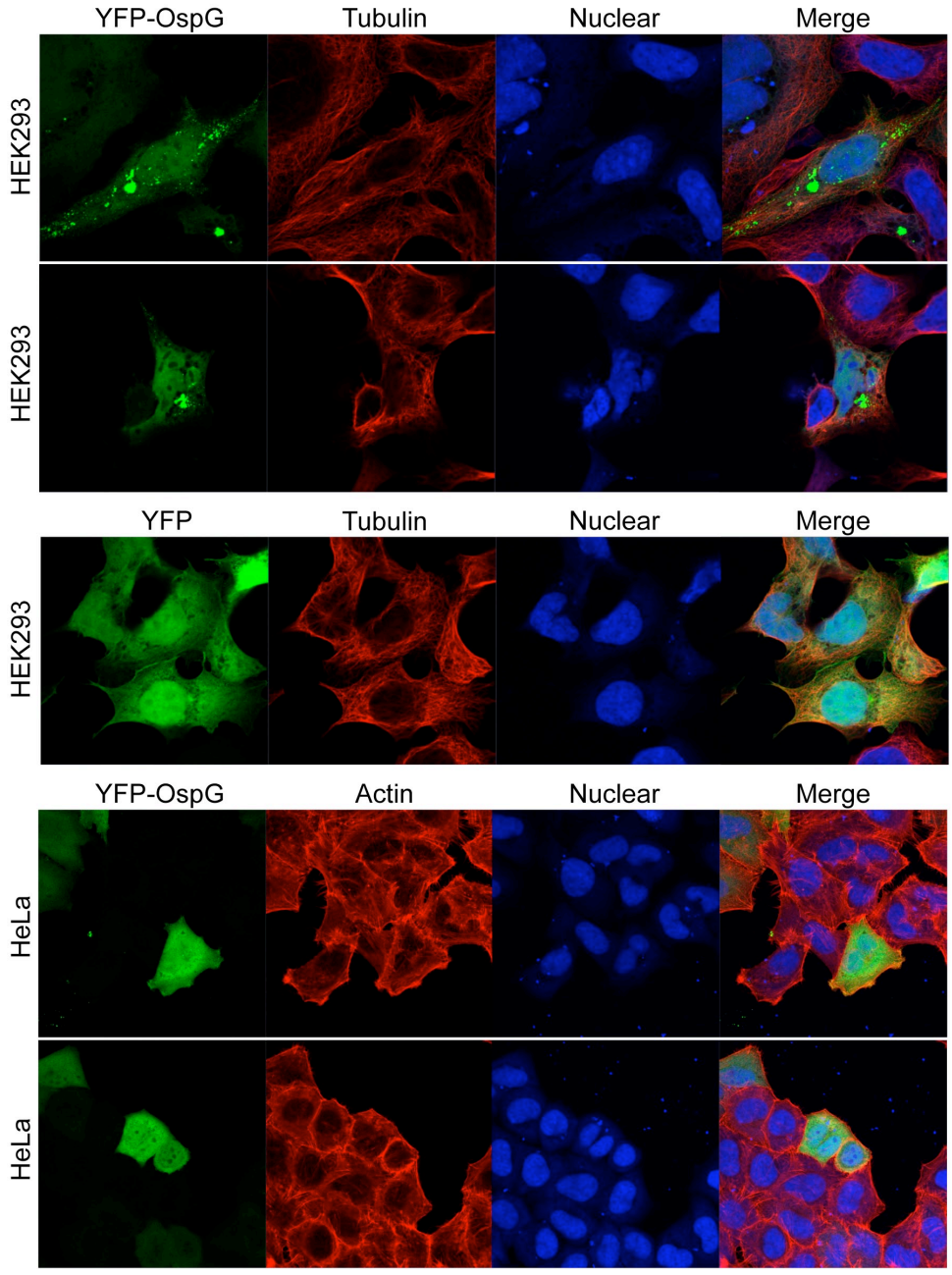

Supplemental Figure 1. YFP-OspG shows cellular localization dependent upon cell type. Tranfection of YFP-tagged OspG (green) into HEK293 and HeLa cell lines. Cytoskeletal and nuclear stains are also shown for reference.

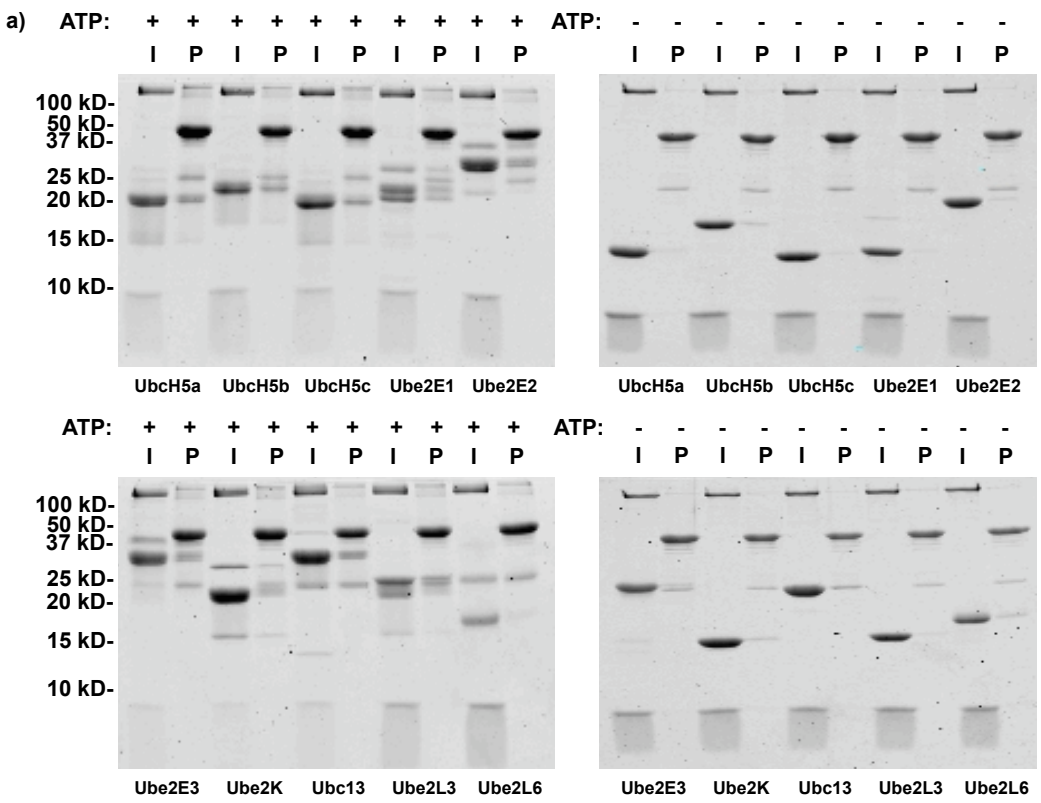

Supplemental Figure 2. GST-OspG pulldowns experiments. (a) GST-OspG pulldowns for a panel of 10 isolated and Ub-loaded E2s. **(b)** Pulldowns of UbcH5c~Ub using GST-OspG, GST, GST-NleH1, or GST-NleH2.

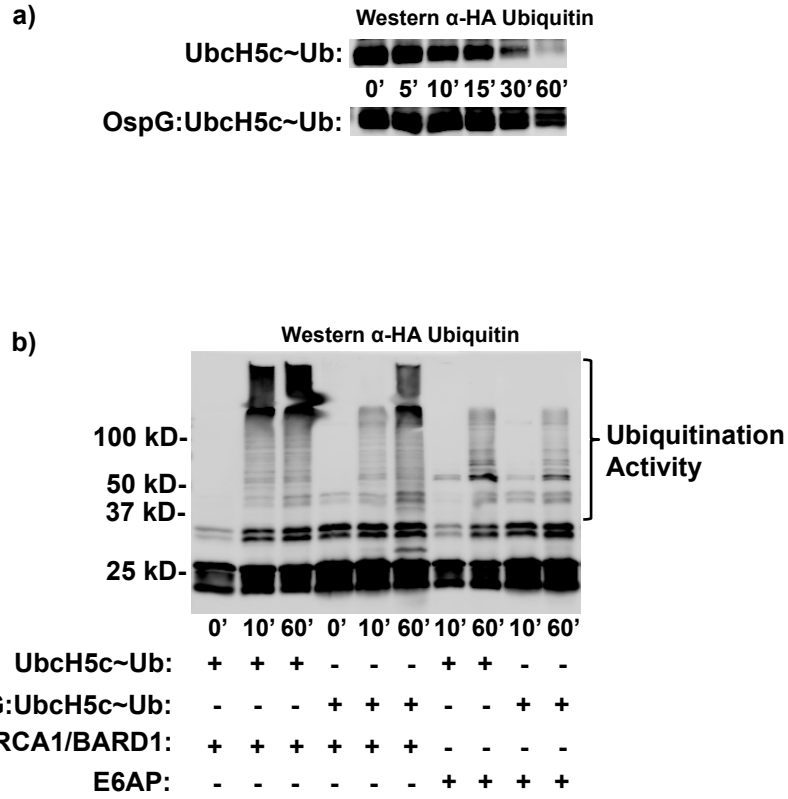

Supplemental Figure 3. Reactivity of the UbcH5c~Ub conjugate within the OspG:UbcH5c~Ub complex. (a) 5μM samples of purified UbcH5c~Ub or OspG:UbcH5c~Ub(HA) were reacted with 50mM Lysine over a 60-minute timecourse. Non-reducing gel samples were separated by SDS-PAGE, transferred to nitrocellulose, and Western blotted for the HA-epitope tag on Ub. Decay of the UbcH5c~Ub species is shown. **(b)** 20μM samples of purified UbcH5c~Ub or OspG:UbcH5c~Ub were reacted with 2μM E3 (BRCA1/BARD1 heterodimeric RING ligase or E6AP HECT ligase) over a 60-minute timecourse. Gel samples were separated by SDS-PAGE, transferred to nitrocellulose, and Western blotted for the HA-epitope tag on Ub. High molecular weight Ub products are indicated.

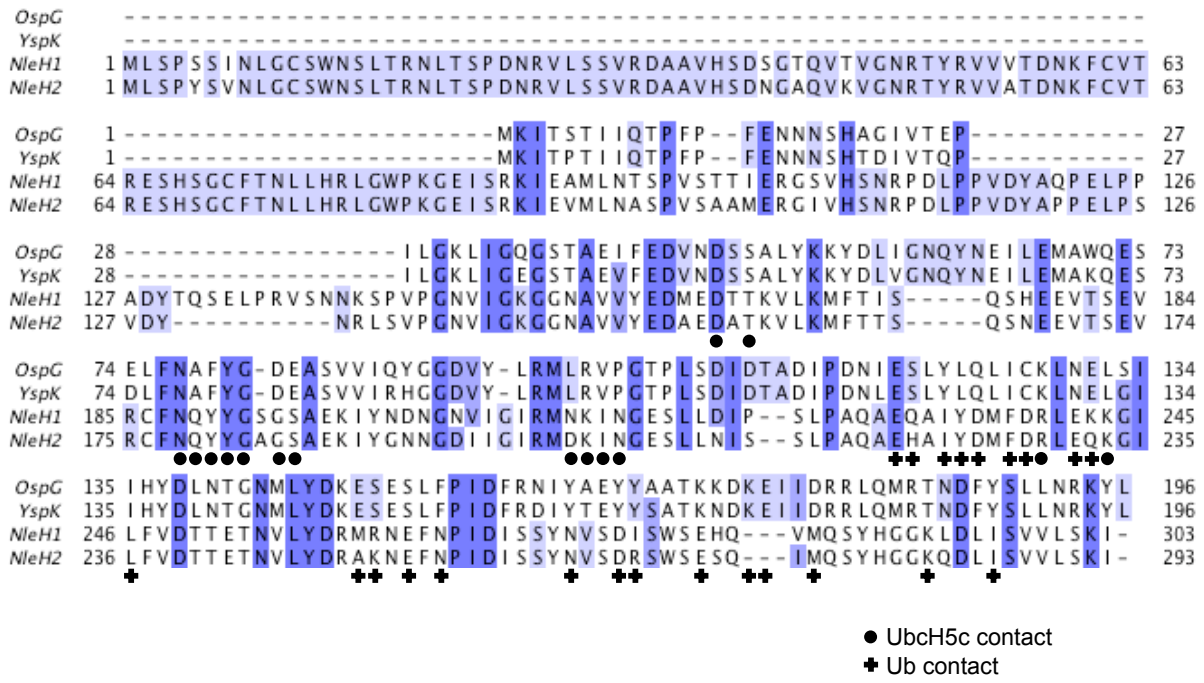

Supplemental Figure 4. Effector kinase sequence alignment. Sequence alignment between OspG and the related effector kinases YspK (*Yersinia pestis*), NleH1, and NleH2 (EHEC *Escherichia coli*). Sequences are colored by conservation. The UbcH5c- and Ub-interfaces on OspG are indicated.

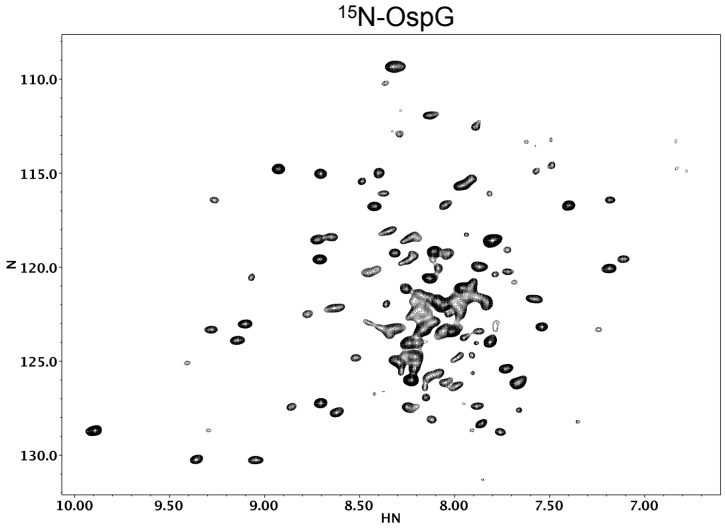

Supplemental Figure 5: OspG shows signs of dynamics. ^{1}H, ^{15}N-HSQC-TROSY spectrum of 265μM ^{15}N-labeled OspG collected at 500 MHz.

Chapter VI – Concluding Remarks

The goal of this thesis work focused on a fairly simple concept: what structural changes are associated with an E3 ligase interacting with an E2~ubiquitin conjugate, and are these changes at all related to ubiquitin (Ub) transfer activity. Although the cartoon representation of the Ub transfer pathway shown in the Introduction portrays this as a relatively straightforward process, the structural characterization and functional understanding of this critical step of ubiquitination are much more complicated. At the inception of this project, very little was known about E2~Ub conjugates or how they interact with E3 ligases. Although it actually represents the product of the Ub transfer reaction, structural biologists had instead focused their efforts on characterizing interactions between E3s and isolated E2s. Though informative for futures studies (including those performed herein), structure after structure of RING E3:E2 complexes was published, each looking nearly identical to the last and each showing virtually no changes when compared to structures of the isolated domains. Knowing that it would unlock secrets critical to understanding E3 function, we set out to determine the structure of a RING E3:E2~Ub complex in a state poised for Ub transfer.

Of course, to fully appreciate the role played by E3 ligases in facilitating Ub transfer, we first had to develop a structural understanding of the E2~Ub conjugate. At that time, only two structures of E2~Ub species had been deposited into the PDB. These structures represented a snapshot of E2~Ubs in a single conformation. However, as our initial studies of the UbcH5c~Ub conjugate indicated that the E2~Ub conjugate is highly dynamic, we adapted our strategies to accommodate this fluid structure. The combination of paramagnetic NMR techniques and small angle X-ray scattering (SAXS) provided the orientation/population information required to generate appropriate models of both the UbcH5c~Ub and Ubc13~Ub conjugates. Interestingly,

the pattern of E2~Ub conformations differed for the two E2s, which may have implications for how they interact with other cellular proteins.

Based on the NMR and SAXS information, the UbcH5c~Ub conjugate prefers extended conformations in which the conjugated Ub is positioned directly below the active site. Using this as a starting point, we incorporated RING E3 ligases into our structural studies to find that E3 binding causes a shift in the population of UbcH5c~Ub states toward more closed conformations. Additional structural and biochemical work showed that these closed conformations are strictly required for E3-mediated Ub transfer activity, and are commonly utilized by diverse E2s and RING-type E3s. From this work, we identified a basic residue conserved among RING/U-box E3s, and proposed that this was the "allosteric linchpin" responsible for activating E2~Ub conjugates. We have shown this structurally and functionally through mutation of the ligases BRCA1/BARD1 and Ube4b, and have heard anecdotally from other groups that the analogous mutation in their E3 of choice also disrupts Ub transfer activity. Hopefully, with time, other labs will introduce this mutation into their E3s and its ability to commonly inactivate ligases will be truly put to the test. As RING/U-box E3 ligases do not carry a conventional active site, the identification of a truly "ligase-dead" mutant has proven difficult. To date, the most commonly utilized mutations target either structural positions such as Zn-liganding cysteines in RING domains (e.g. BRCA1 C61G) or residues that contribute to E3:E2 binding (e.g. BRCA1 I26A). Mutation of a catalytic position such as the allosteric linchpin could create a more appropriate control for studies involving E3 functionality and substrate identification.

To further understand what aspects of an E3 ligase contribute to the activation of E2~Ub conjugates, we collaborated with Stan Fields' lab to perform a deep mutational scan of the Ube4b U-box domain. After screening nearly 100,000 variants, rare mutations were identified

that dramatically increased Ube4b ligase activity. Detailed structural analyses grouped these activating mutations into two main categories: those that increase E3:E2 binding affinity and those that enhance the allosteric capacity of the U-box domain to promote closed E2~Ub conformations. The success of this screen in identifying rare mutations that enhance ligase activity opens avenues of research that could utilize this method to address key biochemical questions plaguing the ubiquitin field. First, a slightly modified version of this method could be used to create "non-native" E3:E2 pairs that could be used to further distinguish E3- from E2-dependent functions. For example, suppositions that E3s control substrate specificity and E2s dictate product formation (e.g. mono- vs. poly-ubiquitination) could be examined with the proper switches of E3:E2 pairings. Second, the comparison of two screens performed with different E2 enzymes could identify "E2-specific" mutations; that is to say, mutations that enhance activity for one E2, but decrease activity for another. These mutations could be used to dissect the roles of specific E3:E2 pairs in biological pathways and even identify which E2 an E3 uses for ubiquitination of a particular target protein.

The identification of ligase-activating mutations, be they universal or E2-specific, provide powerful tools for studies aimed at identifying *in vivo* substrates of particular E3 ligases, particularly those studies using large-scale mass spectrometry approaches. In combination with ligase-dead mutants (such as those incorporating mutation of the allosteric linchpin), ligase-activating mutants could expand the dynamic range of ubiquitinated products in a SILAC-based approach and allow for the identification of ubiquitination events that are dependent upon the E3 of choice. Thus, our findings on the role of the E3 ligase in enacting Ub transfer have both furthered our understanding of ubiquitin biology and contributed molecular tools to be used for future research.

As an interesting twist on Ub research, part of my thesis work looked at the E2~Ub conjugate from the perspective of bacterial effector proteins. These proteins are secreted into the host cell during bacterial invasion and often circumvent host cellular pathways to promote their survival. I spent some time looking at a class of bacterial E3 ligases that hijack our ubiquitination machinery to target novel substrates, but the majority of my bacterial effector work focused on the *Shigella* kinase OspG. This protein shows a high level of preference for the Ub-loaded form of the E2, and through crystallographic and biochemical studies we showed that OspG kinase activity is stimulated through association with the E2~Ub conjugate. Ultimately the goal of this research would be to develop a better picture of how OspG contributes to *Shigella* pathogenesis by identifying a substrate for its kinase activity. Unfortunately, as with ubiquitination, identifying substrates of kinase activity can be difficult. Our most promising approach has used a SILAC-based strategy to identify variations in the phospho-proteome of cells that have been infected with either wild type or Δ*ospg* strains of *Shigella flexneri*. With continued optimization and detailed follow-up studies, this approach will hopefully successfully identify an OspG substrate and verify this approach as a technique that can be used to identify substrates of other bacterial effector enzymes, such as E3 ligases. The short exposure I have received to effector proteins involved in bacterial pathogenesis has given me a strong appreciation for the "ingenuity" displayed by bacteria in their development of secretory molecules that can intercalate and redirect host biology. In the course of studying these effector proteins, it has become apparent that, in addition to describing their role in pathogenesis, these molecules can also reveal novel facets of human biology that had previously gone unnoticed. Thus, bacterial effector proteins offer a unique "outside the box" approach to attacking lingering biological questions.

Curriculum Vitae – Jonathan N. Pruneda

Education:

2008: **B.S. Biochemistry, minor in Chemistry – *Summa Cum Laude***
Washington State University, Pullman, WA

2008: **B.S. Microbiology, minor in Molecular Biology – *Summa Cum Laude***
Washington State University, Pullman, WA

Research Experience:

Spring 2008 to Present: **Graduate Student**
Dr. Rachel Klevit, Department of Biochemistry, University of Washington, Seattle, WA
Structural and biochemical studies of protein-protein interactions responsible for transfer of the signaling molecule ubiquitin.

Fall 2007 to Spring 2008: **Undergraduate Researcher**
Dr. Lisa Gloss, School of Molecular Biosciences, Washington State University, Pullman, WA
Enzymatic and protein folding studies on *H. volcanii* dihydrofolate reductase for identification of factors that contribute to function under extremely high salt conditions.

Summers of 2005-2007: **Biological Science Aide**
Dr. Lawrence Lacey, USDA-ARS, Wapato, WA
Assessment of biological agents for insect biocontrol, with focus on several insect baculoviridae, as well as some bacteria, fungi, and nematodes.

Workshops/Other Training:

January 2010: **Biological Small Angle Scattering**, Copenhagen, Denmark

Presentations:

November 2012: **Oral**, "Activation of *Shigella* effector OspG requires binding to host cell ubiquitination machinery" American Society for Microbiology Northwest Conference, Seattle, WA.

June 2012: **Oral and Poster**, "Working outside the box: A non-canonical role for E2~Ub conjugates in the activation of the bacterial effector protein OspG" Ubiquitin and Cellular Regulation FASEB Conference, Saxtons River, VT. Awarded Young Scientist Award for best talk by a young scientist.

September 2011: **Oral**, "Conformational activation of E2~Ub conjugates by RING-type E3 ligases" Seattle Ubiquitin Research Group, Seattle, WA

May 2011: **Poster**, "Conformational activation of E2~Ub conjugates by RING-type E3 ligases" The Ubiquitin Family Conference, Cold Spring Harbor, NY

Teaching Experience:

Spring 2010: **Basic Techniques in Biochemistry Lab Teaching Assistant**, University of Washington

Fall 2009: **Intro to Protein Structure and Intermediary Metabolism Teaching Assistant**, University of Washington

Fall 2007 to Spring 2008: **Multicultural Student Mentor**, Washington State University
Spring 2008: **Advanced Organic Chemistry Lab Assistant**, Washington State University
Fall 2006 to Fall 2008: **Organic Chemistry Tutor**, Washington State University

Honors and Awards:

2012: **Young Scientist Award,** Ubiquitin and Cellular Regulation FASEB Conference, Saxtons River, VT (award given to best oral presentation by a young scientist)
2009 to 2012: **NIH Cellular and Molecular Biology Trainee**
2011: **Best Poster Award,** The Ubiquitin Family Conference, Cold Spring Harbor, NY
2011: **Schultz Travel Fellowship**
2010: **NSF Graduate Research Fellowship "Honorable Mention"**
2010: **Schultz Travel Fellowship**
2009: **NSF Graduate Research Fellowship "Honorable Mention"**
2004 to 2008: **Washington State University President's Honor Roll**
2007 to Present: **Member of Phi Beta Kappa**
2007: **Thomas S. Foley Institute for Public Policy and Public Service Award**
2005: **Science Opportunity Scholarship**

Publications:

Pruneda, J. N., Littlefield, P. J., Soss, S. E., Nordquist, K. A., Chazin, W. J., Brzovic, P. S., and Klevit, R. E. (2012) Structure of an E3:E2~Ub complex reveals an allosteric mechanism shared among RING/U-box ligases. *Molecular Cell*. *47*, 933-942. PMC3462262.

Page, R. C.*, **Pruneda, J. N.***, Amick, J., Klevit, R. E., and Misra, S. (2012) Structural insights into the conformation and oligomerization of E2~Ubiquitin conjugates. *Biochemistry*. *51*, 4175-4187. PMC3366460.

Juang, Y. C.*, Landry, M. C.*, Sanches, M., Vittal, V., Leung, C., Ceccarelli, D. F., Mateo, A. R. F., **Pruneda, J. N.**, Mao, D., Szilard, R. K., Orlicky, S., Munro, M., Brzovic, P. S., Klevit, R. E., Sicheri, F. and Durocher, D. (2012) OTUB1 co-opts Lys48-linked ubiquitin recognition to suppress E2 enzyme function. *Molecular Cell. 45*, 384-397. PMC3306812.

Korotkov, K. V., Johnson, T. L., Jobling, M. G., **Pruneda, J.**, Pardon, E., Héroux, A., Turley, S., Steyaert, J., Holmes, R. K., Sandkvist, M., and Hol, W. G. (2011) Structural and Functional Studies on the Interaction of GspC and GspD in the Type II Secretion System. *PLOS Pathog. 7*, e1002228. PMC3169554.

Pruneda, J. N.*, Stoll, K. E.*, Bolton, L. J., Brzovic, P. S., and Klevit, R. E. (2011) Ubiquitin in Motion: Structural studies of the ubiquitin-conjugating enzyme~ubiquitin conjugate. *Biochemistry. 50*, 1624-1633. PMC3056393.

Arthurs, S., Lacey, L., **Pruneda, J.**, and Rondon, S. (2008) Semi-field evaluation of a granulovirus (PoGV) and *Bacillus thuringiensis* ssp. kurstaki for season-long control of the potato tuber moth, *Phthorimaea operculella*. *Entomol. Exp. Appl. 127*, 276-285.

***Authors contributed equally**

ELSEVIER LICENSE
TERMS AND CONDITIONS

Dec 03, 2012

This is a License Agreement between Jonathan Pruneda ("You") and Elsevier ("Elsevier") provided by Copyright Clearance Center ("CCC"). The license consists of your order details, the terms and conditions provided by Elsevier, and the payment terms and conditions.

All payments must be made in full to CCC. For payment instructions, please see information listed at the bottom of this form.

Supplier	Elsevier Limited The Boulevard,Langford Lane Kidlington,Oxford,OX5 1GB,UK
Registered Company Number	1982084
Customer name	Jonathan Pruneda
Customer address	1705 NE Pacific St. Seattle, WA 98195
License number	3010290985356
License date	Oct 15, 2012
Licensed content publisher	Elsevier
Licensed content publication	Molecular Cell
Licensed content title	Structure of an E3:E2~Ub Complex Reveals an Allosteric Mechanism Shared among RING/U-box Ligases
Licensed content author	Jonathan N. Pruneda,Peter J. Littlefield,Sarah E. Soss,Kyle A. Nordquist,Walter J. Chazin,Peter S. Brzovic,Rachel E. Klevit
Licensed content date	9 August 2012
Licensed content volume number	
Licensed content issue number	
Number of pages	1
Start Page	
End Page	
Type of Use	reuse in a thesis/dissertation
Portion	full article
Format	both print and electronic
Are you the author of this Elsevier article?	Yes
Will you be translating?	No
Order reference number	

Title of your thesis/dissertation	Conformational Manipulation of E2~Ub Conjugates
Expected completion date	Dec 2012
Estimated size (number of pages)	100
Elsevier VAT number	GB 494 6272 12
Permissions price	0.00 USD
VAT/Local Sales Tax	0.00 USD / GBP
Total	0.00 USD
Terms and Conditions	

and conditions.

8. License Contingent Upon Payment: While you may exercise the rights licensed immediately upon issuance of the license at the end of the licensing process for the transaction, provided that you have disclosed complete and accurate details of your proposed use, no license is finally effective unless and until full payment is received from you (either by publisher or by CCC) as provided in CCC's Billing and Payment terms and conditions. If full payment is not received on a timely basis, then any license preliminarily granted shall be deemed automatically revoked and shall be void as if never granted. Further, in the event that you breach any of these terms and conditions or any of CCC's Billing and Payment terms and conditions, the license is automatically revoked and shall be void as if never granted. Use of materials as described in a revoked license, as well as any use of the materials beyond the scope of an unrevoked license, may constitute copyright infringement and publisher reserves the right to take any and all action to protect its copyright in the materials.

9. Warranties: Publisher makes no representations or warranties with respect to the licensed material.

10. Indemnity: You hereby indemnify and agree to hold harmless publisher and CCC, and their respective officers, directors, employees and agents, from and against any and all claims arising out of your use of the licensed material other than as specifically authorized pursuant to this license.

11. No Transfer of License: This license is personal to you and may not be sublicensed, assigned, or transferred by you to any other person without publisher's written permission.

12. No Amendment Except in Writing: This license may not be amended except in a writing signed by both parties (or, in the case of publisher, by CCC on publisher's behalf).

13. Objection to Contrary Terms: Publisher hereby objects to any terms contained in any purchase order, acknowledgment, check endorsement or other writing prepared by you, which terms are inconsistent with these terms and conditions or CCC's Billing and Payment terms and conditions. These terms and conditions, together with CCC's Billing and Payment terms and conditions (which are incorporated herein), comprise the entire agreement between you and publisher (and CCC) concerning this licensing transaction. In the event of any conflict between your obligations established by these terms and conditions and those established by CCC's Billing and Payment terms and conditions, these terms and conditions shall control.

14. Revocation: Elsevier or Copyright Clearance Center may deny the permissions described in this License at their sole discretion, for any reason or no reason, with a full refund payable to you. Notice of such denial will be made using the contact information provided by you. Failure to receive such notice will not alter or invalidate the denial. In no event will Elsevier or Copyright Clearance Center be responsible or liable for any costs, expenses or damage incurred by you as a result of a denial of your permission request, other than a refund of the amount(s) paid by you to Elsevier and/or Copyright Clearance Center for denied permissions.

LIMITED LICENSE

The following terms and conditions apply only to specific license types:

15. **Translation**: This permission is granted for non-exclusive world **English** rights only unless your license was granted for translation rights. If you licensed translation rights you

may only translate this content into the languages you requested. A professional translator must perform all translations and reproduce the content word for word preserving the integrity of the article. If this license is to re-use 1 or 2 figures then permission is granted for non-exclusive world rights in all languages.

16. **Website**: The following terms and conditions apply to electronic reserve and author websites:
Electronic reserve: If licensed material is to be posted to website, the web site is to be password-protected and made available only to bona fide students registered on a relevant course if:
This license was made in connection with a course,
This permission is granted for 1 year only. You may obtain a license for future website posting,
All content posted to the web site must maintain the copyright information line on the bottom of each image,
A hyper-text must be included to the Homepage of the journal from which you are licensing at http://www.sciencedirect.com/science/journal/xxxxx or the Elsevier homepage for books at http://www.elsevier.com , and
Central Storage: This license does not include permission for a scanned version of the material to be stored in a central repository such as that provided by Heron/XanEdu.

17. **Author website** for journals with the following additional clauses:

All content posted to the web site must maintain the copyright information line on the bottom of each image, and the permission granted is limited to the personal version of your paper. You are not allowed to download and post the published electronic version of your article (whether PDF or HTML, proof or final version), nor may you scan the printed edition to create an electronic version. A hyper-text must be included to the Homepage of the journal from which you are licensing at http://www.sciencedirect.com/science/journal/xxxxx . As part of our normal production process, you will receive an e-mail notice when your article appears on Elsevier's online service ScienceDirect (www.sciencedirect.com). That e-mail will include the article's Digital Object Identifier (DOI). This number provides the electronic link to the published article and should be included in the posting of your personal version. We ask that you wait until you receive this e-mail and have the DOI to do any posting.

Central Storage: This license does not include permission for a scanned version of the material to be stored in a central repository such as that provided by Heron/XanEdu.

18. **Author website** for books with the following additional clauses:
Authors are permitted to place a brief summary of their work online only.
A hyper-text must be included to the Elsevier homepage at http://www.elsevier.com . All content posted to the web site must maintain the copyright information line on the bottom of each image. You are not allowed to download and post the published electronic version of your chapter, nor may you scan the printed edition to create an electronic version.

Central Storage: This license does not include permission for a scanned version of the material to be stored in a central repository such as that provided by Heron/XanEdu.

19. **Website** (regular and for author): A hyper-text must be included to the Homepage of the journal from which you are licensing at http://www.sciencedirect.com/science/journal/xxxxx. or for books to the Elsevier homepage at http://www.elsevier.com

20. **Thesis/Dissertation**: If your license is for use in a thesis/dissertation your thesis may be submitted to your institution in either print or electronic form. Should your thesis be published commercially, please reapply for permission. These requirements include permission for the Library and Archives of Canada to supply single copies, on demand, of the complete thesis and include permission for UMI to supply single copies, on demand, of the complete thesis. Should your thesis be published commercially, please reapply for permission.

21. **Other Conditions**: Permission is granted to submit your article in electronic format. This license permits you to post this Elsevier article online on your Institution's website if the content is embedded within your thesis. You are also permitted to post your Author Accepted Manuscript online however posting of the final published article is prohibited. Please refer to Elsevier's Posting Policy for further information:
http://www.elsevier.com/wps/find/authors.authors/postingpolicy

v1.6

If you would like to pay for this license now, please remit this license along with your payment made payable to "COPYRIGHT CLEARANCE CENTER" otherwise you will be invoiced within 48 hours of the license date. Payment should be in the form of a check or money order referencing your account number and this invoice number RLNK500877346.
Once you receive your invoice for this order, you may pay your invoice by credit card. Please follow instructions provided at that time.

Make Payment To:
Copyright Clearance Center
Dept 001
P.O. Box 843006
Boston, MA 02284-3006

For suggestions or comments regarding this order, contact RightsLink Customer Support: customercare@copyright.com or +1-877-622-5543 (toll free in the US) or +1-978-646-2777.

Gratis licenses (referencing $0 in the Total field) are free. Please retain this printable license for your reference. No payment is required.